EXPERIMENTAL AND SIMULATION-BASED ASSESSMENT OF THE HUMAN POSTURAL RESPONSE TO SAGITTAL PLANE PERTURBATIONS WITH LOCALIZED MUSCLE FATIGUE AND AGING

BY

BRADLEY STEVEN DAVIDSON

Dissertation submitted to the Faculties of
Virginia Polytechnic Institute and State University
and
Wake Forest University
in partial fulfillment of the requirements for the degree of

Doctor of Philosophy
in
Biomedical Engineering

Michael L. Madigan, Ph.D. (chair)
Maury A. Nussbaum, Ph.D.
Bradley G. Klein, Ph.D.
Anthony P. Marsh, Ph.D.
Steve C. Southward, Ph.D
Kevin P. Granata, Ph.D.

October 12, 2007
Blacksburg, Virginia

keywords: falls, fatigue, balance, neural control, optimal control theory

Experimental and simulation-based assessment of the human postural response to sagittal plane perturbations with localized muscle fatigue and aging

Bradley Steven Davidson

(ABSTRACT)

This research was motivated by occupational falls, which are one of the leading causes of fatalities in skilled labor divisions. The effects of localized muscle fatigue (LMF) on surrogate measures of postural sway are well-established. This is significant since these increases have been linked to elevated risk of falls, and workers with increased risks of falling fatality frequently engage in fatiguing tasks.

An initial study was conducted to investigate the effects of LMF and aging on balance recovery from postural perturbations without stepping. Sagittal plane perturbations were administered to young and older individuals before and after fatiguing exercises. Measures of balance recovery (BR) were based on the center of mass (COM) and center of pressure (COP) trajectories and the maximum perturbation that could be withstood. Changes in BR measures were consistent with an LMF- and aging-induced decrement in recovering from the perturbations.

The second study investigated the effects of aging and LMF on the neural control of upright stance during small postural perturbations. Small magnitude postural perturbations were administered to young and older individuals before and after fatiguing exercises. A single degree of freedom (DOF) human body model was developed that accurately simulated the experimental data. Feedback gains and time-delay were optimized for each participant, and a delay margin analysis was performed to assess system robustness. Results indicated that older individuals had a longer "effective" time-delay and exhibited greater reliance on afferent velocity information. No changes in feedback controller gains, time-delay, or delay

margins were found with LMF in either age group.

The final study investigated using a nonlinear controller to simulate responses to large magnitude postural perturbations. A three DOF model of the human body was developed and controlled with the state-dependent Riccati equation (SDRE). Parameters of the SDRE were optimized to fit the experimentally recorded kinematics. Unlike other nonlinear controllers, the SDRE provides meaningful parameters for interpretation in the system identification. The SDRE approach was successful at stabilizing the dynamical system; however, accurate results were not obtained. Explanations for this are presented along with an alternative formulation to the time-delayed optimal control problem using Roesser state space equations.

in memory of Dr. Kevin P. Granata

scholar, teacher, and friend

Acknowledgments

I gratefully acknowledge my advisor, Dr. Michael Madigan for his leadership and patience during my time in Blacksburg. Thank you for your setting such an unwavering example of integrity, excellent scholarship, and valuable friendship that I can only hope to emulate in my professional and personal life.

Many thanks to Dr. Maury Nussbuam for working closely with me on this project. It's a delight to collaborate with such a fine scholar.

To my advisory committee: Dr. Anthony Marsh, Dr. Bradley Klein, and Dr. Steve Southward. Your patience and input throughout this process has been valuable.

Thank you to Anoop Varghese for taking time to provide a tutorial on programming in Fortran90. Also, I am indebted to Dr. Sylvester (Skip) Thompson at Radford University for his assistance and persistence in debugging the delayed differential equation solver used for the numerical simulations.

To the unbelievable friends I have had in the Musculoskeletal Biomechanics Laboratory: Dr. Madigan, Katie Bieryla, Dennis Anderson, Michael Whitley, Sara Matrangola, Mike Diersing, Steve Hanson, Greg Slota, Tim Franklin, Martin Tanaka, Hyunwook Lee, Pranitha Gottipati, Kevin Groth, Mike Renner, and the honorary MSB members – Jul Davis and Corrie Spoon. You have made my hours spent in (and out of) Norris Hall some of the most entertaining in Blacksburg.

To "my undergrads" – Blair Padula, Melina Ciccarone, Katie Murray, Scott Kramer, Frances Davis, Nu Ma, Michael Whitley, and Sara Matrangola. Without you, I would still be collecting and processing data into old age.

To my parents, who have always encouraged me to discover. For years you have modeled the three valuable things: constantly learning new things, forever caring for people, and always loving our God. And to my brother, whom I miss dearly. Thank you for all the conversations about work, life, bicycles, etc. I'm honored to have a brother like you.

Finally, to my bride. You have endured lonely evenings while I worked, dirty dishes as I procrastinated, endless stacks of journal articles, and random napkins and post-its full of "numberless math." How could I have ever survived without you? I love you, sweetheart.

Soli Deo Gloria

Bradley Davidson

Table of Contents

List of Tables

List of Figures

List of Abbreviations

AD	anteriorly-directed.
AP	anteroposterior.
ARMAX	autoregressive moving average model with exogenous inputs.
ARE	algebraic Riccati equation.
BR	balance recovery.
CE	characteristic equation.
COM	center of mass.
COP	center of pressure.
DOF	degree of freedom.
FFH	falls from height.
ICC	intraclass correlation coefficient.
LQR	linear quadratic regulator.
LTI	linear time invariant.
LMF	localized muscle fatigue.
ML	mediolateral.
MVC	maximum voluntary contraction.
NIOSH	National Institute of Occupational Safety and Health.
NQR	nonlinear quadratic regulator.
ODE	ordinary differential equation.
OSHA	Occupational Safety and Health Administration.

RIPID	Recurrent integrator proportional, integral, derivative.
PID	proportional, integral, and derivative.
PD	posteriorly-directed. (Chapters 3,6,8)
PD	proportional, derivative. (Chapters 4,5)
SD	standard deviation.
SDC	state-dependent coefficient.
SDRE	state-dependent Riccati equation.
SISO	singe input single output.

List of Symbols and Notation

$\mathbf{A}^{-1}$	Inverse of square matrix $\mathbf{A}$.
$\mathbf{A}^{T}$	Transpose of matrix $\mathbf{A}$.
$\mathcal{L}\{\cdot\}$	Laplace transform.
$\frac{\partial}{\partial t}$	Partial derivative with respect to time.
$\frac{\partial V(\mathbf{x})}{\partial \mathbf{x}}$	Gradient of the scalar function $V(\mathbf{x})$ with respect to the vector $\mathbf{x}$, taken as a column vector $\left[\begin{array}{cccc} \frac{\partial V(\mathbf{x})}{\partial x_1} & \frac{\partial V(\mathbf{x})}{\partial x_2} & \cdots & \frac{\partial V(\mathbf{x})}{\partial x_n} \end{array} \right]^T$.

Chapter 1

Background and problem statement

1.1 Falls from heights

Falls accounted for 14.2% of the 5,703 reported occupational fatalities in the United States in 2004 (BLS, 2005), which marks a record high for fatal falls (Figure 1.1). Almost all of these falls (90%) occurred from an elevated surface (BLS, 2005), hereafter referred to as falls from height (FFH). Examples include falls from ladders and roofs. Not only problematic in the United States, FFH is the number one cause of occupational fatality and injury in Great Britain. In its attempt to ensure a safe working environment, the Health and Safety Executive of Great Britain has recently implemented the "Height Aware 2006" campaign designed to help workers identify when they are at risk of falling from height.

Virtually every industrial sector is exposed to risk of FFH. The potential for FFH exists for an iron worker connecting steel columns 200 feet in the air, to the worker washing windows on a suspended scaffold, and even a stock clerk retrieving goods using a 4-foot step ladder (NIOSH, 2000). Using data taken from occupational accident reports, those jobs with the greatest hazard of FFH lie within skilled labor divisions such as construction, mining, agriculture/forestry, and manufacturing (NIOSH, 2000). Accordingly, the National Institute of Occupational Safety and Health (NIOSH) has produced several publications which specifically address prevention of falls while erecting communications towers (NIOSH, 2001), trimming trees (NIOSH, 1992a), working on scaffolds (NIOSH, 1992b, 1993), and working on roofs near skylights or roof openings (NIOSH, 1989, 2004).

Workers in the construction industry are at particularly high risk of FFH (Derr et al.,

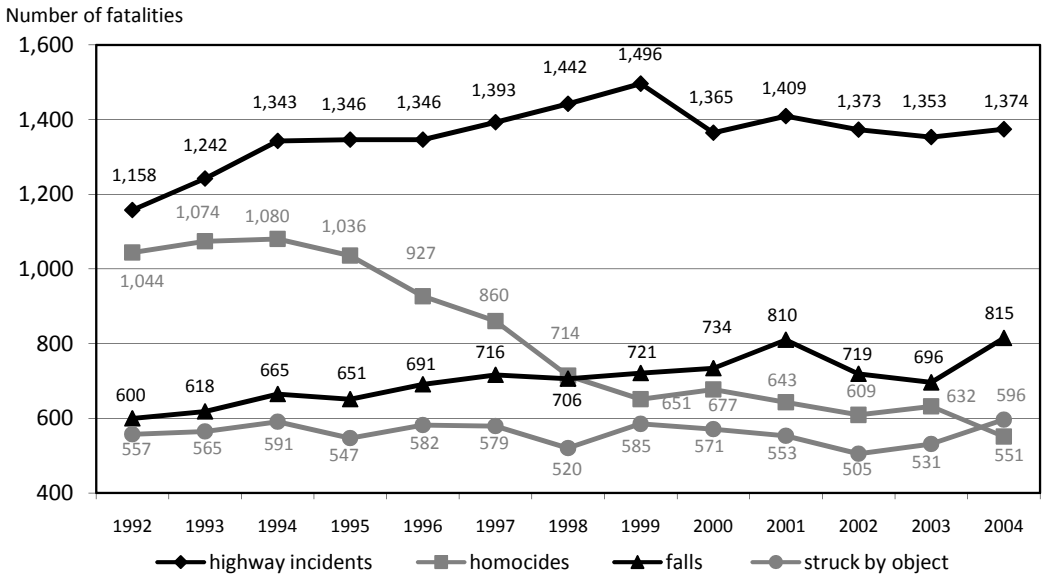

Figure 1.1: Data from the Bureau of Labor Statistics shows falls to be of the four most frequent work-related fatal events in the United States. As can be seen, 2004 marked an all-time high in these falls. (BLS, 2005)

2001). For example, a report on worker deaths by falls revealed that construction workers accounted for 50% of all FFH fatalities. This is well above the contributions from any other industry – the second highest being industrial manufacturing at 12% (NIOSH, 2000). Falls are the predominant cause of fatality in this industry where elevated work environments are common, most often off of ladders, roofs, and through openings in floors and roofs (NIOSH, 2004).

In addition to employment as a laborer in the industrial sector, age also contributes to risk of falling. The National Census of Fatal Occupational Injuries showed that 39% of fatal falls in 2004 were from workers 55 years and older BLS (2005). This is a disproportionate trend since this age group composes only 17% of the total workforce according to annual surveys by the U.S. Department of Labor. Figure 1.2 demonstrates this trend in increased fall incidents with older workers. Notice that the construction industry shows both a greater overall percentage of FFH deaths as well as greater increase in deaths at higher ages.

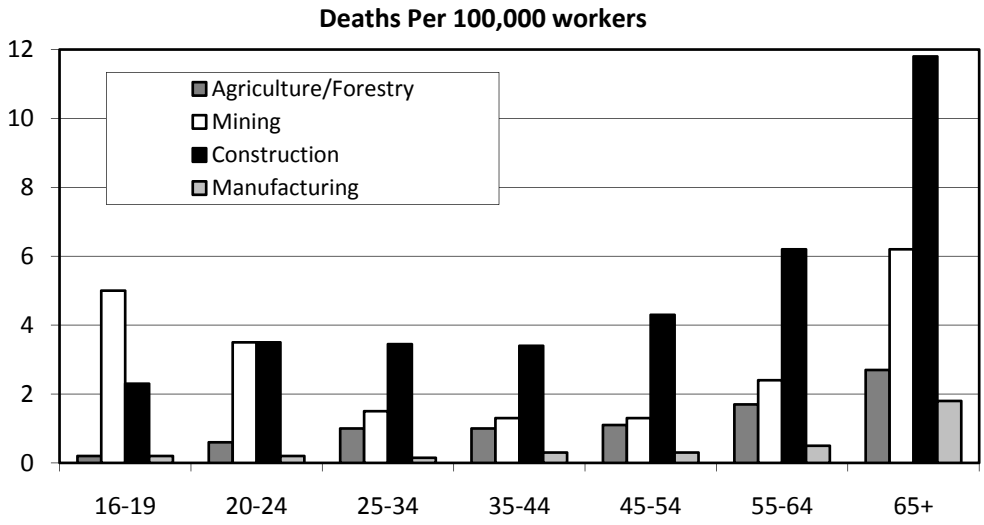

Figure 1.2: Worker deaths by falls categorized by age. Two important trends emerge here. First is the considerably larger percentage of falls for the construction industry when compared to other industries which report high rates of falling fatality. Also, note the remarkable increase in deaths by falling in the construction industry for the older workers. (NIOSH, 2000)

1.2 Fall interventions

The mechanism of a fall can be defined as an imbalance with a failed attempt at recovering balance that causes potential injury or fatality (Gauchard et al., 2001). Interventions aimed at preventing injuries and fatalities from FFH are typically categorized as either fall protection or fall prevention (Hsiao and Simeonov, 2001).

The goal of fall protection is to safely arrest a fall after it has occurred. Occupational Safety and Health Administration (OSHA) standards exist which address falls with this approach, and a large amount of research has been conducted throughout the country in designing the necessary devices used for fall protection (Lough, 2004). Despite the readily available safety equipment and government regulation of those industries with a high risk of falls, many workers fail to use fall protection devices appropriately (David, 1996). Thus, upwards of two-thirds of FFH fatalities reported by NIOSH (2000) occurred while fall protection devices remained unused.

The goal of fall prevention is to prevent a fall from occurring. To devise methods of

fall prevention it is necessary to identify and understand underlying factors, both extrinsic and intrinsic that contribute to occupational falls. Examples of extrinsic factors are type of activity, urgency of activity, and work environment (Gauchard et al., 2001). Prevention tactics which address these situations often consist of additional safety training, altering work schedules, or improving the work area by reducing known hazards. Examples of intrinsic factors are use of judgment-impairing substances, attention level, experience level, weakness, and muscle fatigue (Gauchard et al., 2001). To develop methods designed to prevent FFH due to these intrinsic factors, a thorough knowledge is necessary of how these may contribute to a fall.

1.3 Fatigue effects on postural control and balance

The most reported cause of falls in roofers is a "loss of balance" (Hsiao and Simeonov, 2001). Although common in everyday usage, a definitive definition of "balance" does not exist (Ekdahl et al., 1989; Pollock et al., 2000). For our purposes, human balance will be defined as the ability of a person to remain in an upright standing posture. Upright stance is an inherently unstable posture in which a human essentially behaves as an inverted pendulum (Gage et al., 2004; Winter, 1995) with roughly two-thirds mass distributed at two-thirds height above the ground (Winter, 1993). Maintaining balance, or upright stance, is accomplished by the postural control system. The postural control system involves many interactive elements (Massion, 1994) such as sensory reception, signal transmission, neural control, and muscle excitation-contraction. The sensory information used by the postural control system is comprised of afferent signals from three sources: vision, vestibular organs, and somatosensory system (Shumway-Cook and Woollacott, 1995). This information is transmitted to the neural controller, a portion of the postural control system that integrates the sensory information and generates corrective motor commands based on the difference between actual and desired postures (Massion, 1994). These motor commands are transmitted via

motor units to the postural muscles, and the resulting contractions influence maintenance of balance. Balance and postural control are most often assessed by surrogate measures of postural sway calculated from the center of mass (COM) or center of pressure (COP) trajectories during quiet stance.

One intrinsic factor that has been shown to affect COM- and COP-based measures of balance and postural control is localized muscle fatigue. Increases in these measures during quiet stance have been demonstrated after fatiguing muscles that are directly associated with upright stance and those that are not. For instance, many investigations have focused on fatigue of the ankle musculature (Caron, 2003; Corbeil et al., 2003; Gribble and Hertel, 2004; Lundin et al., 1993; Yaggie and McGregor, 2002). It is well-accepted that the ankle musculature are primary in controlling quiet stance, and so it is of little surprise that localized changes such as fatigue would adversely affect postural sway. However, recent investigations have demonstrated that fatigue of non-postural muscles such as the neck (Gosselin et al., 2004; Schieppati et al., 2003) and shoulder (Nussbaum, 2003) have had similar effects on these measures. A review of fatigue and balance literature is found in Chapter 2.

The purpose of this investigation is to further our understanding of the effects of localized muscle fatigue (LMF) and aging on balance and the postural control system. A series of laboratory experiments were performed and analyzed to evaluate the effects of LMF and aging on recovery of upright stance following a postural perturbation. Theoretical models of the human body were developed in conjunction with the collected experimental data to assess changes in neural control of balance. It is anticipated that this work will provide the foundations for future postural modeling and simulation in the presence of fatigue and age and potentially aid in the design of interventions aimed at reducing FFH.

1.4 Document organization

This thesis is organized into nine chapters and is arranged in a progressive sequence: from an experimental and measurement-based analyses to theoretical and simulation-based analyses. Chapter 2 introduces the reader to the body of "fatigue and balance" literature, and Chapter 3 presents the first study from the series – "Effects of localized muscle fatigue on recovery from a postural perturbation without stepping." Chapter 4 initiates the shift toward modeling of the postural control system with a brief review of dynamical modeling and feedback control systems. Chapter 5 introduces past studies that performed feedback-controlled simulations of the upright stance. Chapter 6 presents the second study – "Effects of aging and localized muscle fatigue on neural control of posture during small magnitude perturbations." Chapter 7 introduces the reader to the theory and implementation of optimal controls, and Chapter 8 expands on these ideas in the third and final study – "Neural controller approximation using the nonlinear state-dependent Riccati equation during postural responses to large magnitude sagittal plane perturbations." Chapter 9 highlights the major findings and contributions from the individual studies.

References

BLS: (2005) National census of fatal occupational injuries in 2004. United States Department of Labor

Caron O (2003) Effects of local fatigue of the lower limbs on postural control and postural stability in standing posture. *Neurosci Lett* 340(2): 83–6

Corbeil P, Blouin JS, Begin F, Nougier V, Teasdale N (2003) Perturbation of the postural control system induced by muscular fatigue. *Gait Posture* 18(2): 92–100

David D A J (1996) Proper fall protection training. *Occup Health Saf* 65(6): 54–6, 58–9

Derr J, Forst L, Chen HY, Conroy L (2001) Fatal falls in the us construction industry, 1990 to 1999. *J Occup Environ Med* 43(10): 853–60

Ekdahl C, Jarnlo GB, Andersson SI (1989) Standing balance in healthy subjects. evaluation of a quantitative test battery on a force platform. *Scand J Rehabil Med* 21(4): 187–95

Gage WH, Winter DA, Frank JS, Adkin AL (2004) Kinematic and kinetic validity of the inverted pendulum model in quiet standing. *Gait Posture* 19(2): 124–32

Gauchard G, Chau N, Mur JM, Perrin P (2001) Falls and working individuals: role of extrinsic and intrinsic factors. *Ergonomics* 44(14): 1330–9

Gosselin G, Rassoulian H, Brown I (2004) Effects of neck extensor muscles fatigue on balance. *Clin Biomech (Bristol, Avon)* 19(5): 473–9

Gribble PA, Hertel J (2004) Effect of lower-extremity muscle fatigue on postural control. *Arch Phys Med Rehabil* 85(4): 589–92

Hsiao H, Simeonov P (2001) Preventing falls from roofs: a critical review. *Ergonomics* 44(5): 537–61

Lough D (2004) Horizontal fall arrest systems: rigid systems vs. flexible line systems. *Occup Health Saf* 73(9): 162, 164, 166–7

Lundin T, Feuerbach J, Grabiner M (1993) Effect of plantar flexor and dorsiflexor fatigue on unilateral postural control. *J Appl Biomech* 9: 191–201

Massion J (1994) Postural control system. *Curr Opin Neurobiol* 4(6): 877–87

NIOSH: (1989) Niosh alert: Preventing worker deaths and injuries from alls through skylights and roof opening. National Institute of Occupational Safety and Health

NIOSH: (1992a) Niosh alert: Preventing falls and electrocution during tree trimming. National Institute of Occupational Safety and Health

NIOSH: (1992b) Niosh alert: Preventing worker injuries and deaths caused by falls from suspension scaffolds. National Institute of Occupational Safety and Health

NIOSH: (1993) Niosh issues nationwide alert on dangers of working from scaffolds. National Institute of Occupational Safety and Health

NIOSH: (2000) Worker deaths by falls: a summary of surveillance findings and investigative case reports. National Institute of Occupational Safety and Health

NIOSH: (2001) Niosh alert: Preventing injuries and deaths from falls during construction and maintenance of telecommunication towers. National Institute of Occupational Safety and Health

NIOSH: (2004) Niosh alert: Preventing falls of workers through skylights and roof and floor openings. National Institute of Occupational Safety and Health

Nussbaum MA (2003) Postural stability is compromised by fatiguing overhead work. *AIHA J (Fairfax, Va)* 64(1): 56–61

Pollock AS, Durward BR, Rowe PJ, Paul JP (2000) What is balance? *Clin Rehabil* 14(4): 402–6

Schieppati M, Nardone A, Schmid M (2003) Neck muscle fatigue affects postural control in man. *Neuroscience* 121(2): 277–85

Shumway-Cook A, Woollacott M: *Motor Control: Theory and Practical Applications* (Baltimore: Williams and Wilkins 1995)

Winter DA: *A.B.C of Balance During Standing and Walking* (Waterloo: University of Waterloo 1993)

Winter DA (1995) Human balance and posture control during standing and walking. *Gait & Posture* 3(4): 193–214

Yaggie JA, McGregor SJ (2002) Effects of isokinetic ankle fatigue on the maintenance of balance and postural limits. *Arch Phys Med Rehabil* 83(2): 224–8

Chapter 2

Fatigue and balance literature

2.1 Introduction

Balance is a term which is frequently used in everyday conversation as well as by clinicians. Every individual has some qualitative understanding of balance or loss of balance. Despite its widespread use, there is no universally accepted definition of balance (Ekdahl et al., 1989; Pollock et al., 2000). As such, many approaches have been used to quantify balance. Investigators have used the duration of a participant to remain in a certain stance, ability to control a moving platform, various measures of center of mass (COM) and center of pressure (COP) trajectories, as well as a myriad of other commercial devices to assess balance and changes in balance.

A common biomechanical description of balance is the body's ability to maintain its center of mass within its base of support (Hall, 1991; Kreighbaum and Barthels, 1990; Massion, 1994; Pollock et al., 2000). COM movement (also referred to as sway) is controlled by movement of the COP primarily by the ankle and hip musculature during quiet standing. Because a human body has approximately two-thirds of its mass located two-thirds its height above the ground, the body is inherently unstable and requires continuous adjustment of the COP (Winter, 1993). Movement of the COP, although not identical, is generally in phase with movement of the COM. This quality, along with its relative ease of collection, has made measures of the COP trajectory an attractive method of quantitative assessment of postural sway and balance. Changes in these measures have been associated with increased falls in the elderly (Lichtenstein et al., 1989; Riach and Starkes, 1994) and may also indicate risk of

falling outside of this population.

The following sections review the current literature investigating the effects of fatigue on measures of postural sway and are organized into three sections. The first section outlines the earliest studies reporting the effects of fatigue on balance. Next, more recent studies are addressed beginning with localized muscle fatigue in the lower extremities. The third section introduces the reader to muscle fatigue not located in the lower extremities. Finally, a summary of the investigation using perturbations from our laboratory is presented.

2.2 Earliest reported studies investigating the effects of fatigue on balance

Although the last decade has presented an increase in the number of studies investigating the effects of fatigue on measures of balance, this topic is not new. As long ago as 1949 the effects of fatigue induced by a physical efficiency test on balance were investigated by Scott and Matthews. Slocum (1953) performed a similar study. A more recent publication (Nielson and Johnson, 1973) reported that both studies found improved balance performance following the efficiency test, and Slocum hypothesized that the improvement resulted from a warm-up effect. The first scientific evidence of potential balance impairment due to fatigue was offered by Culhane (1956) in an unpublished Master's thesis. Here, a slight loss in static balance performance is reported following two minutes of cycling; however, the loss was not statistically significant. It was suggested that the exercise was not strenuous enough to produce "genuine fatigue."

The topic of fatigue effects on balance was relatively quiet until 1973, when Nielson and Johnson analyzed the effects of "general fatigue" and "local fatigue" on static balance. Local fatigue was administered through maximum number of one-legged toe raises while general fatigue was administered through maximum number of squat thrusts. Static balance was quantified by the length of time which participants could remain in a one-legged stance.

It was found that both heel raises and squat thrusts significantly reduced the length of one-legged standing, but the effects of the squat thrusts were more detrimental.

Three years later, an investigation was performed which compared the fatigue of several different muscle groups on balance as measured with a "dynabalometer" (Miller and Bird, 1976). Four muscle groups were fatigued: dorsiflexors; plantar flexors; abdominals; knee and hip flexors and extensors). Twenty participants were randomly assigned to each muscle group and twenty were used as a control group. Only the group which fatigued the knee and hip flexors and extensors with squats demonstrated a significant difference in balance as measured by the "time in balance" while standing on an unstable platform.

Almost fifteen years transpired before the next study pertaining to fatigue effects on balance. During this interlude, biomechanics was revolutionized by technological advances and improved methodology. Equipment such as force platforms and motion monitoring systems were developed and, along with vast improvement of computer processing and data collection, the current era of biomechanical analysis arrived.

2.3 Investigations of localized muscle fatigue in lower extremities

By far, the largest number of studies investigating the effects of fatigue on postural sway or postural control has involved localized muscle fatigue of muscle groups in the lower extremities, specifically the ankle musculature. Lundin et al. (1993) determined that combining dorsiflexor and plantar flexor fatigue increased sway parameters in the anteroposterior (AP) and mediolateral (ML) directions during unilateral stance as measured by a Chattecx Balance System. An anterior shift in COP location was also observed which has been demonstrated by other authors following fatigue (Sparto et al., 1997). Contrary to Lundin et al. (1993) and Nielson and Johnson (1973), Adlerton and Moritz (1996) found no changes after plantar flexor fatigue. One other investigation of the effects of plantar flexor fatigue on postural

sway during bilateral stance (Corbeil et al., 2003) demonstrated increased COP mean velocity, mean radius, and median frequency. This study concluded that "fatigue places higher demands on the postural control system by increasing the frequency of actions needed to regulate the upright stance."

Vuillerme et al. (2001, 2002, 2003), while presuming the destabilizing effect of plantar flexor fatigue, has investigated different effects of afferent input on the balance system. In 2001, Vuillerme et al.determined that the presence of visual cues allowed the body to more quickly compensate for the effects of fatigue. Vuillerme et al. (2002) tested the combined effects of plantar flexor fatigue and muscle vibration on postural sway measures. These two conditions alone caused a deleterious effect on postural sway. However, when muscle vibration was applied following fatigue, there was no additional increase in sway. Two hypotheses were offered to account for this: 1) fatigued muscles are less sensitive to vibration or 2) the CNS relies less on afferent information from fatigued muscles to control postural sway. Vuillerme and Nougier (2003) reported on the effects of light finger touch on postural sway following plantar flexor fatigue with similar results as Vuillerme et al. (2002). They concluded that haptic cues from the finger, which contribute to total proprioceptive feedback, possibly increased following fatigue.

Yaggie and McGregor (2002) sought to add fatigue of ankle inverters and everters to the treatment of ankle fatigue and postural sway. Increases of non-directional and both AP/ML sway measures were reported. However, because the measures of sway were not clearly defined, definitive interpretation is not possible.

Investigations of ankle dorsiflexor fatigue by Caron (2003, 2004) have explored the relationship between postural control and "postural stability." Stability is defined here as movement of the COM while postural control is quantified by the COP trajectory. Dorsiflexor fatigue was selected for this research because "plantar flexors are rarely involved in quiet stance" (Okada, 1973). In particular, these studies sought to first assess COM and COP relationship in the presence of ankle dorsiflexor fatigue (Caron, 2003), and then to

determine if there is interaction effects of local fatigue and vision (2004). In each study, COP measures significantly changed with dorsiflexors fatigue while measures of the COM trajectory did not. Effects in Caron (2004) were more pronounced in the eyes open condition. These results indicate that changes in postural control (mean velocity, frequency) do not necessarily imply a decrease in postural stability. This hypothesis was derived from an earlier investigation which employed a comparative analysis of COM and COP trajectories (Caron et al., 2000).

Instead of focusing on the effects of a single muscle group, Gribble and Hertel have compared the effects of fatiguing different lower body muscles on COP mean velocity. In a study which separately fatigued the ankle, knee, and hip muscles in the sagittal plane, an increase in COP mean velocity was found in each condition (Gribble and Hertel, 2004b). Interestingly, the increase in mean velocity was present in both the AP and ML directions, and was larger following knee and hip fatigue than following ankle fatigue. In a similar investigation which fatigued the lower extremity joints (ankle, hip) in the frontal plane (Gribble and Hertel, 2004a), changes were only found following hip fatigue. Although these studies only examined mean velocity of the COP trajectory, they have provided evidence to suggest that muscular fatigue more central to the body would cause an adaptive change in postural control.

2.4 Investigations of localized muscle fatigue distant from lower extremities

All of the studies previously mentioned which involve localized muscle fatigue have focused on the lower extremity musculature. Since lower extremity muscles are commonly associated with the control of upright posture and balance, these changes are somewhat intuitive. Recently, several studies have reported the effect of localized fatigue in muscles not primarily thought to be responsible for balance control.

A series of investigations from our laboratory (Davidson et al., 2004; Madigan et al., 2006; Wilson et al., 2006) have addressed the effects of lumbar extensor fatigue on measures of balance. In each of these, fatigue was induced by a series of controlled back extension exercises and was assessed by measuring the decline of maximum voluntary contraction. The first publication (Davidson et al., 2004) established the effect of low back fatigue on traditional measures of postural sway during quiet standing. In addition, no influence of fatiguing rate was observed. Madigan et al. (2006) demonstrated that a local investigation of joint kinematics may be necessary to discern fatigue effects instead of the widely used COM- and COP-based measures of sway. Along with Wilson et al. (2006), this is only the second study in contemporary fatigue and balance literature which departs from the standard measures.

Nussbaum (2003) investigated the effects of localized shoulder fatigue following overhead work on COP measures of sway. Fatigue was induced by a series of repetitive overhead tapping sessions lasting a total of three hours (or until participants chose to terminate the task). COP data was collected before and after each tapping session. Here, the effect of prolonged fatiguing work on postural sway measures was assessed. Participants who did not complete all of the tapping sessions showed a significantly larger increase in sway measures than those who did finish.

Both Schieppati et al. (2003) and Gosselin et al. (2004) investigated the effects of neck extensor muscle fatigue on COP measures of sway, and arrived at comparable conclusions. Gosselin et al. (2004) recorded COP data while participants stood quietly with closed eyes, and reported increases in displacement and velocity measures overall and in the AP direction. Schieppati et al. (2003) determined that the effects on postural sway were significant only in an eyes closed condition. The authors speculated that neck extensor fatigue was sends abnormal sensory input to the CNS which is overcome by visual information.

2.5 Investigations of localized muscle fatigue with use of external perturbations

Unique to the body of fatigue and balance literature is a study from our laboratory by Wilson et al. (2006). Instead of having the participants remain still during balance collections, dynamic perturbations were employed to examine the balance system. In this experiment participants were fatigued using similar methods to Davidson et al. (2004) and Madigan et al. (2006); however, an anteriorly-directed perturbation was given via a ballistic pendulum. Postural strategies were analyzed using measures of joint kinematics and kinetics during recovery from the perturbation revealing that those using more of a hip strategy previous to the fatigue were more affected. A proactive change in strategy was also observed in that participants adopted a slight forward lean following fatigue. Changes in reactive strategies included a shift toward more hip motion during the perturbations following fatigue.

References

Adlerton AK, Moritz U (1996) Does calf-muscle fatigue affect standing balance? *Scand J Med Sci Sports* 6(4): 211–5

Caron O (2003) Effects of local fatigue of the lower limbs on postural control and postural stability in standing posture. *Neurosci Lett* 340(2): 83–6

Caron O (2004) Is there interaction between vision and local fatigue of the lower limbs on postural control and postural stability in human posture? *Neurosci Lett* 363(1): 18–21

Caron O, Gelat T, Rougier P, Blanchi JP (2000) A comparative analysis of the center of gravity and center of pressure trajectory path lengths in standing posture: an estimation of active stiffness. *J Appl Biomech* 16(3): 234–47

Corbeil P, Blouin JS, Begin F, Nougier V, Teasdale N (2003) Perturbation of the postural control system induced by muscular fatigue. *Gait Posture* 18(2): 92–100

Culhane M: (1956) *The effect of leg fatigue on balance.* Master's thesis, State University of Iowa, Iowa City, IA

Davidson BS, Madigan ML, Nussbaum MA (2004) Effects of lumbar extensor fatigue and fatigue rate on postural sway. *Eur J Appl Physiol* 93(1-2): 183–9

Ekdahl C, Jarnlo GB, Andersson SI (1989) Standing balance in healthy subjects. evaluation of a quantitative test battery on a force platform. *Scand J Rehabil Med* 21(4): 187–95

Gosselin G, Rassoulian H, Brown I (2004) Effects of neck extensor muscles fatigue on balance. *Clin Biomech (Bristol, Avon)* 19(5): 473–9

Gribble PA, Hertel J (2004a) Effect of hip and ankle muscle fatigue on unipedal postural control. *J Electromyogr Kinesiol* 14(6): 641–6

Gribble PA, Hertel J (2004b) Effect of lower-extremity muscle fatigue on postural control. *Arch Phys Med Rehabil* 85(4): 589–92

Hall S: *Basic Biomechanics* (St Louis: Mosby Year Book 1991)

Kreighbaum E, Barthels K: *Biomechanics: A Qualitative Approach for Studying Human Movement* (New York: MacMillan 1990)

Lichtenstein MJ, Shields SL, Shiavi RG, Burger C (1989) Exercise and balance in aged women: a pilot controlled clinical trial. *Arch Phys Med Rehabil* 70(2): 138–43

Lundin T, Feuerbach J, Grabiner M (1993) Effect of plantar flexor and dorsiflexor fatigue on unilateral postural control. *J Appl Biomech* 9: 191–201

Madigan ML, Davidson BS, Nussbaum MA (2006) Postural sway and joint kinematics during quiet standing are affected by lumbar extensor fatigue. *Hum Mov Sci*

Massion J (1994) Postural control system. *Curr Opin Neurobiol* 4(6): 877–87

Miller PK, Bird AM (1976) Localized muscle fatigue and dynamic balance. *Percept Mot Skills* 42(1): 135–8

Nielson JK, Johnson BL (1973) Effects of local and general fatigue on static balance. *Percept Mot Skills* 37(2): 615–8

Nussbaum MA (2003) Postural stability is compromised by fatiguing overhead work. *AIHA J (Fairfax, Va)* 64(1): 56–61

Okada M (1973) An electromyographic estimation of the relative muscular load in different human postures. *J Hum Ergol (Tokyo)* 1(1): 75–93

Pollock AS, Durward BR, Rowe PJ, Paul JP (2000) What is balance? *Clin Rehabil* 14(4): 402–6

Riach C, Starkes J (1994) Velocity of centre of pressure excursions as an indicator of postural control systems in children. *Gait Posture* 2: 167–172

Schieppati M, Nardone A, Schmid M (2003) Neck muscle fatigue affects postural control in man. *Neuroscience* 121(2): 277–85

Scott M, Matthews H (1949) A study of fatigue effects induced by an efficiency test for college women. *Research Quarterly* 20: 134–141

Slocum H: (1953) *The effects of fatigue induced by physical activity on tests of kinesthesis.* Doctoral dissertation, State University of Iowa, Iowa City, IA

Sparto PJ, Parnianpour M, Reinsel TE, Simon S (1997) The effect of fatigue on multijoint kinematics, coordination, and postural stability during a repetitive lifting test. *J Orthop Sports Phys Ther* 25(1): 3–12

Vuillerme N, Danion F, Forestier N, Nougier V (2002) Postural sway under muscle vibration and muscle fatigue in humans. *Neurosci Lett* 333(2): 131–5

Vuillerme N, Nougier V (2003) Effect of light finger touch on postural sway after lower-limb muscular fatigue. *Arch Phys Med Rehabil* 84(10): 1560–3

Vuillerme N, Nougier V, Prieur JM (2001) Can vision compensate for a lower limbs muscular fatigue for controlling posture in humans? *Neurosci Lett* 308(2): 103–6

Wilson EL, Madigan ML, Davidson BS, Nussbaum MA (2006) Postural strategy changes with fatigue of the lumbar extensor muscles. *Gait Posture* 23(3): 348–54

Winter DA: *A.B.C of Balance During Standing and Walking* (Waterloo: University of Waterloo 1993)

Yaggie JA, McGregor SJ (2002) Effects of isokinetic ankle fatigue on the maintenance of balance and postural limits. *Arch Phys Med Rehabil* 83(2): 224–8

Chapter 3

Effects of localized muscle fatigue on recovery from a postural perturbation without stepping

Abstract

The purpose of this study was to investigate the effects of localized muscle fatigue (LMF) on balance recovery from a postural perturbation without stepping. Postural perturbations were administered to thirty-two participants (16 young, 16 older) with ballistic pendulums before and after exercises to fatigue the lumbar extensors or ankle plantar flexors. Measures of balance recovery were based on the center of pressure (COP) and center of mass (COM) trajectories and the maximum perturbation that could be withstood without stepping. Increased COM displacement ($p = 0.003$) and time to return ($p = 0.002$) were consistent with an LMF-induced decrement in the ability to recover from the perturbations without stepping. Simultaneous decreases in the COP displacement ($p < 0.001$) were consistent with an altered postural strategy following LMF. The decrease in maximum perturbation that could be withstood without stepping exhibited a trend toward significance following LMF ($p = 0.086$). Age was associated with an impaired ability to recover from the perturbations.

3.1 Introduction

Localized muscle fatigue (LMF) increases surrogate measures of postural sway during quiet standing (Corbeil et al., 2003; Davidson et al., 2004; Gribble and Hertel, 2004b; Lundin

et al., 1993; Nussbaum, 2003). For example, Corbeil et al. (2003) reported increases in mean velocity, mean radius, and median frequency of the center of pressure (COP) following plantar flexor fatigue. Gribble and Hertel (2004b) fatigued the plantar flexors, knee extensors, and hip flexors separately and found that COP velocity increased in each case. Based on reports that increased postural sway is linked to an increased risk of falling (albeit among older adults) (Fernie et al., 1982; Lichtenstein et al., 1988; Lord et al., 1999; Maki et al., 1994, 1991), these findings may indicate that LMF increases the risk of falling.

Quiet standing is not a particularly challenging task under normal circumstances for most individuals. Because of this, many falls are likely caused by postural perturbations. As such, investigating the effects of LMF on balance recovery from a postural perturbation may provide improved external validity over quiet stance. Furthermore, the added challenge and larger kinematic range induced by the perturbations may provide additional insight into the effects of LMF on balance recovery than measures recorded during quiet stance. Lumbar extensor fatigue has been shown to elicit a subtle shift from the so-called "ankle strategy" to more of a "hip strategy" in response to a postural perturbation (Wilson et al., 2006). This shift may represent a neuromuscular adaptation to mitigate potentially deleterious effects of LMF on postural control. However, it is not clear whether this change in strategy was beneficial in regard to the ability to recover from a postural perturbation.

Therefore, the goal of this investigation was to examine the effects of LMF on balance recovery (BR) following a postural perturbation. Two different age groups were recruited and two different muscle groups were fatigued to also investigate any interactive effects of LMF with age and fatigued muscle group. We hypothesized that LMF would produce changes in BR indicative of a diminished ability to recover from a postural perturbation, and that aging would exacerbate these changes.

3.2 Methods

Thirty-two participants were recruited from the local community including 16 young (age mean±SD = 19.4 ± 1.4 years, mass = 71.411.1 kg, height = 174.8 ± 8.3 cm) and 16 older adults (age = 62.2 ± 5.1 years, mass = 74.0 ± 10.9 kg, height = 167.8 ± 8.9 cm). Each age group had an equal number of males and females. Participants were screened for self-reported musculoskeletal disorders and medications that could affect balance. In addition, older participants were required to pass a medical exam to exclude those with neurological, cardiac, respiratory, vestibular, or musculoskeletal disorders, or any falling incidents within the past year. This experiment was approved by the Virginia Tech Institutional Review Board, and participants provided informed consent prior to participation.

Participants visited the laboratory for two experimental sessions separated by approximately one week. In each session, participants underwent a series of postural perturbations both before and after fatiguing exercises. Both sessions were identical except that in one session the ankle plantar flexors were fatigued, and in the other session the lumbar extensors were fatigued. Presentation order of the two fatiguing exercises was counterbalanced.

Prior to the perturbations the participants were instructed to "stand in a relaxed manner" with their feet together, eyes closed, and hands clasped together behind their back to eliminate upper extremity movement (Allum et al., 2002; Otten, 1999). Perturbations were administered with padded pendulums (mass≈13 kg) positioned in the back and front of the participants in the mid-sagittal plane (Figure 3.1). To apply a perturbation, both pendulums were pulled away from the participants in the median plane, and one was released so as to swing in a ballistic manner until impact. The release point was selected to achieve a specified pendulum velocity just before impact. Perturbation magnitude was defined as the linear momentum just before impact. The rear pendulum was used to administer anteriorly-directed (AD) perturbations, and impacted the body just inferior to the scapula (Brown and Frank 1997). The front pendulum was used to administer posteriorly-directed (PD) pertur-

bations, and impacted the body just inferior to the jugular notch of the sternum. Each series of perturbations consisted of equal numbers of AD and PD perturbations, ordered randomly to prevent anticipation of perturbation direction. Only results for AD perturbations are described here. Earmuffs were worn by the participants to eliminate auditory cues to a perturbation.

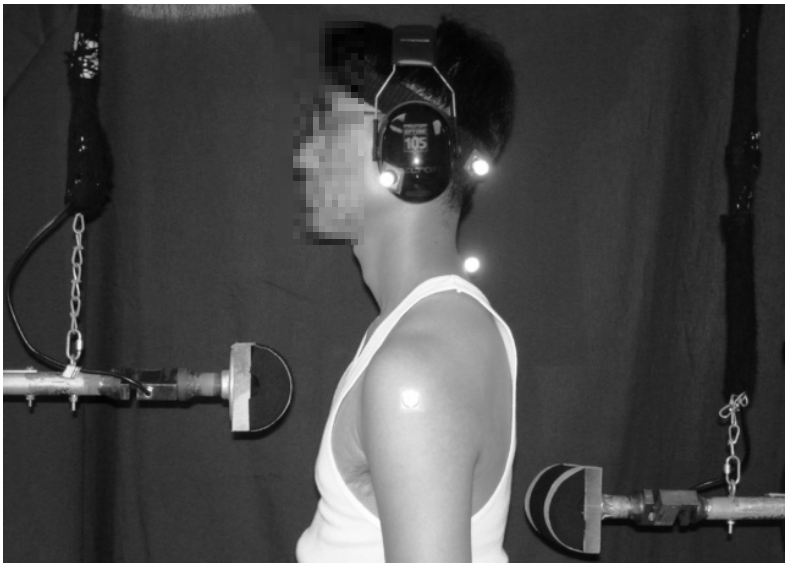

Figure 3.1: Participants were perturbed in the anterior and posterior directions with padded and weighted ballistic pendulums. Perturbations were administered by pulling the pendulums away from the participant and releasing one from a fixed location to yield the desired perturbation magnitude.(photo by Bradley Davidson)

The experiment began with an initial series of 20 moderately low magnitude perturbations (Figure 3.2). These perturbation magnitudes (10 N·s AD, 7 N·s PD) were selected as small enough such that participants could recover their balance without stepping. Exposing the participants to these initial perturbations allowed any adaptation to occur prior to investigating the effects of LMF. Subsequently, the maximum perturbation that could be withstood without stepping was determined by applying a series of AD and PD perturbations beginning at 6 N·s AD and 5 N·s PD and increasing incrementally by 2 N·s AD and 1 N·s PD after each successful recovery without stepping. This was continued until two stepping responses were elicited for a given magnitude. Sixteen perturbations were then

administered at a perturbation magnitude of 4 N·s and 2 N·s below the maximal AD and PD perturbations that could be withstood without stepping, respectively. The decreases in perturbation magnitude, based upon qualitative laboratory trials, were were chosen so that the the participant was sufficiently challenged without necessitating a stepping response.

Figure 3.2: Overall schematic of experimental protocol. Participants underwent five separate series of perturbations with an intervening fatiguing exercise of the ankle plantar flexors or lumbar extensors. (photos by Bradley Davidson)

The fatiguing protocol was similar to earlier experiments (Davidson et al., 2004; Madigan et al., 2006; Wilson et al., 2006), and involved multiple sets of dynamic exertions designed to fatigue the participants to a desired fatigue level over a fixed duration. A fixed duration was used due to the potential of fatigue time to modulate the effects of LMF on balance (Pline et al., 2006). The protocol began by obtaining an isometric maximum voluntary contraction (MVC) of the targeted muscle group (ankle plantar flexors or lumbar extensors). All MVCs and fatiguing exercises were performed on a seated calf-raise device (New York Barbell, Elmira, NY) for the ankle plantar flexors, or on a Biodex System 3 Pro dynamometer (Biodex Medical Systems, Inc., Shirley, NY) for lumbar extensors (Figure 3.3). Ankle plantar flexor MVCs were performed with the ankle in the anatomical position, and lumbar extensor MVCs while the lumbar spine was flexed 45°. Throughout the duration of the fatiguing protocol, participants performed one set of concentric contractions of the ankle plantar flexors or lumbar extensors every minute. Repetitions were performed at a rate of 23 per minute with resistance set at 45% of the unfatigued MVC. Every two minutes an isometric MVC was performed and the number of repetitions in each set was adjusted in an attempt to decrease the MVC in a linear fashion to 70% of the unfatigued MVC over 14 minutes of exercise

(Figure 3.4). If the MVC had not dropped below 70% by the end of 14 minutes, two minutes of exercise were added along with an increase in repetitions. This process was repeated until the participants were fatigued to 70% of their unfatigued MVC. Immediately following the fatiguing protocol, the maximum perturbation that could be withstood without stepping was again determined in the same manner described above, and 16 fatigued perturbations with the same magnitude as the unfatigued perturbations were administered.

Figure 3.3: Fatiguing exercise were performed with a seated calf raise device for ankle plantar flexor fatigue (left), and with a custom attachment designed for the Biodex System 3 Pro dynamometer for lumbar extensor fatigue (right).

Full body kinematic data and ground reaction data were collected during all trials using a Vicon 460 Motion Analysis System (Lake Forest, CA) and a six degree-of-freedom force platform (Model OR6-5, Advanced Mechanical Technology Inc., Watertown, MA), respectively. Participants were instrumented with 16 reflective markers (Figure 3.5) placed at selected anatomical locations. Marker positions were sampled at 100 Hz and low-pass filtered at 5 Hz (4th order zero-phase-lag Butterworth). Bilateral marker positions were averaged across the left and right sides of the body to create a six-segment sagittal plane model (feet, shanks, thighs, pelvis, torso/arms, and head). Segment inertial parameters were taken from Pavol et al. (2002) and de Leva (1996) and used to approximate the trajectory of the body center of mass (COM). Ground reaction forces and moments were sampled at 1000 Hz, low-pass

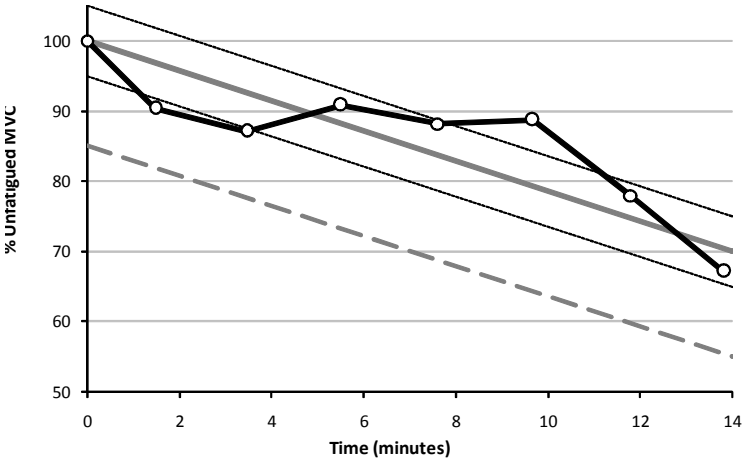

Time (min)	% MVC	Repetitions
0:00	100.0	10
1:29	90.3	10
3:28	87.1	11
5:31	90.9	13
7:37	88.2	15
9:41	88.7	18
11:48	78.0	19
13:50	67.2	-

Figure 3.4: Sample fatigue data showing decline of MVC from 100% to below 70% within 14 minutes. The plot on the left graphically demonstrates the decline of MVC. The bold line represents the target fatigue level. Lines parallel to the target indicate $\pm 5\%$ and -30% deviations from the target line. Number of repetitions is determined by the time course of MVC through these regions. The right side corresponds with the plot on the left and demonstrates change in number of repetitions with MVC throughout the exercise.

filtered at 7 Hz (4th order zero-phase-lag Butterworth), and mathematically transformed to obtain the COP trajectory in the anteroposterior direction (Winter, 1993). An in-line load cell (Cooper Instruments and Systems, Warrenton, VA) attached to the pendulum was used to identify perturbation onset time, which was the time at which the load cell force exceeded two standard deviations above the baseline mean.

Measures of BR included the maximum perturbation that could be withstood without stepping and descriptors of the COM and COP trajectories following a postural perturbation. These descriptors included: peak displacement relative to initial position, time-to-peak displacement, peak velocity, time-to-peak velocity (Brown and Frank 1997), minimum time-to-boundary (van Emmerik and van Wegen, 2002), and time-to-return to within 20% of peak displacement relative to initial position (Horak et al., 1989). COM- and COP-based displacement measures were normalized by ankle-to-toe length. Similarly, COM- and COP-based velocity measures were normalized by multiplying by participant mass (yielding units of momentum).

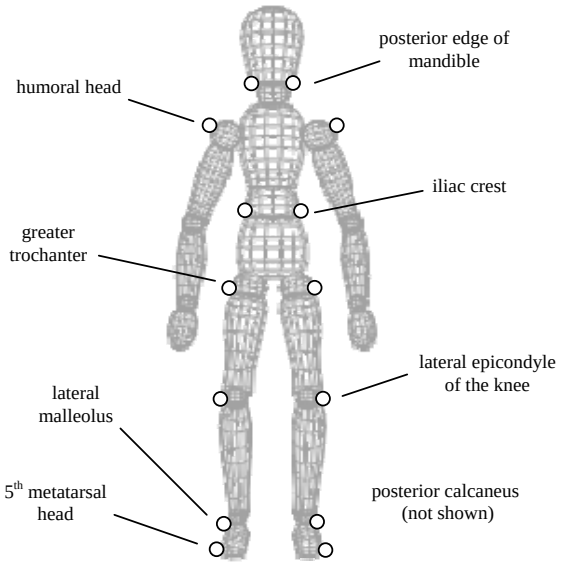

Figure 3.5: Cartoon demonstrating the anatomical locations of the reflective markers placed on the participant.

Between-session reliability of the BR measures was assessed using intraclass correlation coefficients (ICC) model (2,1) based on single measurements (Portney and Watkins, 2000) using the pre-fatigue data in each session. A repeated measures analysis of variance was used to determine the effects of fatigue (unfatigued, fatigued), muscle (ankle plantar flexor, lumbar extensor), and age (young, older) on BR measures. Only interactions of fatigue $\times$ muscle and fatigue $\times$ age were included as higher order effects in the statistical model. Additionally, three covariates (initial COM or COP position, initial COM or COP velocity, and measured perturbation magnitude) were included in the analysis of COM- and COP-based measures. Effects were considered statistically significant when $p \leq 0.05$, and trends toward significance were noted when $p \leq 0.10$.

3.3 Results

Several measures of BR were affected by LMF (Table 3.1). The maximum perturbation that could be withstood without stepping exhibited a trend toward significance with LMF ($p = 0.086$). Four of the six COM-based measures were affected by LMF including a 2.7% increase in peak COM displacement ($p = 0.003$), a 4.1% increase in time-to-peak COM peak displacement ($p < 0.001$), a 0.6% increase in peak COM velocity ($p = 0.011$), and a 3.5% increase in time-to-return within 20% of peak COM displacement ($p = 0.002$). In addition, two COP-based measures were affected by LMF including a 3.1% decrease in peak COP displacement ($p < 0.001$) and a 3.0% decrease in time-to-peak COP velocity ($p < 0.001$). Peak COP velocity had a significant fatigue $\times$ age interaction due to a 2.3% increase with LMF in the older group, and no change in the young group (Figure 3.6). Peak COP velocity also had a significant fatigue $\times$ muscle interaction, with a 3.6% increase with LMF of the lumbar extensors, but no change after LMF of the ankle plantar flexors. Time-to-return within 20% of peak COP displacement had a significant fatigue $\times$ age interaction due to an 8.5% increase with LMF in the older group, and no change in the young group (Figure 3.6).

Several measures of BR were affected by age (Table 3.1). The maximum perturbation that could be withstood without stepping was 17.8% lower among the older adults ($p = 0.029$). Two COM-based measures demonstrated a difference between age groups, with an 8.65% higher peak COM velocity ($p = 0.006$) and a 4.6% lower time-to-peak COM velocity ($p = 0.042$) in the older group. Among the COP-based measures, there was an 11.8% higher peak COP displacement ($p = 0.004$) and a 14.9% lower COP time-to-boundary ($p = 0.070$) in the older group.

The range of the ICCs calculated for the unfatigued COM- and COP-based measures of BR between sessions was 0.82 to 0.99 (Table 3.1). ICC of the maximum perturbation magnitude was 0.91. Of the 12 total COM- and COP-based measures of BR, all but one (time-to-peak COM velocity) were linearly dependent on initial position at the time of

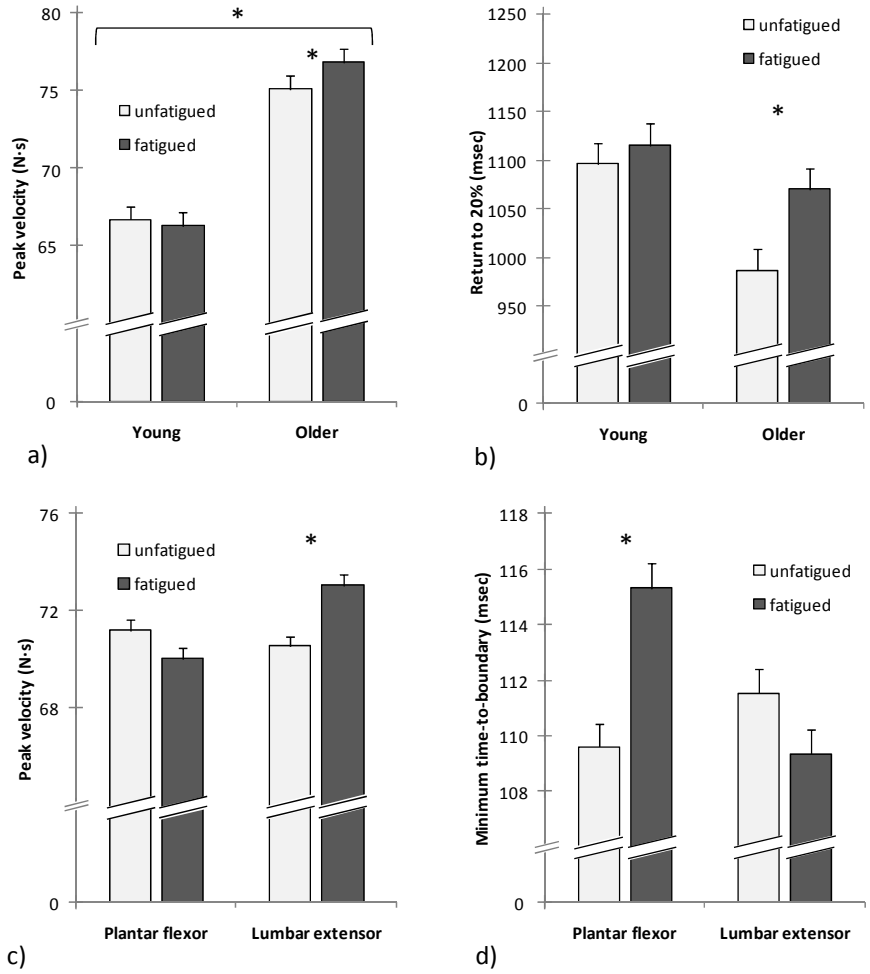

Figure 3.6: Least square means (with standard error) of COP-based balance recovery measures that exhibited fatigue × age and fatigue × muscle interactions. * indicates significant difference ($p \leq 0.05$).

Table 3.1: Intraclass correlations (ICC) and main effects of fatigue and age for each balance recovery measure (least squares mean ± standard error).

Dependent Measure	ICC	Fatigue Level		Age	
		unfatigued	fatigued	young	old
Stepping response					
max. perturbation magnitude (N·s)	0.91	$6.88 \pm 0.10^{\P}$	6.63 ± 0.10	7.41 ± 0.41	$6.09 \pm 0.41^{*}$
Center of mass					
peak displacement (%)	0.97	25.6 ± 0.1	$26.3 \pm 0.1^{*}$	26.4 ± 0.8	25.5 ± 0.8
time-to-peak displacement (msec)	0.93	564.6 ± 2.9	$587.8 \pm 3.2^{*}$	599.7 ± 14.3	552.7 ± 14.5
peak velocity (N·s)	0.99	17.27 ± 0.03	$17.38 \pm 0.03^{*}$	16.61 ± 0.25	$18.03 \pm 0.25^{*}$
time-to-peak velocity (msec)	0.96	143.1 ± 0.3	142.6 ± 0.3	146.2 ± 1.8	$139.5 \pm 1.7^{*}$
min. time-to-boundary (msec)	0.93	580.1 ± 3.6	578.3 ± 4.0	571.6 ± 16.7	586.8 ± 16.2
return 20% (msec)	0.82	1316 ± 10	$1361 \pm 11^{*}$	1346 ± 36	1332 ± 37
Center of pressure					
peak displacement (%)	0.98	49.8 ± 0.1	$48.3 \pm 0.1^{*}$	46.3 ± 0.9	$51.8 \pm 0.9^{*}$
time-to-peak displacement (msec)	0.87	362.5 ± 5.0	359.6 ± 3.2	348.1 ± 11.8	374.0 ± 11.9
peak velocity (N·s)	0.97	–	$-^{\dagger,\ddagger}$	–	–
time-to-peak velocity (msec)	0.97	146.3 ± 0.3	$142.0 \pm 0.4^{*}$	145.3 ± 2.3	143.0 ± 2.3
min. time-to-boundary (msec)	0.95	–	$-^{\S}$	120.4 ± 5.0	$102.5 \pm 5.0^{*}$
return 20% (msec)	0.91	–	$-^{\dagger}$	–	–

* significant ($p \leq 0.05$) main effect of age or fatigue
† fatigue × age interaction where older participants increased with fatigue while young participants remained unchanged
‡ fatigue × muscle interaction where lumbar extensor fatigue caused an increase while plantar flexor did not change
§ fatigue × muscle interaction where plantar flexor fatigue caused an increase while lumbar extensor did not change
¶ trend ($p \leq 0.10$) toward significant main effect of fatigue

perturbation (Table 3.2). Seven of the 12 BR measures were linearly dependent upon initial velocity, all of which were also linearly dependent upon perturbation magnitude and initial position. Ten BR measures were linearly dependent upon perturbation magnitude (excluding time-to-peak COM and time-to-peak COP).

Table 3.2: Linear covariate slopes for each balance recovery measure. An asterisk indicates covariate slope is significantly different from zero ($p \leq 0.05$).

	Covariate Multipliers		
Dependent Measure	perturbation magnitude	initial position	initial velocity
Center of mass			
peak displacement	0.0239*	0.2290*	0.0176*
time-to-peak displacement	21.548	828.4*	21.79*
peak velocity	1.237*	-2.123*	0.379*
time-to-peak velocity	-0.3378	-1.449	-0.370
min. time-to-boundary	-32.69*	-587.9*	-16.34*
return 20%	50.12*	893.8*	58.56
Center of pressure			
peak displacement	0.0209*	-0.6174*	-0.0030*
time-to-peak displacement	19.19*	409.1*	0.6994
peak velocity	2.302*	-0.6453*	-118.1*
time-to-peak velocity	-0.7963	-16.71*	-0.0185
min. time-to-boundary	-7.395*	70.13*	0.5286*
return 20%	49.53*	-0.3847*	1254

3.4 Discussion

LMF has been shown to affect the postural strategy used during BR from a postural perturbation (Wilson et al., 2006). These changes in postural strategy suggest changes in the postural control system, and may result in a change in the ability to recover from a postural perturbation without stepping. Therefore, the purpose of this study was to further investigate the effects of LMF on BR following a postural perturbation. The maximum perturbation that could be withstood without stepping was not significantly affected by LMF, but did exhibit a trend toward significance. In general, COM excursion increased during

BR after LMF, while COP excursion exhibited more complex trends. The effects of age and interactions between LMF and age were also identified.

Values of the COM- and COP-based measures of BR were comparable to other studies employing similar measures. For example, mean values of COM displacement and COM time-to-peak displacement were similar to those reported by Brown and Frank (1997). Schulz et al. (2006) reported a stepping threshold based on the COM minimum time-to-boundary as 0.57-0.58 sec for healthy young and 0.66-0.67 sec for healthy older participants, which are comparable to the 0.40-0.72 sec for healthy young and 0.57-0.61 sec for healthy older reported here. The slight discrepancies may have resulted from the differing perturbation methods, or perhaps because we instructed participants to "recover balance without stepping if possible" while Schulz et al. instructed participants to "respond naturally." Changes in COM- and COP-based measures with LMF ranged from 0.5-8.5%. While not large, these effect sizes were comparable to other studies reporting fatigue-induced changes in anteroposterior postural sway during quiet standing (Gribble and Hertel, 2004a; Lundin et al., 1993; Yaggie and McGregor, 2002).

COM-based measures of BR exhibited greater excursions with LMF. Both peak COM displacement and time-to-return within 20% of the peak displacement indicated that the perturbed COM not only moved closer to the base-of-support boundary, but was displaced for a longer period of time following LMF. Increases in the peak COM velocity and time-to-peak COM displacement corresponded with an increase in peak angular momentum and a delay in reversing the direction of momentum, respectively. When considered together, these changes imply a greater likelihood of stepping, and possibly a decrease in the ability to recover without stepping. Consistent with this interpretation, the maximum perturbation that could be withstood without stepping tended to decrease with LMF. However, the increment in perturbation magnitude used to identify this maximum perturbation may have, in retrospect, been too large to detect small effects of LMF.

Most studies employing the COP trajectory during quiet or perturbed stance use this

trajectory as a surrogate for the COM trajectory. COP is relatively easy to collect in the laboratory and clinic, but when used to analyze posture it is best interpreted as a controller of body kinematics and used keep the COM within the base-of-support (Horak, 2006; Morasso et al., 1999; Rietdyk et al., 1999). As such, the COP is a measure of passive components (due to intrinsic stiffness and damping and tonic muscle activity) and active components (due to joint torques produced by automatic feedback control and descending cognitive command) used by the postural control system. Therefore, it is appropriate to interpret the results COP-based measures alongside the COM when available and is treated here as the net torque (time derivative of angular momentum) used to control body kinematics.

Following LMF, a decrease in peak COP displacement occurred with a simultaneous increase in peak COM displacement and a slower return of the COM to the pre-perturbation position. The observed increase in these COM-based measures is consistent with a decrease in the maximal net torque as demonstrated by the decreased peak COP displacement. One reason for this change could be a decreased ability to generate ankle plantar flexor or lumbar extensor torque due to muscle fatigue. Another explanation could be a shift in postural strategy following LMF toward the "hip strategy" as demonstrated with LMF in Wilson et al. (2006). Use of a "hip strategy" results in a larger displacement and longer time for the body to return to a vertical position, in comparison to an ankle strategy (Kuo, 1995; Kuo and Zajac, 1993).

Time-to-peak COP velocity decreased by 4 msec with LMF, indicating that LMF caused a reduced response time for generating net torque following the perturbation. The magnitudes of this variable were less than estimated delays in the central feedback loop of 150 msec (Cordo et al., 1994), but corresponded well with long-loop reflex delays in the ankle musculature, which have been measured at 90-120 msec (Di Fabio et al., 1992; Diener et al., 1985). The observed decrease in time-to-peak COP velocity with LMF may be the result of increased pre-perturbation muscle activity, which would provide a faster response by increasing muscle stiffness (Morasso et al., 1999). Although we controlled for variations in

ankle torque prior to perturbations by including initial COP position as a covariate in our statistical analysis, increased agonist-antagonist cocontraction may have occurred following LMF as a proactive postural strategy.

Selected measures of BR exhibited an interaction of fatigue level with age. Peak COP velocity was higher in the older group and increased only in the older group following LMF. This is consistent with the higher peak COP displacement in the older group, since further anterior travel in the same time period necessitates a higher velocity. Perhaps most notable is the large LMF-induced change in the older group in COP time-to-return within 20% of the peak displacement. Most changes in the COM- and COP-based measures were modest (0.6 to 4.1%), but this measure increased 8.5%. Similar to the time-to-return to 20% threshold for the COM, the increase in its COP analogue indicates that a longer time was needed to complete the recovery from the perturbation. This increase occurred only in the older group, suggesting that they found the postural perturbations more difficult to recover from than the young group.

Peak velocity and time-to-boundary of the COP trajectory dependent measures revealed significant interactions of fatigue level and muscle group (Figure 3.6c and d). These results indicate that COP characteristics are affected differently by fatigue of various muscle groups. Since calculating the time-to-boundary measures involves dividing by the COP velocity, the inverse relationships between the time-to-boundary and peak velocity as displayed in Figure 3.6 are internally consistent. However, at present we cannot offer a precise explanation for these outcomes, but they may be elucidated in future investigations designed specifically to address fatigue level and muscle group interactions.

Several limitations must be noted in this investigation. First, the participants were aware that they were going to be perturbed. As a result, we cannot infer how their responses would be different in an unexpected perturbation such as could occur outside the laboratory. Second, we could not ensure that the participants remained relaxed during the perturbations as instructed, and the results may have been influenced by preactivation or cocontraction

prior to the perturbations. Lastly, participants were instructed to recover balance without stepping, if possible. As such, it is likely that the participants did not respond naturally to the perturbations. However, there may be analogous situations (e.g., in the workplace) when stepping to recover balance is not possible. It is also possible that the ability to recover balance without stepping is correlated to the ability to recover with stepping.

3.5 Conclusions

In summary, LMF increased COM excursion following a postural perturbation and exhibited a trend toward a decrease in maximum perturbation that could be withstood without stepping. These results imply a decreased ability to recover from a postural perturbation following LMF. Changes in the COP with LMF were consistent with a change in postural strategy. Interaction effects with age indicated recovering balance following LMF was more difficult among older individuals.

References

Allum JH, Carpenter MG, Honegger F, Adkin AL, Bloem BR (2002) Age-dependent variations in the directional sensitivity of balance corrections and compensatory arm movements in man. *J Physiol* 542(Pt 2): 643–63

Brown L, Frank J (1997) Postural compensations to the potential consequences of stability: kinematics. *Gait Posture* 6: 89–97

Corbeil P, Blouin JS, Begin F, Nougier V, Teasdale N (2003) Perturbation of the postural control system induced by muscular fatigue. *Gait Posture* 18(2): 92–100

Cordo P, Carlton L, Bevan L, Carlton M, Kerr GK (1994) Proprioceptive coordination of movement sequences: role of velocity and position information. *J Neurophysiol* 71(5): 1848–61

Davidson BS, Madigan ML, Nussbaum MA (2004) Effects of lumbar extensor fatigue and fatigue rate on postural sway. *Eur J Appl Physiol* 93(1-2): 183–9

de Leva P (1996) Adjustments to zatsiorsky-seluyanov's segment inertia parameters. *J Biomech* 29(9): 1223–30

Di Fabio RP, Graf B, Badke MB, Breunig A, Jensen K (1992) Effect of knee joint laxity on long-loop postural reflexes: evidence for a human capsular-hamstring reflex. *Exp Brain Res* 90(1): 189–200

Diener HC, Ackermann H, Dichgans J, Guschlbauer B (1985) Medium- and long-latency responses to displacements of the ankle joint in patients with spinal and central lesions. *Electroencephalogr Clin Neurophysiol* 60(5): 407–16

Fernie GR, Gryfe CI, Holliday PJ, Llewellyn A (1982) The relationship of postural sway in standing to the incidence of falls in geriatric subjects. *Age Ageing* 11(1): 11–6

Gribble PA, Hertel J (2004a) Effect of hip and ankle muscle fatigue on unipedal postural control. *J Electromyogr Kinesiol* 14(6): 641–6

Gribble PA, Hertel J (2004b) Effect of lower-extremity muscle fatigue on postural control. *Arch Phys Med Rehabil* 85(4): 589–92

Horak FB (2006) Postural orientation and equilibrium: what do we need to know about neural control of balance to prevent falls? *Age Ageing* 35 Suppl 2: ii7–ii11

Horak FB, Diener HC, Nashner LM (1989) Influence of central set on human postural responses. *J Neurophysiol* 62(4): 841–53

Kuo AD (1995) An optimal control model for analyzing human postural balance. *IEEE Trans Biomed Eng* 42(1): 87–101

Kuo AD, Zajac F: Human standing posture: multijoint movement strategies based on biomechanical constraints. In Allum J, Allum-Mecklenburg D, Harris F, Probst R, eds., *Progress in Brain Research: Vol. 97: Natural and Artificial Control of Hearing and Balance*, page 349âE“58 (Amsterdam: Elsevier 1993)

Lichtenstein MJ, Shields SL, Shiavi RG, Burger MC (1988) Clinical determinants of biomechanics platform measures of balance in aged women. *J Am Geriatr Soc* 36(11): 996–1002

Lord SR, Rogers MW, Howland A, Fitzpatrick R (1999) Lateral stability, sensorimotor function and falls in older people. *J Am Geriatr Soc* 47(9): 1077–81

Lundin T, Feuerbach J, Grabiner M (1993) Effect of plantar flexor and dorsiflexor fatigue on unilateral postural control. *J Appl Biomech* 9: 191–201

Madigan ML, Davidson BS, Nussbaum MA (2006) Postural sway and joint kinematics during quiet standing are affected by lumbar extensor fatigue. *Hum Mov Sci*

Maki BE, Holliday PJ, Topper AK (1991) Fear of falling and postural performance in the elderly. *J Gerontol* 46(4): M123–31

Maki BE, Holliday PJ, Topper AK (1994) A prospective study of postural balance and risk of falling in an ambulatory and independent elderly population. *J Gerontol* 49(2): M72–84

Morasso PG, Baratto L, Capra R, Spada G (1999) Internal models in the control of posture. *Neural Netw* 12(7-8): 1173–1180

Nussbaum MA (2003) Postural stability is compromised by fatiguing overhead work. *AIHA J (Fairfax, Va)* 64(1): 56–61

Otten E (1999) Balancing on a narrow ridge: biomechanics and control. *Philos Trans R Soc Lond B Biol Sci* 354(1385): 869–75

Pavol MJ, Owings TM, Grabiner MD (2002) Body segment inertial parameter estimation for the general population of older adults. *J Biomech* 35(5): 707–12

Pline KM, Madigan ML, Nussbaum MA (2006) Influence of fatigue time and level on increases in postural sway. *Ergonomics* 49(15): 1639–48

Portney L, Watkins M: *Foundations of clinical research: applications to practice* (Upper Saddle River, NJ: Prentice-Hall, Inc. 2000), 2nd edition

Rietdyk S, Patla AE, Winter DA, Ishac MG, Little CE (1999) Nacob presentation csb new investigator award. balance recovery from medio-lateral perturbations of the upper body during standing. north american congress on biomechanics. *J Biomech* 32(11): 1149–58

Schulz BW, Ashton-Miller JA, Alexander NB (2006) Can initial and additional compensatory steps be predicted in young, older, and balance-impaired older females in response to anterior and posterior waist pulls while standing? *J Biomech* 39(8): 1444–53

van Emmerik RE, van Wegen EE (2002) On the functional aspects of variability in postural control. *Exerc Sport Sci Rev* 30(4): 177–83

Wilson EL, Madigan ML, Davidson BS, Nussbaum MA (2006) Postural strategy changes with fatigue of the lumbar extensor muscles. *Gait Posture* 23(3): 348–54

Winter DA: *A.B.C of Balance During Standing and Walking* (Waterloo: University of Waterloo 1993)

Yaggie JA, McGregor SJ (2002) Effects of isokinetic ankle fatigue on the maintenance of balance and postural limits. *Arch Phys Med Rehabil* 83(2): 224–8

Chapter 4

Mathematical modeling and control of dynamical systems

4.1 Introduction

Biomechanical systems are often simulated and analyzed using quantitative mathematical models with parameters which have physical meaning. The goal of this chapter is to provide a foundation on which to assemble the subsequent investigations. By no means an exhaustive review, this chapter will introduce mathematical modeling of dynamical systems and its application in selected topics of feedback control.

4.2 Dynamical systems

4.2.1 Equations of motion

Dynamic behavior of a system is generally quantified by ordinary differential equations (ODEs) based on the physical laws of motion. ODEs are equations which contain the derivatives of one or more dependent variables. In dynamical systems, the independent variables are differentiated with respect to time, t. For a simple mass, spring, and damper system (Figure 4.1),we use Newton's 2$^{\text{nd}}$ Law of motion to derive the representative differential equation for the system (equation of motion) as

$$m\frac{d^2y(t)}{dt^2} + m\frac{dy(t)}{dt} + ky(t) = p(t) \tag{4.1}$$

where $y(t)$ is a coordinate based in a fixed Newtonian inertial frame, $p(t)$ is a time-dependent force, and, m, b, and k are physical properties of the system which are proportional to the acceleration, velocity, and position of the system. Using the "dot" notation, a more compact form of (4.1) is

$$m\ddot{y}(t) + b\dot{y}(t) + ky(t) = p(t) \tag{4.2}$$

Second-order ODEs such as this comprise the foundational basis for dynamics. Equations of motion are derived based upon prior knowledge and assumptions of the system being modeled.

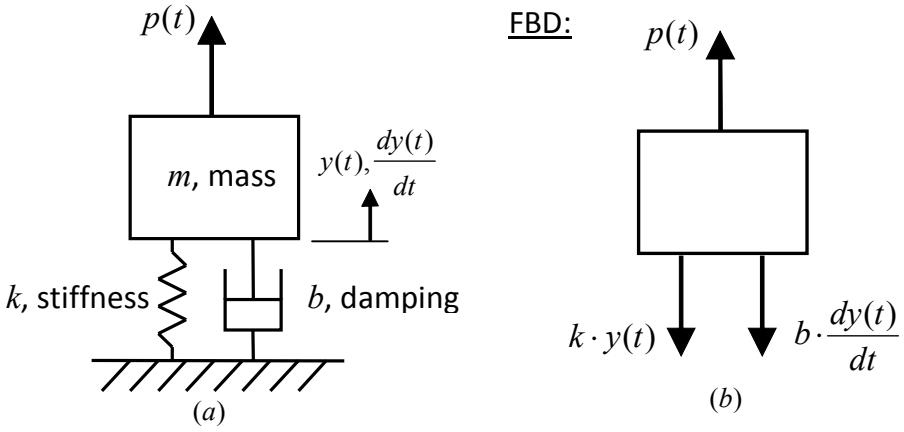

Figure 4.1: (a) Mass, spring, and damper system. (b) A free body diagram (FBD) of the system demonstrating the forces produced by each element on the mass

One of the most convenient ways to derive the equations of motion for a system is using Lagrange's method, which is described as follows: First, the kinetic energy scalar, $T(q_1 \dots q_j \dots q_n, \dot{q}_1 \dots \dot{q}_j \dots \dot{q}_n, t)$, and the potential energy scalar, $V(q_1 \dots q_j \dots, t)$, are formed for the system, where q_j and $\dot{q}_j$ represent the generalized coordinates and their time derivatives, respectively, and n is the total number of degrees of freedom in the system. The equations of motion are obtained by calculating

$$\frac{d}{dt}\left(\frac{\partial T}{\partial \dot{q}_j}\right) - \frac{\partial T}{\partial q_j} + \frac{V}{\partial q_j} = Q_j^* \tag{4.3}$$

where

$$Q_j^* = \sum_{Elements} \left(\mathbf{F} \cdot \frac{\partial \dot{\mathbf{r}}_A}{\partial \dot{q}_j} + \mathbf{M}_A \cdot \frac{\partial \boldsymbol{\omega}}{\partial \dot{q}_j} \right) \tag{4.4}$$

represents the generalized forces and moments; $\mathbf{F}$ is a force vector acting on the system, $\dot{\mathbf{r}}_A$ is a translational velocity vector acting at point A, $\mathbf{M}_A$ is a moment vector located at point A, and $\boldsymbol{\omega}$ is the angular velocity vector of the element.

4.2.2 Linearization

The majority of dynamical systems are modeled as linear systems. A linear system is one that satisfies two conditions:

Principle of homogeneity

if $y = f(x)$ then $\beta y = f(\beta x)$

Principle of superposition

if $y = f(x)$ then $y_1 + y_2 = f(x_1 + x_2)$

Even when the requirements are not satisfied, a nonlinear system can be approximated as a linear system by making the assumption of only small changes in a variable around a given operating point. Assuming a continuous function, $y = g(x)$, we can linearize using a Taylor Series Expansion:

$$y = g(x) = g(x_0) + \left.\frac{dg}{dx}\right|_{x=x_0} \frac{x - x_0}{1!} + \left.\frac{d^2g}{dx^2}\right|_{x=x_0} \frac{(x - x_0)^2}{2!} + \cdots + \left.\frac{d^ng}{dx^n}\right|_{x=x_0} \frac{(x - x_0)^n}{n!} \tag{4.5}$$

The slope, $\frac{dg}{dx}$, is a good approximation around the operating point, x_0, so

$$y = g(x) = g(x_0) + \left.\frac{dg}{dx}\right|_{x=x_0} (x - x_0) = y_0 + \mu(x - x_0) \tag{4.6}$$

where μ is the slope, or

$$(y - y_0) + \mu(x - x_0) \rightarrow \Delta y = \mu(x - x_0) \tag{4.7}$$

which is a linear equation. Any dynamical system can be linearized in a similar manner. The linearized system, which establishes an input-output relationship between the variables, is the basis for the following discussion of feedback controls.

4.3 Feedback control of dynamical systems

A control system is an interconnection of components forming a system configuration that will provide a desired system response. Controls techniques are divided into two related methodologies: Classical Methods and State Space Methods. There is some overlap between the two approaches, particularly in single input single output (SISO) systems. Although more capabilities exist using State Space Methods, the classical approach is more intuitive, and will be described first.

4.3.1 Classical methods

Control systems are typically classified as either open-loop or closed-loop (Figure 4.2). In an open-loop system, the desired response is given to the controller which then sends a controlling signal to the plant (equations of motion) that produces the system output. A closed-loop system contains the same components of an open-loop system, except that the system output is "fed" back to the beginning of the system and the system error is given to the controller.

In a linear system, the blocks in the "block diagrams" displayed in Figure 4.2 represent transfer functions which when directly connected by a line indicate that the transfer functions are to be multiplied together. A transfer function in linear ODEs refers to the ratio of the Laplace transform of the output variable to the Laplace transform of the input variable. For example:

$$\frac{\mathcal{L}\{\text{output}\}}{\mathcal{L}\{\text{input}\}} = G(s) \tag{4.8}$$

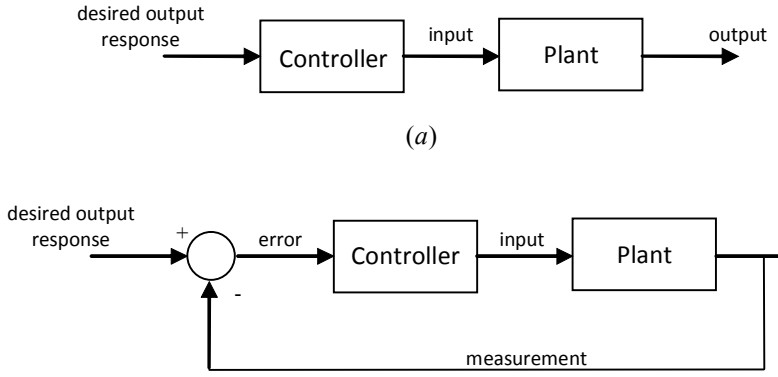

Figure 4.2: Block diagrams of (a) open-loop control (b) closed-loop control systems

where s is called the Laplace variable (detailed information on using Laplace transforms to solve linear ODEs can be found in any differential equations textbook). The Laplace variable can be considered to be a differential operator

$$s \equiv \frac{d}{dt} \tag{4.9}$$

Likewise, the integral operator can be represented in the Laplace domain as

$$\frac{1}{s} \equiv \int_{0-}^{t} dt \tag{4.10}$$

Recall (4.2) which describes the mass, spring, and damper system in the time domain. When converting to the Laplace domain we obtain

$$Y(s)(ms^2 + bs + k) = P(s) \tag{4.11}$$

The resulting open-loop transfer function for the system is

$$\frac{\mathcal{L}\{\text{output}\}}{\mathcal{L}\{\text{input}\}} = G(s) = \frac{Y(s)}{P(s)} = \frac{1}{ms^2 + bs + k} \tag{4.12}$$

where $P(s)$ is the input force and $Y(s)$ is the resulting output in the Laplace domain. When adding unity feedback and a controller which operates on the system error (Figure 4.3), the system equation in the Laplace domain becomes

$$Y(s) = \frac{C(s)G(s)}{1 + C(s)G(s)} X(s) \tag{4.13}$$

where $X(s)$ is the desired output and $C(s)$ is the controller in the Laplace domain. Therefore, the engineering task becomes that of designing the controller, $C(s)$, so that the system remains stable, and that the desired response is obtained.

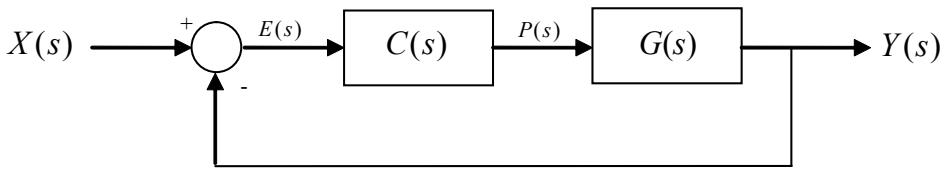

Figure 4.3: Block diagrams of the transfer function $G(s)$ incorporated within a feedback control loop.

Stability of a linear system in the Laplace domain is based upon setting the denominator of the transfer equal to zero. This is called the characteristic equation (CE).

$$1 + C(s)G(s) = 0 \tag{4.14}$$

Solving for s, the roots of the characteristic equation, called poles, determine the character of the time response. In particular, if the real parts of the poles are negative, then the system is considered to be asymptotically stable. In other words, the system is attracted to a certain equilibrium point, and if no disturbances are added, will eventually arrive at the

attractor. Should any real portion of a pole be greater than zero, the system is considered to be unstable (Figure 4.4).

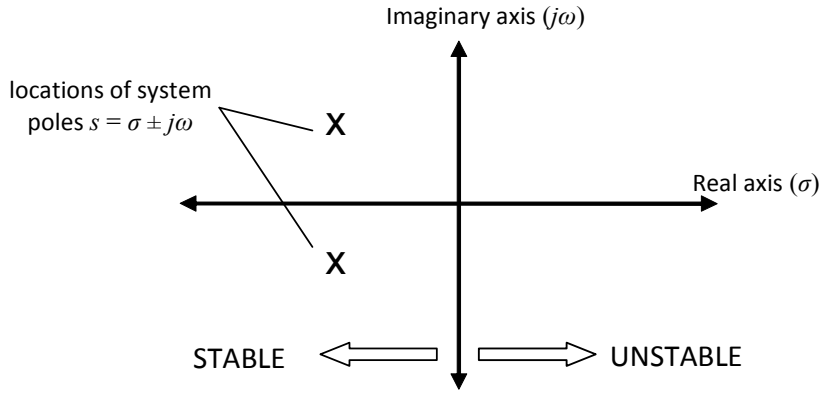

Figure 4.4: Stability is assessed by determining the location of the poles in the Laplace domain (s-plane). Values in the s-plane are made up of real (σ) and imaginary ($j\omega$) components. If the real portions of system poles are negative, the system is considered to be stable.

The most common classical controller design is a proportional, integral, derivative (PID) controller. This controller calculates the input to the plant as a summation of three time-invariant gains operating on the error, time-derivative of the error, and the integrated error. Provided that the system remains stable, these PID gains can be adjusted to achieve the desired system response. It is also necessary to point out that the controls engineer is not limited to basic PID control as long as the system remains stable.

4.3.2 State space methods

Whereas classical control methods are centered on dynamical systems in the Laplace domain, state space methods are based completely in the time domain. State space is a representation of 2$^{\text{nd}}$ order linear ODEs with twice as many coupled 1$^{\text{st}}$ order ODEs that are dependent upon the system state. The format of the linear state space equations is

$$\dot{\mathbf{x}}(t) = \mathbf{A}\mathbf{x}(t) + \mathbf{B}\mathbf{u}(t) \tag{4.15}$$

where $\mathbf{A} \in \mathbb{R}^{n\times n}$ is called the state matrix, $\mathbf{B} \in \mathbb{R}^{n\times m}$ is the input matrix, $\mathbf{x}(t) \in \mathbb{R}^n$ is the state vector, and $\mathbf{u}(t) \in \mathbb{R}^m$ is the input vector. Although, no restrictions exist upon choosing what to include in the state vector, we will assume that only position and velocity information are included from each element of the system. Again, we will consider the mass, spring, damper system from (4.2). To place this equation into state space format, it must first be divided into two 1st order ODEs as follows:

$$\dot{y}_1(t) = y_2(t) \tag{4.16}$$

$$\dot{y}_2(t) = -\frac{k}{m}y_1(t) - \frac{b}{m}y_2(t) + \frac{1}{m}p(t) \tag{4.17}$$

where $y_1(t) = y(t)$ and $y_2(t) = \dot{y}(t)$.

In state space form, the equations become

$$\begin{Bmatrix} \dot{y}_1(t) \\ \dot{y}_2(t) \end{Bmatrix} = \begin{bmatrix} 0 & 1 \\ -k/m & -b/m \end{bmatrix} \begin{Bmatrix} y_1(t) \\ y_2(t) \end{Bmatrix} + \begin{Bmatrix} 0 \\ 1/m \end{Bmatrix} p(t) \tag{4.18}$$

Stability of the system can be assessed very easily from this form. The eigenvalues of the state matrix, $\mathbf{A}$, are equivalent to the poles of the system, the same stability criteria are true concerning the pole locations on the s-plane.

To add feedback, the input vector is taken to be a function of the state vector

$$\mathbf{u}(t) = -\mathbf{K}\mathbf{x}(t) \tag{4.19}$$

where $\mathbf{K} \in \mathbb{R}^{m\times n}$ is a matrix containing feedback gains that operate directly on the system state. Thus, (4.15) becomes

$$\dot{\mathbf{x}}(t) = \mathbf{A}\mathbf{x}(t) - \mathbf{B}\mathbf{K}\mathbf{x}(t) \tag{4.20}$$

and reduces to

$$\dot{\mathbf{x}}(t) = (\mathbf{A} - \mathbf{B}\mathbf{K})\,\mathbf{x}(t) = \mathbf{A}_c\mathbf{x}(t) \tag{4.21}$$

where $\mathbf{A}_c \in \mathbb{R}^{n \times n}$ is called the closed-loop state matrix. Likewise, to determine the stability of a state space system with feedback the eigenvalues of $\mathbf{A}_c$ must be in the left half of the s-plane.

Therefore, if a one degree of freedom system is to be controlled so the state $\mathbf{x}(t)$ goes to zero, the corresponding feedback gains in $\mathbf{K}$ will be equivalent to the proportional and derivative (PD) gains in a classical feedback controller. Applying this to the spring, mass, damper in (4.18) we arrive at

$$\begin{Bmatrix} \dot{y}_1(t) \\ \dot{y}_2(t) \end{Bmatrix} = \begin{bmatrix} 0 & 1 \\ -k/m & -b/m \end{bmatrix} \begin{Bmatrix} y_1(t) \\ y_2(t) \end{Bmatrix} - \begin{Bmatrix} 0 \\ 1/m \end{Bmatrix} \begin{Bmatrix} g_1 & g_2 \end{Bmatrix} \begin{Bmatrix} y_1(t) \\ y_2(t) \end{Bmatrix} \tag{4.22}$$

which simplifies to become

$$\begin{Bmatrix} \dot{y}_1(t) \\ \dot{y}_2(t) \end{Bmatrix} = \begin{bmatrix} 0 & 1 \\ \frac{-k-g_1}{m} & \frac{-b-g_2}{m} \end{bmatrix} \begin{Bmatrix} y_1(t) \\ y_2(t) \end{Bmatrix} \tag{4.23}$$

where g_1 and g_2 are the PD feedback gains, respectively.

The advantage of the state space approach becomes apparent when controlling a system with more than one degree of freedom. In these situations we are able to incorporate full-state feedback control. In full-state feedback, the system input(s) are a function of all of the system states contained in the state vector $\mathbf{x}(t)$. This is particularly powerful because the control designer is allowed to move the system poles to any desired location in the s-plane by changing the fully populated gain matrix, $\mathbf{K}$. Several approaches exist that are commonly used to choose the elements of $\mathbf{K}$. An optimal approach to selecting feedback gains will be introduced in Chapter 7.

4.4 Conclusions

The information in this chapter is presented to construct a foundation for subsequent chapters that utilize concepts from feedback control theory to model the postural control system. For further information on these topics, several texts are recommended in the References.

References

Bedford A, Fowler W: *Engineering Mechanics: Dynamics* (Reading, MA: Addison-Wesley 1995)

Dorf R, Bishop R: *Modern Control Systems* (Upper Saddle river, NJ: Pearson/Prentice-Hall 2005), 10th edition

Friedland B: *Control System Design: An Introduction to State Space Methods* (Boston, MA: McGraw-Hill 1986)

Greenwood D: *Classical Dynamics* (Mineola, NY: Dover 1977)

Greenwood D: *Principles of Dynamics* (Englewood Cliffs, NJ: Prentice-Hall 1988), 2nd edition

Zill D, Cullen M: *Differential Equations with Boundary-value Problems* (Pacific Grove, CA: Brooks/Cole 1997)

Chapter 5

Feedback-controlled postural modeling literature

5.1 Introduction

A brief overview of modeling and control of dynamical systems was presented in Chapter 4. These ideas can be applied to the study of human movement since the human body acts a controlled dynamical system. Human motion is typically modeled using a series of connected rigid-body segments that is driven by torques acting at the joints. In the human body these torques are produced by muscle contractions acting across the joints. It is a complex and uncertain task to estimate in vivo forces produced by individual muscles, and most investigations model the joint torques as lumped torque parameters. Feedback-controlled models of the human body are particularly useful in investigations of balance and upright stance because of the known afferent sensory information from the visual, vestibular, and somatosensory systems.

The following sections contain a review of published literature that has incorporated feedback-controlled models to analyze the neural control of upright stance. In the first section, investigations that used proportional, integral, derivative (PID) control of balance are presented. Second, investigations that used optimal control techniques are presented. The last section highlights key studies that incorporated feedback control within a system identification approach.

5.2 Investigations using a PID controller

The most common method of controlling single input single output systems is with the proportional, integral, derivative (PID) controller or variation of the PID. PID control has been thoroughly studied and is well-established within engineering design. As such, many studies have incorporated this method when simulating posture. Johansson et al. (1988) used a model-based analysis of center of pressure (COP) trajectories that included a PID controller during body sway that was induced by calf muscle vibration. The PID gains were fit using an autoregressive moving average with an exogenous input (ARMAX), and the linear model was reported to fit the experimental data well.

Peterka (2002, 1995) have used the PID controller successfully to model integration of the vestibular, visual, and somatosensory systems into control of quiet stance. Using randomly oscillating visual surroundings and support surface as stimuli, the multisensory approach revealed nonlinear behavior with increased stimulus amplitudes. In addition, patients with vestibular loss exhibited increased stiffness (proportional gain), perhaps as a compensation mechanism.

In another study using a PID-controlled model to investigate sensory reweighting, Maurer et al. (2006) investigated the integration of the vestibular, proprioceptive, and force inputs. The results demonstrated variations in gain and phase of the responses as a function of stimulus frequency, and also in relation to the absence of vestibular and proprioceptive cues. Gain was also dependent upon stimulus amplitude, reflecting nonlinearity in the control.

Maurer and Peterka (2005) presented a PID-controlled model of quiet stance that was able to reproduce 15 different COP-based measures of postural sway. Model parameters were estimated using a Nelder-Mead search for two age groups (young and older). The results demonstrated increases in stiffness (proportional gain) and damping (differential gain) in the older group along with a large increase in noise. In studies from 1987 and 1997, Ishida et al. used a subset of the PID controller, the proportional, derivative (PD) controller to

control posture during quiet stance. They introduced a method of parameterizing the neural controller with a direct estimation of the frequency response function between the sway angle and the ankle torque. This approach, called the maximum likelihood principle, provided a least-squares approximation of the PD controller. van der Kooij et al. (2005) has recently criticized this and other direct estimation methods (e.g., cross-correlation between EMG and COP as in Masani et al. (2003)) when used in systems with feedback since they assume an open-loop transfer function. When used to identify closed-loop systems other parts of the feedback dynamics are ignored and distort the identified component.

In a series of publications by Alexandrov et al. (2001a,b), the concept of eigenmovements during upright stance were presented. These eigenmovements, based on the mode shapes of a three-segment inverted pendulum, were added together to produce the time-domain motion. In 2005, Alexandrov et al. incorporated PD feedback control of the eigenmovements during platform perturbations. Since the eigenmovements are decoupled from each other, separate PD controllers were supplied for each mode, creating independent eigenmovement control. Two key aspects of this method were highlighted: 1) the eigenmovement feedback is more accurate than joint level feedback and 2) it requires fewer parameters than a typical full-state feedback-controlled system.

Iqbal and Roy (2004) and Jo and Massaquoi (2004) deviated from the trend to drive the postural model with a lumped torque about each joint. Iqbal and Roy developed a single segment model that included force and kinematic feedback produced by dynamic representations of the Golgi tendon organs and muscle spindles. The model was driven with a Hill-type muscle and activated by a second-order low-pass function. They were able to successfully demonstrate the existence of stabilizing PID parameters for the system and suggested an algorithm to select stabilizing gains.

Jo and Massaquio augmented the PID controller into a recurrent integrator proportional, integral, derivative (RIPID) controller. The goal in this experiment was to demonstrate the feasibility of modeling the cerebrum and cerebellum interaction on the control of posture

during translational platform perturbations. The model included three degrees of freedom and was driven by both monoarticulate and biarticulate muscles. Gain scheduling in the RIPID controller was able to produce realistic "mixed ankle-hip strategies" with the addition small amounts of cocontraction. In general, this study demonstrated that this method bypasses the need for an explicit representation of internal model dynamics (see below) and offers an explanation of how the cerebellum might accomplish such calculations.

5.3 Investigations using optimal control

Several studies have employed optimal control theory in postural simulation. One of the first was by He et al. (1991) in which the cat hind limb was modeled during upright stance using three segments driven by 10 muscle-tendon actuators. When small perturbations were applied, the model performed well in reproducing experimentally collected ground reaction force data.

In 1995, Kuo created an optimally controlled model of balance recovery in humans during platform perturbations. The purpose of the modeling was to simulate the selection of either an "ankle strategy" or "hip strategy". A decade later, Kuo (2005) expanded this design by adding a state estimator that incorporated dynamics in the sensory system. The optimal state estimator (also called a Kalman filter) was used to simulate an internal model of the body. It is theorized that the central nervous system formulates an internal representation of body motion and kinematics using the available sensory information (Morasso et al., 1999). The internal model is used to predict motion and to supply anticipatory and motor control commands. Using this internal model, Kuo successfully predicted statistical properties of human sway.

Two studies by van der Kooij et al. have contributed significantly to the use of optimal controls in postural modeling. In 1999, an optimally controlled model with an extended Kalman filter was used to simulate platform perturbations. The predictive element of the

model was crucial to success because removal of this component caused the system to become unstable. In a paper from 2001, the previous work was expanded to include adaptive control of stance dynamics while reducing the number of input parameters to include only sensory dynamics. Using this model, thresholds of stability in platform sway referencing was produced and determined to be mediated by the vestibular system.

Most recently, Qu et al. (2007)developed an optimally controlled model of quiet stance. This single-segment model was used to predict changes due to aging and fatigue in parameters related to postural sway. Unique to this model was that the state realization used provided an analytical solution to the time-delay problem, and was able to be simulated without incorporating a delayed differential equation solver.

5.4 Investigations using system identification

System identification is defined as the process of using experimental data to build a dynamic model of the system being studied (Westwick and Kearney, 2003). Parameters defined in the system identification are often interpretable, and can provide insight into the characteristics of the system.

The earliest attempts to identify the neural controller of posture using system identification techniques were performed by Hemami et al. in the late seventies. In 1975, Golliday and Hemami speculated on feedback control mechanisms incorporated by humans during standing and locomotion. Assuming a general model, they demonstrated the effectiveness of using linear simulations, and also presented a method to reduce the number of externally controlled actuators by applying physiologically relevant kinematic constraints. Building upon their previous study, Camana et al. (1977) developed one and two degree of freedom models to determined feedback gains used during platform perturbations. The modeled feedback included kinematic information from the ankle proprioceptors and the vestibular organs. The transfer function of the vestibular organs was based on modeling by Nashner

(1973). Feedback gains were chosen based on a gradient-based algorithm and were also tested for sensitivity to potential errors in anthropometry such as weight, segment lengths, and inertias.

In 1988, Johansson et al. undertook the topic of vibration-induced sway using spectral analyses, and quantified control performance by calculating parameters such as swiftness, stiffness, and damping. One major finding was that parametric identification of the transfer function between a stimulus and response can be made with higher confidence than parametric identification of spontaneous motion.

Recently, Peterka and Maurer have contributed the most publications to system identification of upright stance than any other group. Studies from this group have dealt with sensorimotor integration (Peterka, 2002, 1995), multisensory control and sensory reweighting (Maurer et al., 2006; Mergner et al., 2003), and interpretation of sway measures (Maurer and Peterka, 2005). In fact, the recent study investigating quiet stance was lauded as an important and novel advancement in postural modeling (Pavol, 2005).

Also, van der Kooij et al. have contributed to the identification of neural control of posture using multisegment models. They have incorporated approximations of the sensory dynamics within an optimal controls structure (van der Kooij et al., 1999, 2001). Recently, they have offered critique of some identification practices, and presented solutions to increase the validity of system identification in feedback-controlled systems (van der Kooij et al., 2005).

References

Alexandrov AV, Frolov AA, Horak FB, Carlson-Kuhta P, Park S (2005) Feedback equilibrium control during human standing. *Biol Cybern* 93(5): 309–22

Alexandrov AV, Frolov AA, Massion J (2001a) Biomechanical analysis of movement strategies in human forward trunk bending. i. modeling. *Biol Cybern* 84(6): 425–34

Alexandrov AV, Frolov AA, Massion J (2001b) Biomechanical analysis of movement strategies in human forward trunk bending. ii. experimental study. *Biol Cybern* 84(6): 435–43

Camana PC, Hemami H, Stockwell CW (1977) Determination of feedback for human posture control without physical intervention. *Cybernet Syst* pages 199–225

Golliday C, Hemami H (1975) Postural stability of the two-degree-of-freedom biped by general linear feedback. *IEEE Trans Auto Contr* AC-21(1): 74–79

He J, Levine W, Loeb G (1991) Feedback gains for correcting small perturbations to standing posture. *IEEE Trans Auto Contr* 36(3): 322–332

Iqbal K, Roy A (2004) Stabilizing pid controllers for a single-link biomechanical model with position, velocity, and force feedback. *J Biomech Eng* 126(6): 838–43

Ishida A, Imai S, Fukuoka Y (1997) Analysis of the posture control system under fixed and sway-referenced support conditions. *IEEE Trans Biomed Eng* 44(5): 331–6

Ishida A, Miyazaki S (1987) Maximum likelihood identification of a posture control system. *IEEE Trans Biomed Eng* 34(1): 1–5

Jo S, Massaquoi SG (2004) A model of cerebellum stabilized and scheduled hybrid long-loop control of upright balance. *Biol Cybern* 91(3): 188–202

Johansson R, Magnusson M, Akesson M (1988) Identification of human postural dynamics. *IEEE Trans Biomed Eng* 35(10): 858–69

Kuo AD (1995) An optimal control model for analyzing human postural balance. *IEEE Trans Biomed Eng* 42(1): 87–101

Kuo AD (2005) An optimal state estimation model of sensory integration in human postural balance. *J Neural Eng* 2(3): S235–49

Masani K, Popovic MR, Nakazawa K, Kouzaki M, Nozaki D (2003) Importance of body sway velocity information in controlling ankle extensor activities during quiet stance. *J Neurophysiol* 90(6): 3774–82

Maurer C, Mergner T, Peterka RJ (2006) Multisensory control of human upright stance. *Exp Brain Res* 171(2): 231–50

Maurer C, Peterka RJ (2005) A new interpretation of spontaneous sway measures based on a simple model of human postural control. *J Neurophysiol* 93(1): 189–200

Mergner T, Maurer C, Peterka RJ (2003) A multisensory posture control model of human upright stance. *Prog Brain Res* 142: 189–201

Morasso PG, Baratto L, Capra R, Spada G (1999) Internal models in the control of posture. *Neural Netw* 12(7-8): 1173–1180

Nashner LM: Vestibular and reflex control of normal standing. In Stein R, Pearson K, Smith RS, Redford JB, eds., *Advances in behavioral biology, vol. 7, Control of posture and locomotion* (New York: Plenum 1973)

Pavol MJ (2005) Detecting and understanding differences in postural sway. focus on "a new interpretation of spontaneous sway measures based on a simple model of human postural control". *J Neurophysiol* 93(1): 20–1

Peterka RJ: Simple model of sensory interaction in human postural control. In Mergner T, Hlavacka F, eds., *Multisensory Control of Posture*, pages 281–288 (New York: Plenum Press 1995)

Peterka RJ (2002) Sensorimotor integration in human postural control. *J Neurophysiol* 88(3): 1097–118

Qu X, Nussbaum MA, Madigan ML (2007) A balance control model of quiet upright stance based on an optimal control strategy. *J Biomech*

van der Kooij H, Jacobs R, Koopman B, Grootenboer H (1999) A multisensory integration model of human stance control. *Biol Cybern* 80(5): 299–308

van der Kooij H, Jacobs R, Koopman B, van der Helm F (2001) An adaptive model of sensory integration in a dynamic environment applied to human stance control. *Biol Cybern* 84(2): 103–15

van der Kooij H, van Asseldonk E, van der Helm FC (2005) Comparison of different methods to identify and quantify balance control. *J Neurosci Methods* 145(1-2): 175–203

Westwick D, Kearney R: *Identification of nonlinear physiological systems* (Piscataway, NJ: IEEE Press 2003)

Chapter 6

Effects of aging and localized muscle fatigue on neural control of posture during small magnitude perturbations

Abstract

This study investigated the effects of aging and localized muscle fatigue on the neural control of upright stance during small postural perturbations. Sixteen young (aged 18-24 years) and 16 older (aged 55-74 years) participants were exposed to anteriorly-directed small magnitude postural perturbation before and after fatiguing exercises. A single degree of freedom model of the human body was used to accurately simulate the experimentally collected kinematics during recovery of upright stance following the perturbations. The model included a neural controller that multiplied time-delayed kinematics by invariant feedback gains. Feedback gains and time-delay were optimized for each participant according to experimentally collected kinematics and a novel delay margin analysis was performed to assess system robustness. Results demonstrated that the older group exhibited a 10.9% longer "effective" time-delay (p=0.010), and a 31.1% greater reliance upon velocity feedback information (p=0.001) than the young group. Calculated delay margins indicated that the older participants adopted a more robust control scheme during small perturbations. No changes in neural controller gains, time-delay, or delay margin with LMF were found in either age group.

6.1 Introduction

Age-related increases in postural sway during quiet standing are well-documented (Baloh et al., 1994; Du Pasquier et al., 2003; Fujita et al., 2005; Nakamura et al., 2001; Prieto et al., 1996). These increases could result from age-related degradation of sensory information from the proprioceptive (McChesney and Woollacott, 2000; Shaffer and Harrison, 2007) and vestibular (Baloh et al., 2001; Lopez et al., 1997; Park et al., 2001) systems. Increases in sway could also result from inaccurate or imprecise muscle forces resulting from excitation-contraction uncoupling (Delbono, 2003; Wang et al., 2000). Localized muscle fatigue (LMF) has been shown to increase the measures of postural sway during quiet standing (Davidson et al., 2004; Gribble and Hertel, 2004; Lundin et al., 1993; Nussbaum, 2003). Several of these reports have speculated that these changes are the result of LMF-induced decreases in proprioceptive acuity in the fatigued muscles (Caron, 2003; Davidson et al., 2004; Lundin et al., 1993; Vuillerme et al., 2002, 2001).

In addition to changes in sensory systems and muscles, increases in postural sway with aging and LMF could be due to changes in the neural controller employed by the postural control system. For the purpose of this study, the neural controller will be operationally defined as the portion of the postural control system that processes information from the sensory systems (vestibular, somatosensory, and visual), and elicits appropriate motor commands to the musculature in order to regulate upright posture. In support of this idea, increases in postural sway have been observed following LMF of muscles not commonly thought to have a critical role in maintaining upright posture such as the neck extensors (Gosselin et al., 2004; Schieppati et al., 2003) and shoulder flexors (Nussbaum, 2003). Moreover, deficits in ankle proprioceptive acuity have been reported with LMF of the lumbar extensors (Pline et al., 2005) and deficits in shoulder proprioceptive acuity with LMF of the contralateral shoulder (Sharpe and Miles, 1993). These studies suggest a possible alteration in central processing of proprioceptive signals with LMF (Gandevia, 2001). The neural controller may adapt to

environmental or internal factors (aging and/or LMF) by reweighting different kinematic afferents or sensory modalities. Previous research of alterations in the neural controller have primarily focused on reweighting the contributions of the three sensory modalities (visual, vestibular, somatosensory), most often within the context of conflicting sensory information (Carver et al., 2006; Peterka and Loughlin, 2004).

Several feedback-controlled models of standing posture have been developed to gain insight into the neural controller by simulating quiet stance (Ishida et al., 1997; Kuo, 2005; Maurer and Peterka, 2005; Peterka, 2002) or a response to a postural perturbation (Alexandrov et al., 2005; Jo and Massaquoi, 2004; Kuo, 1995; Park et al., 2004). Some of these have used a system identification approach to identify physiologically relevant neural controller parameters (Johansson et al., 1988; Maurer and Peterka, 2005; Peterka, 2002, 1995; Peterka and Loughlin, 2004). Recently, Maurer and Peterka (2005) employed a time domain identification that included time-delayed sensory feedback to parameterize proportional, integral, and differential gains during unperturbed quiet stance in young and older adults. The system was driven by a stochastic input and produced sagittal plane center of pressure trajectories having the same sway characteristics as experimentally recorded data. To our knowledge, this study was the first to use system identification to investigate the changes in the neural controller with aging (or any other factor).

Physiological time-delay is present within the human postural control system due to the accumulation of afferent and efferent neural transmission delays, as well as delays encountered during central processing in the neural controller. This is an important concept since system stability is often not independent of time-delay in feedback-controlled systems (Gu et al., 2003). Few studies have simulated standing posture with a model that includes time-delay in the feedback loop (Alexandrov et al., 2005; Maurer and Peterka, 2005; Peterka, 2002). Kuo (1995) estimated a value for the maximum tolerable time-delay based on the phase margin and crossover frequency of the system. However, relating these maximum values to system time-delays were not possible since time-delay was not included in the sys-

tem dynamics. Such a measure would allow insight into how variations in neural controller parameters affect robustness of the system in relation to physiological time-delay.

The purpose of this study was to investigate the effects of aging and LMF on the neural control of upright stance during postural perturbations. A system identification approach, similar to Maurer and Peterka (2005), was used to parameterize a mathematical model of the postural control system that included invariant proportional and differential neural controller gains and time-delay in the sensory feedback. Perturbations were used instead of quiet stance because a more challenging environment may facilitate identification of the effects of aging and LMF. In addition, by increasing the kinematic range with the perturbations, the relatively small stochastic kinematics associated quiet stance may be neglected (Riley et al., 1997; Rougier, 1999). A novel delay margin analysis was performed on the identified systems to assess changes in system robustness to time-delay with aging and fatigue.

6.2 Methods

Thirty-two participants were recruited from the local community including 16 young (19.4 ± 1.4 years old, 71.4 ± 11.1 kg, 174.8 ± 8.3 cm) and 16 older adults (62.2 ± 5.1 years old, 74.0 ± 10.9 kg, 167.8 ± 8.9 cm). Each age group had an equal number of males and females. All participants were screened for self-reported musculoskeletal disorders and medications that could influence balance. In addition, the older participants were required to pass a medical exam to exclude those with neurological, cardiac, respiratory, vestibular, or musculoskeletal disorders, or a history of multiple falls within the past year. The experiment was approved by the Virginia Tech Institutional Review Board, and all participants provided informed consent prior to participation.

6.2.1 Experimental protocol

Each participant visited the laboratory for two experimental sessions separated by approximately one week. In each session, postural responses to a series of small magnitude perturbations were assessed both before and after fatiguing exercises. In one session, the ankle plantar flexor muscles were fatigued, and in the other session the lumbar extensor muscles were fatigued. The order of these sessions was counterbalanced across all participants so half of the participants underwent plantar flexor fatigue in the first session, and the remaining half underwent lumbar extensor fatigue in the first session.

During postural testing, each participant stood with their eyes closed, feet together, and hands clasped behind their back, and were instructed to "stand in a relaxed manner." Ballistic pendulums were used to administer anteriorly-directed (AD) and posteriorly-directed (PD) perturbations in the mid-sagittal plane (Figure 6.1). Perturbations were administered by pulling the pendulums away from the participant a set distance and releasing from a stationary position. Perturbation magnitude was quantified using the horizontal linear momentum of the pendulum just before impacting the participant. The applied magnitudes were small such that a stepping response was not necessary to maintain upright stance. Although this investigation is concerned only with AD perturbations, both directions were applied in random order to reduce the effects anticipation of an impact in the anterior direction. Hearing protection earmuffs were worn by each participant to eliminate auditory cues of an impending perturbation.

The experiment began with ten AD and ten PD perturbations of moderately-low magnitude (10 N·s AD, 7 N·s PD). The purpose of these perturbations was to habituate the participant to the perturbations and allow any performance adaptation to occur. After a one minute break, five AD and five PD small magnitude perturbations (6 N·s AD and 5 N·s PD) were administered in a random order. It was these trials, along with those collected after the fatiguing exercise (see below), that were used for this investigation. Next,

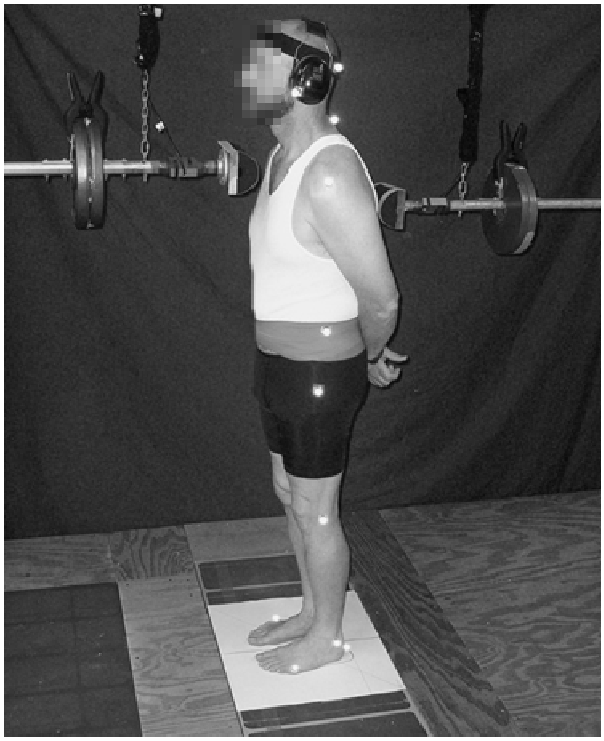

Figure 6.1: The participant was perturbed in the anterior and posterior directions with padded and weighted ballistic pendulums that impacted the participant just below the inferior margin of the scapulae and just below the jugular notch. The perturbations were administered by pulling the pendulums away from the participant and releasing them from a point that corresponded to the desired perturbation magnitude (linear momentum). The perturbation magnitudes chosen in this study did not cause a stepping response in the participants.(photo by Bradley Davidson)

either the lumbar extensors or ankle plantar flexors were fatigued to 70% of their unfatigued maximum voluntary contraction (MVC) moment with isotonic contractions performed on a System 3 Isokinetic Dynamometer (Biodex Medical Systems, Shirley, NY) or a seated calf raise machine (New York Barbell Corp., Elmira, NY). This fatigue level was accomplished by systematically adjusting the number of repetitions performed based on intermittent MVCs so that MVC decreased 30% over 14 minutes (Davidson et al., 2004; Madigan et al., 2006). After the fatiguing exercises, 10 small magnitude perturbations were administered in the same manner as before the exercise.

During all trials, each participant was instrumented with reflective markers placed on each shoulder and ankle (Vicon Motion Analysis System, Lake Forest, CA). Marker position data were sampled at 100 Hz and low-pass filtered at 5 Hz (3rd order zero-phase-lag Butterworth) during post-processing. Sagittal plane body orientation was defined by calculating the angle from vertical of a line connecting each ankle/shoulder pair and averaging across the body. A load cell (Cooper Instruments and Systems, Warrenton, VA) was attached inline to the pendulum to sample perturbation force at 1000 Hz. These data were used to determine perturbation onset time, and the time series of force was implemented into the dynamic simulations.

6.2.2 Model development

A two-dimensional, time-delayed, feedback-controlled dynamic human model of upright stance was created to simulate the experimentally recorded data. The model consisted of a single inertially-correct body segment (Figure 6.2) based on subject specific anthropometry (de Leva, 1996; Pavol et al., 2002) with passive ankle stiffness and damping, and an active ankle torque determined by the neural controller (Figure 6.3). Input to the model was the experimentally recorded pendulum force, $F(t)$. The active ankle torque, $T_A(t)$, was based on time-invariant proportional (K_P) and differential (K_D) feedback gains operating on the system state delayed by τ_d seconds. An arbitrary reference angle, θ_{ref}, was included in the

dynamics to account for the naturally occurring slight forward lean during upright stance.

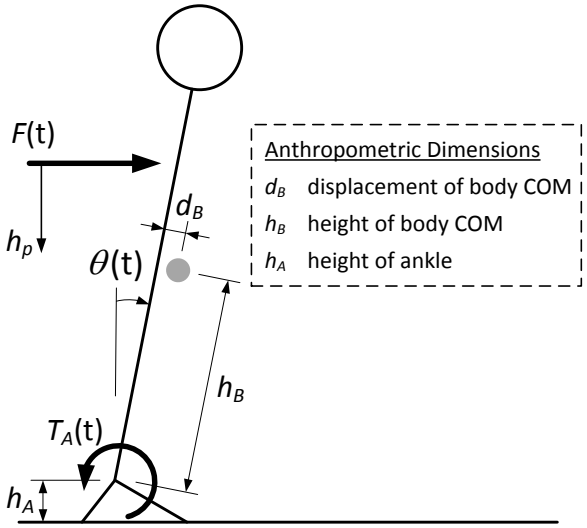

Figure 6.2: Free body diagram of the human model (i.e., the plant). $F(t)$ represents the experimentally recorded pendulum force applied to the participant, and $T_A(t)$ is the resulting ankle torque produced by the neural controller. $\theta(t)$ is body angle relative to vertical. h_P is the height of the pendulum upon contact with the participant. (COM = center of mass).

The equations of motion for this system in linear, first-order form are

$$\begin{Bmatrix} \dot{\theta}(t) \\ \ddot{\theta}(t) \end{Bmatrix} = \underbrace{\begin{bmatrix} 0 & 1 \\ \frac{-K+m_B\,g\,h_B}{J_B} & \frac{-B}{J_B} \end{bmatrix}}_{\mathbf{A}_0} \begin{Bmatrix} \theta(t) \\ \dot{\theta}(t) \end{Bmatrix} + \underbrace{\begin{bmatrix} 0 & 0 \\ \frac{-K_P}{J_B} & \frac{-K_D}{J_B} \end{bmatrix}}_{\mathbf{A}_1} \begin{Bmatrix} \theta(t-\tau_d) \\ \dot{\theta}(t-\tau_d) \end{Bmatrix} + \begin{Bmatrix} 0 \\ \frac{K_P\,\theta_{ref}+m_B\,g\,d_B}{J_B} \end{Bmatrix} + \begin{Bmatrix} 0 \\ \frac{h_p-h_A}{J_B} \end{Bmatrix} F(t) \quad (6.1)$$

where $\theta(t)$, $\dot{\theta}(t)$, and $\ddot{\theta}(t)$ are the time-dependent angle, angular velocity, and angular acceleration of the body segment relative to vertical; g is gravitational acceleration; h_B, d_B, and h_A describe the anthropometrics of the participant (Figure 6.2); m_B and J_B are the mass and the anthropometrically-correct moment of inertia of the body segment about the

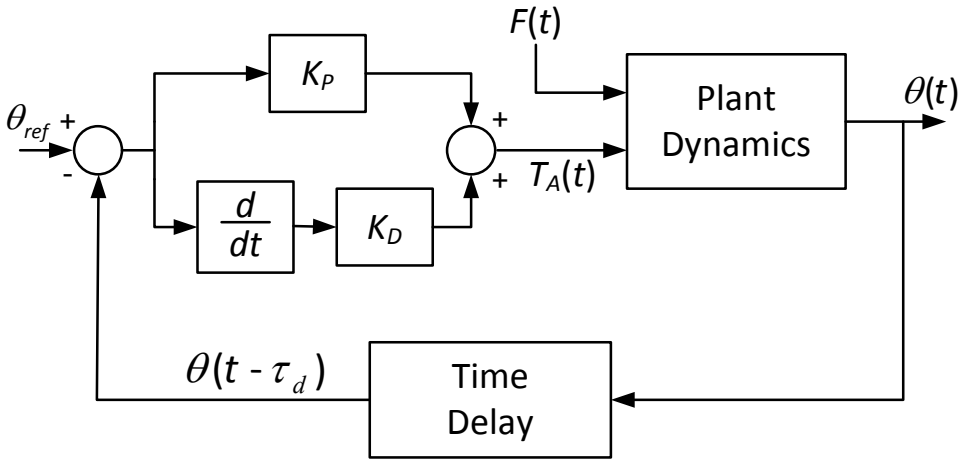

Figure 6.3: Schematic of the controlled system. The input into the system is the experimentally measured pendulum force, $F(t)$. The neural controller calculated the applied ankle torque by multiplying the time-delayed state with two time invariant feedback gains, K_P and K_D (note: passive ankle stiffness and damping are included within the plant dynamics).

ankle, respectively; h_p is the height above the ground that the pendulum contacts the body; K is the passive ankle stiffness taken from Hof (1998); and B is the passive ankle damping calculated using the empirical formula from Loram et al. (2001) as

$$B = 0.76\sqrt{4\, J_B\, K} \tag{6.2}$$

Using body angle from the five AD small magnitude perturbations from each individual, eight model parameters were optimized for each experimental combination of fatigued muscle group (ankle plantar flexor, lumbar extensor) and fatigue level (unfatigued, fatigued). These parameters included the system time-delay τ_d, proportional gain K_P, differential gain K_D, and a five arbitrary reference angles $\theta_{ref}(1 \ldots 5)$, one for each of the AD perturbations in a series. To optimize these parameters the difference between the simulated and experimentally recorded body angles were minimized via the scalar cost function

$$\sum_{n=1}^{pert} \left(\sum_{m=1}^{sample} (\hat{\theta}_{mn} - \theta_{mn})^2 \right) \tag{6.3}$$

where $\hat{\theta}_{mn}$ is data point m from the simulated body angle in perturbation n, and θ_{mn} is data point m from the experimentally recorded body angle in perturbation n. A Nelder-Mead search (Lagarias et al., 1998; Nelles, 2005) was used to perform the optimization (Maurer and Peterka, 2005). Since the Nelder-Mead algorithm is a local nonlinear search, appropriate choice of the initial parameters is crucial in order to obtain physiologically relevant parameters. Accordingly, each simulation began with neural controller gains and time-delay similar to those reported in Maurer and Peterka (2005) and small reference angles (Table 6.1). The simulations began at the time of perturbation onset, and lasted for 1.7 seconds. This simulation length was chosen by identifying the time-delay and neural controller parameters of four randomly selected participants, along with the strength of fit between experimental and simulated data across simulation times of 1-3 seconds (Figure 6.4). All simulations were performed in Fortran90 (Intel Fortran Compiler 9.1, San Jose, CA).

Table 6.1: Parameter seed and specifications for Nelder-Mead optimization. Initial Step Size refers to the step taken during the first series of simplexes based on each parameter.

Parameter	Starting Value	Initial Step Size
τ_d (msec)	170	30
K_P (N·m/rad)	500	200
K_D (N·m·sec/rad)	200	100
$\theta_{ref}(1 \ldots 5)$ (rad)	0.05	0.1

6.2.3 Analysis

Following optimization, robustness of the system to time-delay was quantified by the delay margins of the system. Dynamic systems containing time-delay are not often stable independent of time-delay. As such, an absolute delay margin, or the maximum time-delay the system can withstand before becoming unstable, exists. To calculate the absolute delay margin ($\bar{\tau}_{abs}$) a frequency-sweeping method first proposed by Gu et al. (2003) was used. To

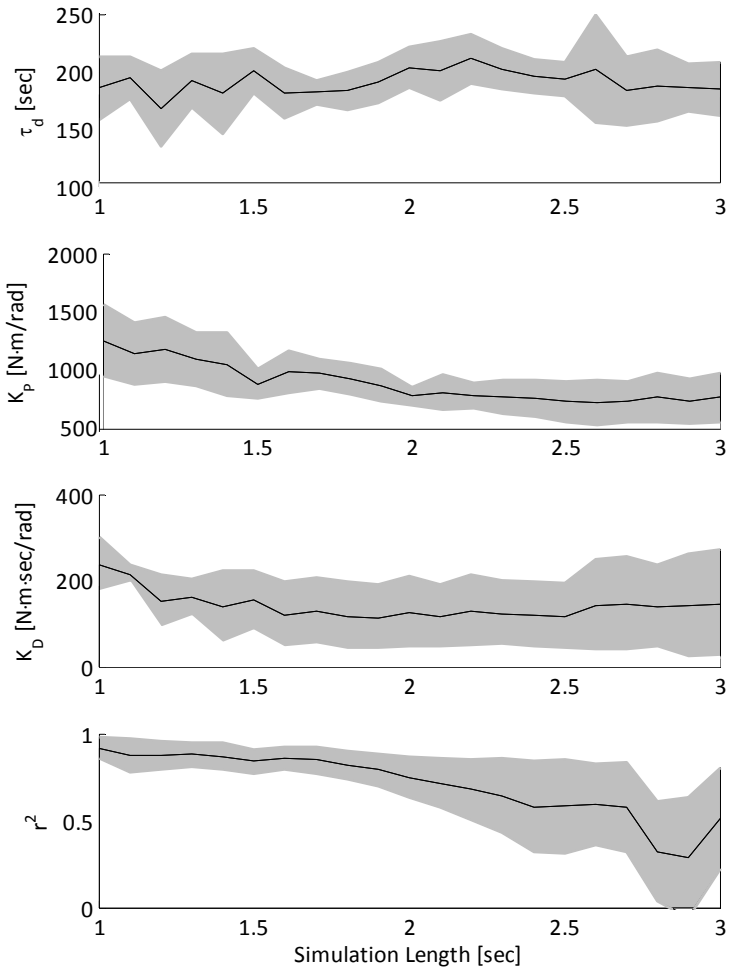

Figure 6.4: Mean ±95% confidence intervals of time-delay (τ_d), neural controller parameters (K_P, K_D), and coefficient of determination (r^2) as a function of simulation length. Selection criteria included the best combination of the following: 1) high r^2-value, 2) low variance in each metric, and 3) mean and variance were stable within the region around the simulation length. Data from four randomly chosen subjects were used to select a simulation length of 1.7 sec for this investigation.

do this, the linear time-delayed dynamics can be written in the following state space form:

$$\dot{\mathbf{x}}(t) = \mathbf{A}_0\mathbf{x}(t) + \mathbf{A}_1\mathbf{x}(t-\tau) + \mathbf{g} + \mathbf{b}F(t) \tag{6.4}$$

where $\mathbf{x}(t)$ is the state vector $[\ \theta(t) \quad \dot{\theta}(t)\ ]^T$, $\mathbf{A}_0$ is the non-delayed state matrix, $\mathbf{A}_1$ is the delayed state matrix, $\mathbf{g}$, is a constant acceleration vector, $\mathbf{b}$ is the input vector, and τ is an arbitrary positive-valued time-delay.

Linear stability is characterized only by the eigenvalues of the matrices $\mathbf{A}_0$ and $\mathbf{A}_1$, which map the state and the delayed state, respectively, to the time-differentiated state. Thus, we can eliminate the forcing term, $\mathbf{b}F(t)$, and constant term, $\mathbf{g}$ from the equation.

Transforming the reduced equation into the Laplace domain gives

$$\mathcal{L}\left\{\dot{\mathbf{x}}(t) = \mathbf{A}_0\mathbf{x}(t) + \mathbf{A}_1\mathbf{x}(t-\tau)\right\} \tag{6.5}$$

$$s\mathbb{X}(s) = \mathbf{A}_0\mathbb{X}(s) + \mathbf{A}_1\mathbb{X}(s)e^{s\tau} \tag{6.6}$$

where s is the Laplace variable, $\mathbb{X}(s)$ is the Laplace transformed $\mathbf{x}(t)$, and $e^{s\tau}$ is the time-delay multiplier. If the system eigenvalues are located in the left half of the Laplace plane ($\mathrm{Re}(s) < 0$), the system is considered to be stable. Assuming that the non time-delayed system is stable, there may exist a time-delay, τ, that will cause a system eigenvalue to cross into the right half of the plane ($\mathrm{Re}(s) > 0$). Thus, by sweeping the frequency domain ($s = j\omega \ \forall\ \omega > 0$), the time-delay that causes an eigenvalue to cross into the right-half plane is found. Constraining the Laplace variable to the imaginary axis yields

$$j\omega\mathbb{X}(j\omega) = \mathbf{A}_0\mathbb{X}(j\omega) + \mathbf{A}_1\mathbb{X}(j\omega)e^{j\omega\tau} \tag{6.7}$$

the terms are rearranged to obtain

$$\left(j\omega\mathbf{I} - \mathbf{A}_0\right)\mathbb{X}(j\omega) = \lambda\mathbf{A}_1\mathbb{X}(j\omega), \quad \lambda = e^{j\omega\tau} \tag{6.8}$$

which is the generalized eigenvalue problem where j is the imaginary variable, ω is the frequency, and $\mathbf{I}$ is a 2×2 identity matrix. Solutions to this problem only exist at a frequency ω, and time delay τ, where the magnitude of λ is equal to the unit modulus according to Euler's formula:

$$|\lambda| = \sqrt{\cos^2(\omega\tau) + \sin^2(\omega\tau)} = 1 \tag{6.9}$$

The solution τ, when simultaneously solving equations (6.8) and (6.9), is considered to be the absolute delay margin and denoted as $\bar{\tau}_{abs}$.

The absolute time-delay provides valuable insight into the overall robustness that the neural controller provides for the system. However, robustness to time-delay must also be considered in light of the existing time-delay present in the postural control system. Therefore, a relative delay margin ($\bar{\tau}_{rel}$) was also calculated using the time-delay identified by the optimization as

$$\bar{\tau}_{abs} = \tau_d - \bar{\tau}_{rel} \tag{6.10}$$

Sensitivity of the simulated dynamics to variations in the identified parameters was assessed. Additional simulations were performed using K_P, K_D, and τ_d from a representative participant and individually varying these parameters between 60-140% of the optimized values. Since characteristics of a linear system are mathematically bounded relative to changes in the neural controller gains and time-delay, qualitative changes in the simulations would be similar across participants regardless of anthropometry. In addition, sensitivity of the absolute delay margin to variations of the neural controller gains K_P and K_D was assessed between 60-140% of a set of neural controller gains from the same representative participant representative.

The strength of fit between simulated angular position and the experimentally recorded angular position were described for the series of five perturbations each session and fatigue level combination by the coefficient of determination (r^2). A two-way repeated measures analysis of variance was used to investigate the effects of age, muscle group, and LMF

on the identified parameters. Independent variables included fatigue level (unfatigued, fatigued), age (young, older), and muscle group (ankle, back). Only interactions of fatigue level with age and fatigue level with muscle group were included as higher order effects in the statistical model. Dependent variables included the optimized neural controller gains (K_P, K_D), time-delay (τ_d), and delay margins ($\bar{\tau}_{abs}$, $\bar{\tau}_{rel}$). Three of the dependent variables (K_D, $\bar{\tau}_{abs}$, $\bar{\tau}_{rel}$) required a square root transformation to achieve normal distributions. Upon finding a significant interaction, pair-wise comparisons were performed using a Tukey HSD analysis. Effects were considered significant when $p \leq 0.05$.

6.3 Results

The optimized dynamic model was able to accurately simulate the experimental data with $r^2 = 0.82 \pm 0.09$ and range of 0.55 - 0.96 (Figure 6.5). Several differences were identified between the young and older age groups (Table 6.2). The older group exhibited 31.1% larger differential gain ($p = 0.001$) and 10.9% longer time-delay ($p = 0.010$). In the delay margin parameters, the older group exhibited 18.5% larger absolute delay margin ($p = 0.001$) and 26.7% larger relative delay margin ($p = 0.001$). No main effects or two-way interactions involving fatigue were present (Table 6.2).

Table 6.2: Mean±standard deviation of identified model parameters (neural controller gains, time-delay) and delay margins (absolute, relative) between age groups and fatigue level

	Young	Older	Unfatigued	Fatigued
Neural controller				
K_P (N·m/rad)	963.9 ± 203.2	864.6 ± 197.3	911.1 ± 223.4	916.6 ± 186.9
K_D (N·m·sec/rad)	98.3 ± 103.5	$129.3 \pm 82.1^*$	111.8 ± 93.4	116.1 ± 95.8
τ_d (msec)	188 ± 16	$211 \pm 21^*$	199 ± 21	200 ± 23
Stability metrics				
$\bar{\tau}_{abs}$ (msec)	331 ± 98	$406 \pm 120^*$	337 ± 128	365 ± 102
$\bar{\tau}_{rel}$ (msec)	143 ± 98	$195 \pm 116^*$	174 ± 122	165 ± 98

* – indicates significant age effect ($p \leq 0.05$)

Varying neural controller gains and time-delay around values representative of the mean

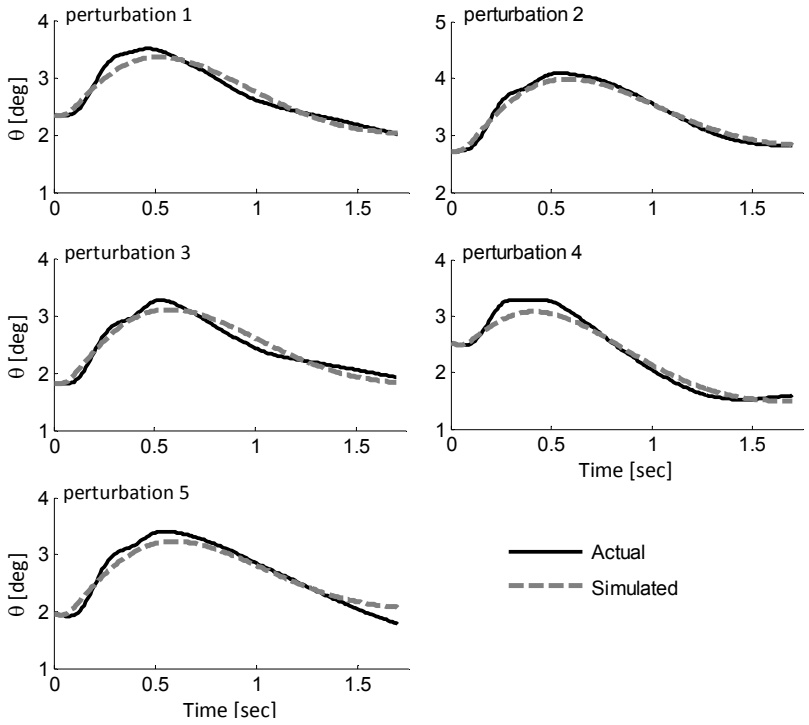

Figure 6.5: Representative time histories from a single subject of experimental and simulated body angle from a single subject during five perturbations. Identified simulation parameters for this series were $K_P = 1033.4$ N·m/rad, $K_D = 152.1$ N·m·s/rad, $\tau_d = 200$ msec, $\theta_{ref}(1) = 0.014$ rad, $\theta_{ref}(2) = 0.019$ rad, $\theta_{ref}(3) = 0.017$ rad, $\theta_{ref}(4) = 0.016$ rad, $\theta_{ref}(5) = 0.019$ rad, $r^2 = 0.91$

across young and older groups revealed distinct changes in the simulated response to a postural perturbation (Figure 6.6). The angular response retained an under-damped shape with variations in τ_d and K_D. Magnitudes of the displacements around the equilibrium point were generally proportional to changes in τ_d and inversely proportional to changes in K_D. Conversely, varying K_P did change the shape of the response where an increase produced a smaller maximum angular displacement with under-damped characteristics. Decreasing K_P caused an increase in the peak displacement and over-damped characteristics. Simultaneously varying K_P and K_D revealed $\bar{\tau}_{abs}$ increased with increasing K_D and decreased with increasing K_P (Figure 6.7).

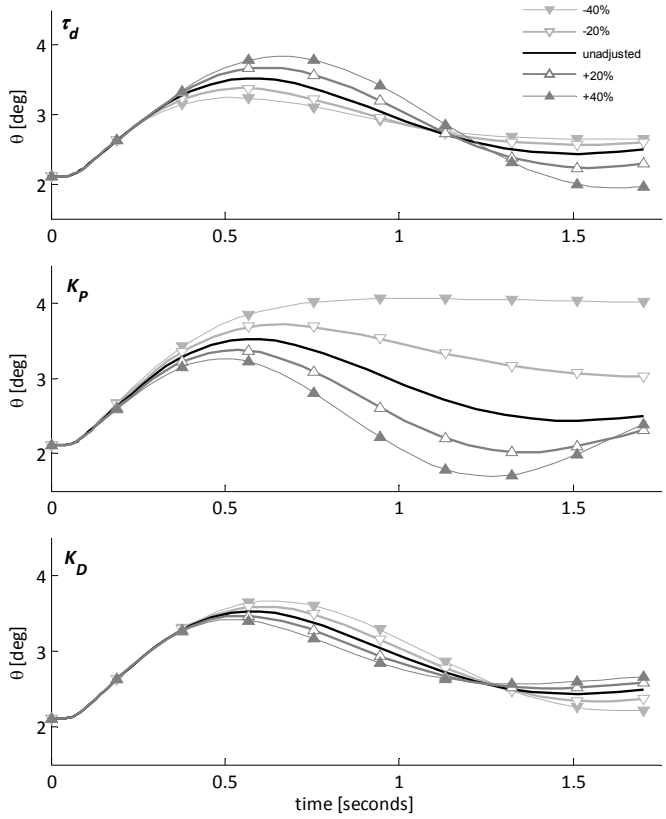

Figure 6.6: Effects of varying model parameters on kinematic response to perturbation. The traces are trajectories as the time-delay and neural controller gains are varied from mean-40% to mean+40% in 20% increments. The shape of the trajectory was most sensitive to change in K_P and least sensitive to changes in K_D.

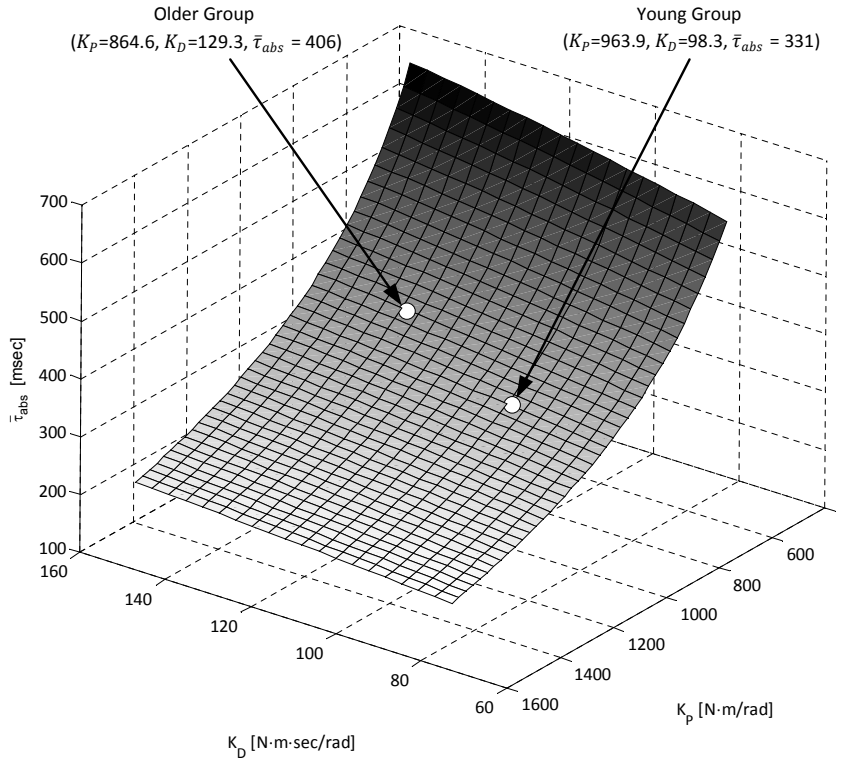

Figure 6.7: Combined effects of neural controller gains (proportional gain K_P and differential gain K_D) on the absolute delay margin ($\bar{\tau}_a bs$). $\bar{\tau}_a bs$ is an indicator of robustness of the system where higher values indicate greater robustness. The interaction of K_D and K_P demonstrated that $\bar{\tau}_a bs$ increased as K_D increased, and tau abs decreased as K_P increased. In general, $\bar{\tau}_a bs$ was more sensitive to changes K_P than K_D, but was dependent upon the specific values of K_P and K_D.

6.4 Discussion

The purpose of this study was to investigate changes in the neural control of upright stance with aging and LMF. Parameters of a feedback-controlled dynamic model of the human body were optimized to match experimentally recorded data during a series of small magnitude postural perturbations. Optimized parameters revealed several differences between age groups including 10.9% longer time-delay and 31.1% higher differential gain in the older group. In addition, the older group had 18.5% and 26.7% larger absolute and relative delay margins, respectively. No changes in neural controller gains, time-delay, or delay margins were found with LMF.

The optimized neural controller gains exhibited similarities to previously published values determined from quiet stance in that $K_P > K_D$ (Maurer and Peterka, 2005), but the actual values (young group: $K_P = 963.9$, $K_D = 98.3$; older group: $K_P = 864.6$, $K_D = 129.3$) were higher than those reported in their model that included intrinsic ankle stiffness and damping (young group: $K_P = 573.0$, $K_D = 19.5$; older group unreported). This could simply be a difference between neural control of quiet stance and postural perturbations, or perhaps due to the slight forward lean used in this study. Values of the identified time-delay (young group: $\tau_d = 188$ msec; older group: $\tau_d = 211$ msec) were consistent with previous estimates of physiological time-delay above 150 msec (Cordo et al., 1994), and are slightly higher than those values identified during quiet stance (young group: $\tau_d = 177$; older group: $\tau_d = 163$) (Maurer and Peterka, 2005). The higher differential gain in older adults found here was similar to the trend reported by Maurer and Peterka (2005) using quiet stance, but the longer time-delay in older adults found here differed from the shorter time-delay reported in the same study.

The longer time-delay in the older group is consistent with documented decrease in nerve conduction velocity with increasing age (Mackenzie and Phillips, 1981; Shaw, 1992; Tong et al., 2004). The identified time-delay can be considered as an "effective" time-delay instead

of an actual physiological value (Alexandrov et al., 2005; Peterka, 2002). This parameter is a lumped quantity that represents feedback loops of shorter and longer delays such as short-latency reflexes, long-latency reflexes, and central feedback loops. We must also consider that an increase in the "effective" time-delay essentially reduces the quality of the feedback information in the simulations. Since age-related losses in proprioceptive (McChesney and Woollacott, 2000; Shaffer and Harrison, 2007) and vestibular acuity (Baloh et al., 2001; Lopez et al., 1997; Park et al., 2001) were not explicitly modeled, these deficits may have emerged as an increase in "effective" time-delay.

Differential gain was significantly larger in the older group. Although this investigation was concerned with perturbed stance, this is an interesting observation given recent findings that the neural controller relies heavily on velocity feedback during quiet stance (Masani et al., 2003, 2006). Since velocity feedback contains implicit information about subsequent positions of the body, the velocity-based motor commands can be considered "anticipatory" in nature. This effectively eliminates the necessity for a feed-forward mechanism to compensate for physiological time-delay. In addition, Jeka et al. (2004) have suggested that afferent velocity information is more accurate than afferent position information. Accordingly, one could surmise that older participants adopt a control scheme with an increased anticipatory element, and also depend more on kinematic information that is more accurate by using a higher differential gain in the neural controller.

The older participants exhibited higher absolute and relative delay margins than the young group. When discussing margins of stability such as delay margins we must bear in mind that these values do not represent the stability of the system, but are indicators of robustness (or sensitivity) of the system towards becoming unstable. To ensure stability, the absolute delay margin must be greater than the system time-delay. Consequently, the higher absolute delay margin indicates that the older participants adopted a more robust control scheme than the young group for small magnitude perturbations.

Relative delay margin, which takes into account the identified time-delay, was higher

in the older participants despite having a higher time-delay than the young group. This additional robustness (resulting from the higher differential gain) is indicative of a more conservative neural control scheme employed by the older group. It is common in older adults to employ a more conservative or cautious approach in other moments such as during gait (Herman et al., 2005; Menz et al., 2003). Reasons for adopting a more conservative control scheme may be to compensate for age-related deficits in sensory acuity (Baloh et al., 2001; Lopez et al., 1997; McChesney and Woollacott, 2000; Park et al., 2001; Shaffer and Harrison, 2007), impaired force production (Delbono, 2003; Wang et al., 2000), or as an additional safeguard against a significant change in recovery strategy.

Although the older participants adopted a more robust neural control scheme than the young group, these results cannot be extrapolated to larger perturbations associated with falls in older adults. Using small perturbations in this investigation allowed accurate simulation using a single body segment with a fixed foot, and the delay margins are unique to these dynamics. To assess robustness during perturbations that elicit a "hip strategy" (Horak and Nashner, 1986; Nashner and Woollacott, 1979), stepping response, or a potential fall, different dynamics must be used.

Sensitivity analysis of the absolute delay margin with respect to changes in neural controller gains revealed a decrease in absolute delay margin with increasing proportional gain and an increase in absolute delay margin with increasing differential gain (Figure 6.7). In comparing proportional and differential gains, the proportional gain had a greater effect on the absolute delay margin over the range of values investigated. Although lowering the proportional gain resulted in a greater delay margin, it introduced a larger anterior displacement (Figure 6.6) and slowed the response such that it may not be physiologically accurate. In contrast, changes in differential gain had a smaller effect on body angle following a perturbation, but still a noticeable effect on the absolute delay margin. These observations are notable because they imply differing roles for each of the neutral controller gains in this system. In this scenario, the proportional gain would be primarily responsible for regulating

body angle, and the differential gain would be increased to a necessary level to ensure an appropriate margin of stability. Although an increase in differential gain would result in a greater absolute delay margin in this system, an excess increase would reduce the speed of the system response such that it may not be physiologically accurate.

Neither ankle plantar flexor nor lumbar extensor fatigue elicited changes in neural controller parameters. This finding suggests that the changes in balance that occur with LMF during quiet stance (Gribble and Hertel, 2004; Lundin et al., 1993; Nussbaum, 2003) and during postural perturbations (as in Chapter 3) do not result from changes in the neural controller. However, this is inconsistent with evidence indicating that LMF alters the central processing of sensory information (Pline et al., 2005; Sharpe and Miles, 1993). Several limitations and/or assumptions in our model and approach may have precluded the identification of changes in the neural controller. First, the system dynamics were linearized and based on a gross simplification of the neural controller. Although the simulations yielded satisfactory fits to the experimental data, physiological systems such as this are highly nonlinear in both dynamics and control structure (Westwick and Kearney, 2003). We chose to linearize the system because few analytical tools currently exist to address these nonlinearities while also permitting a meaningful interpretation of the results. Second, the small magnitude of the perturbations may not have been challenging enough to discern small changes in the neural controller with LMF. Lastly, the model incorporated only a single degree of freedom based on observations of participants employing the so-called "ankle strategy" (Horak and Nashner, 1986; Nashner and McCollum, 1985). A recent report by Creath et al. (2005), however, presented evidence of hip movement during quiet stance that suggests perturbed stance situations such as in this experiment may also merit additional degrees of freedom.

This model has several advancements over previous models used to simulate quiet standing. The simulations in this investigation accounted for the naturally occurring forward lean during standing whereas previous models of upright stance have assumed that the target angle of the body is vertical. This has important implications on estimation of neural con-

troller gains and also on the necessity of incorporating intrinsic ankle stiffness and damping into the dynamic model. This investigation also employed a novel delay margin analysis, which provided a quantitative measure of robustness toward instability.

6.5 Conclusions

In summary, changes in the human neural controller with aging and LMF were investigated using a feedback-controlled dynamic model that accurately simulated experimentally-collected responses to small postural perturbations. The results suugested a longer "effective" time-delay and an increased reliance on velocity feedback in the neural controller in the older group. Calculated delay margins indicated that the older participants adopt a more robust control scheme – potentially to compensate for higher time-delays or poor sensory feedback information.

References

Alexandrov AV, Frolov AA, Horak FB, Carlson-Kuhta P, Park S (2005) Feedback equilibrium control during human standing. *Biol Cybern* 93(5): 309–22

Baloh RW, Enrietto J, Jacobson KM, Lin A (2001) Age-related changes in vestibular function: a longitudinal study. *Ann N Y Acad Sci* 942: 210–9

Baloh RW, Fife TD, Zwerling L, Socotch T, Jacobson K, Bell T, Beykirch K (1994) Comparison of static and dynamic posturography in young and older normal people. *J Am Geriatr Soc* 42(4): 405–12

Caron O (2003) Effects of local fatigue of the lower limbs on postural control and postural stability in standing posture. *Neurosci Lett* 340(2): 83–6

Carver S, Kiemel T, Jeka JJ (2006) Modeling the dynamics of sensory reweighting. *Biol Cybern* 95(2): 123–34

Cordo P, Carlton L, Bevan L, Carlton M, Kerr GK (1994) Proprioceptive coordination of movement sequences: role of velocity and position information. *J Neurophysiol* 71(5): 1848–61

Creath R, Kiemel T, Horak F, Peterka R, Jeka J (2005) A unified view of quiet and perturbed stance: simultaneous co-existing excitable modes. *Neurosci Lett* 377(2): 75–80

Davidson BS, Madigan ML, Nussbaum MA (2004) Effects of lumbar extensor fatigue and fatigue rate on postural sway. *Eur J Appl Physiol* 93(1-2): 183–9

de Leva P (1996) Adjustments to zatsiorsky-seluyanov's segment inertia parameters. *J Biomech* 29(9): 1223–30

Delbono O (2003) Neural control of aging skeletal muscle. *Aging Cell* 2(1): 21–9

Du Pasquier RA, Blanc Y, Sinnreich M, Landis T, Burkhard P, Vingerhoets FJ (2003) The effect of aging on postural stability: a cross sectional and longitudinal study. *Neurophysiol Clin* 33(5): 213–8

Fujita T, Nakamura S, Ohue M, Fujii Y, Miyauchi A, Takagi Y, Tsugeno H (2005) Effect of age on body sway assessed by computerized posturography. *J Bone Miner Metab* 23(2): 152–6

Gandevia SC (2001) Spinal and supraspinal factors in human muscle fatigue. *Physiol Rev* 81(4): 1725–89

Gosselin G, Rassoulian H, Brown I (2004) Effects of neck extensor muscles fatigue on balance. *Clin Biomech (Bristol, Avon)* 19(5): 473–9

Gribble PA, Hertel J (2004) Effect of hip and ankle muscle fatigue on unipedal postural control. *J Electromyogr Kinesiol* 14(6): 641–6

Gu K, Kharitonov V, Chen J: (2003) Stability of time-delay systems

Herman T, Giladi N, Gurevich T, Hausdorff JM (2005) Gait instability and fractal dynamics of older adults with a "cautious" gait: why do certain older adults walk fearfully? *Gait Posture* 21(2): 178–85

Hof AL (1998) In vivo measurement of the series elasticity release curve of human triceps surae muscle. *J Biomech* 31(9): 793–800

Horak FB, Nashner LM (1986) Central programming of postural movements: adaptation to altered support-surface configurations. *J Neurophysiol* 55(6): 1369–81

Ishida A, Imai S, Fukuoka Y (1997) Analysis of the posture control system under fixed and sway-referenced support conditions. *IEEE Trans Biomed Eng* 44(5): 331–6

Jeka J, Kiemel T, Creath R, Horak F, Peterka R (2004) Controlling human upright posture: velocity information is more accurate than position or acceleration. *J Neurophysiol* 92(4): 2368–79

Jo S, Massaquoi SG (2004) A model of cerebellum stabilized and scheduled hybrid long-loop control of upright balance. *Biol Cybern* 91(3): 188–202

Johansson R, Magnusson M, Akesson M (1988) Identification of human postural dynamics. *IEEE Trans Biomed Eng* 35(10): 858–69

Kuo AD (1995) An optimal control model for analyzing human postural balance. *IEEE Trans Biomed Eng* 42(1): 87–101

Kuo AD (2005) An optimal state estimation model of sensory integration in human postural balance. *J Neural Eng* 2(3): S235–49

Lagarias J, Reeds J, Wright M, Wright P (1998) Convergence properties of the nelder-mead simplex method in low dimensions. *SIAM J Optim* 9: 112–147

Lopez I, Honrubia V, Baloh RW (1997) Aging and the human vestibular nucleus. *J Vestib Res* 7(1): 77–85

Loram I, Kelly S, Lakie M (2001) Human balancing of an inverted pendulum: is sway size controlled by ankle impedance? *J Physiol* 532(Pt 3): 879–891

Lundin T, Feuerbach J, Grabiner M (1993) Effect of plantar flexor and dorsiflexor fatigue on unilateral postural control. *J Appl Biomech* 9: 191–201

Mackenzie RA, Phillips L H n (1981) Changes in peripheral and central nerve conduction with aging. *Clin Exp Neurol* 18: 109–16

Madigan ML, Davidson BS, Nussbaum MA (2006) Postural sway and joint kinematics during quiet standing are affected by lumbar extensor fatigue. *Hum Mov Sci* 25(6): 788–89

Masani K, Popovic MR, Nakazawa K, Kouzaki M, Nozaki D (2003) Importance of body sway velocity information in controlling ankle extensor activities during quiet stance. *J Neurophysiol* 90(6): 3774–82

Masani K, Vette AH, Popovic MR (2006) Controlling balance during quiet standing: proportional and derivative controller generates preceding motor command to body sway position observed in experiments. *Gait Posture* 23(2): 164–72

Maurer C, Peterka RJ (2005) A new interpretation of spontaneous sway measures based on a simple model of human postural control. *J Neurophysiol* 93(1): 189–200

McChesney JW, Woollacott MH (2000) The effect of age-related declines in proprioception and total knee replacement on postural control. *J Gerontol A Biol Sci Med Sci* 55(11): M658–66

Menz HB, Lord SR, Fitzpatrick RC (2003) Age-related differences in walking stability. *Age Ageing* 32(2): 137–42

Nakamura H, Tsuchida T, Mano Y (2001) The assessment of posture control in the elderly using the displacement of the center of pressure after forward platform translation. *J Electromyogr Kinesiol* 11(6): 395–403

Nashner L, McCollum G (1985) The organization of human postural movements: A formal basis and experimental synthesis. *Behav Brain Sci* 8: 135–172

Nashner LM, Woollacott M: The organization of rapid postural adjustments of standing humans: An experimental-conceptual model. In Talbott RE, Humphrey DR, eds., *Posture and Movement*, pages 243–257 (New York: Raven Press 1979)

Nelles O: *Nonlinear System Identification* (Berlin: Springer 2005)

Nussbaum MA (2003) Postural stability is compromised by fatiguing overhead work. *AIHA J (Fairfax, Va)* 64(1): 56–61

Park JJ, Tang Y, Lopez I, Ishiyama A (2001) Age-related change in the number of neurons in the human vestibular ganglion. *J Comp Neurol* 431(4): 437–43

Park S, Horak FB, Kuo AD (2004) Postural feedback responses scale with biomechanical constraints in human standing. *Exp Brain Res* 154(4): 417–27

Pavol MJ, Owings TM, Grabiner MD (2002) Body segment inertial parameter estimation for the general population of older adults. *J Biomech* 35(5): 707–12

Peterka RJ: Simple model of sensory interaction in human postural control. In Mergner T, Hlavacka F, eds., *Multisensory Control of Posture*, pages 281–288 (New York: Plenum Press 1995)

Peterka RJ (2002) Sensorimotor integration in human postural control. *J Neurophysiol* 88(3): 1097–118

Peterka RJ, Loughlin PJ (2004) Dynamic regulation of sensorimotor integration in human postural control. *J Neurophysiol* 91(1): 410–23

Pline KM, Madigan ML, Nussbaum MA, Grange RW (2005) Lumbar extensor fatigue and circumferential ankle pressure impair ankle joint motion sense. *Neurosci Lett* 390(1): 9–14

Prieto TE, Myklebust JB, Hoffmann RG, Lovett EG, Myklebust BM (1996) Measures of postural steadiness: differences between healthy young and elderly adults. *IEEE Trans Biomed Eng* 43(9): 956–66

Riley MA, Mitra S, Stroffregan TA, Turvey MT (1997) Influences of body lean and vision on unperturbed postural sway. *Motor Control* 1: 229–246

Rougier P (1999) Influence of visual feedback on successive control mechanisms in upright quiet stance in humans assessed by fractional brownian motion modelling. *Neurosci Lett* 266(3): 157–60

Schieppati M, Nardone A, Schmid M (2003) Neck muscle fatigue affects postural control in man. *Neuroscience* 121(2): 277–85

Shaffer SW, Harrison AL (2007) Aging of the somatosensory system: a translational perspective. *Phys Ther* 87(2): 193–207

Sharpe MH, Miles TS (1993) Position sense at the elbow after fatiguing contractions. *Exp Brain Res* 94(1): 179–82

Shaw NA (1992) Age-dependent changes in central somatosensory conduction time. *Clin Electroencephalogr* 23(2): 105–10

Tong HC, Werner RA, Franzblau A (2004) Effect of aging on sensory nerve conduction study parameters. *Muscle Nerve* 29(5): 716–20

Vuillerme N, Danion F, Forestier N, Nougier V (2002) Postural sway under muscle vibration and muscle fatigue in humans. *Neurosci Lett* 333(2): 131–5

Vuillerme N, Nougier V, Prieur JM (2001) Can vision compensate for a lower limbs muscular fatigue for controlling posture in humans? *Neurosci Lett* 308(2): 103–6

Wang ZM, Messi ML, Delbono O (2000) L-type ca(2+) channel charge movement and intracellular ca(2+) in skeletal muscle fibers from aging mice. *Biophys J* 78(4): 1947–54

Westwick D, Kearney R: *Identification of nonlinear physiological systems* (Piscataway, NJ: IEEE Press 2003)

Chapter 7

Introduction to optimal control and the linear quadratic regulator problem

7.1 Introduction

This chapter provides an introduction to the state-feedback linear quadratic regulator problem in optimal control. The optimization equation is derived using dynamic programming and is solved in terms of a matrix differential equation called the Riccati equation. Finally, a procedure for solving the steady-state Riccati equation is presented. The order of presentation and notation follow closely with Dorato et al. (2000).

7.2 Linear quadratic regulator optimal control

We first define the system dynamics as coupled linear first-order differential equations

$$\dot{\mathbf{x}}(t) = \mathbf{A}\mathbf{x}(t) + \mathbf{B}\mathbf{u}(t) \tag{7.1}$$

that contain the state vector, $\mathbf{x}(t) \in \mathbb{R}^n$, control vector, $\mathbf{u}(t) \in \mathbb{R}^m$, the state matrix $\mathbf{A} \in \mathbb{R}^{n\times n}$, and the input matrix $\mathbf{B} \in \mathbb{R}^{n\times m}$. A control scheme in which the objective is to maintain the state of a dynamical system close to zero via the control law

$$\mathbf{u}(t) = -\mathbf{K}\mathbf{x}(t) \tag{7.2}$$

is called the regulator control problem. The linear optimization problem to determine $\mathbf{K} \in \mathbb{R}^{m \times n}$ is defined by the scalar cost function

$$\int_0^{t_f} \mathbf{x}(t)^T \mathbf{Q}\mathbf{x}(t) + \mathbf{u}(t)^T \mathbf{R}\mathbf{u}(t) dt + \mathbf{x}(t_f)^T \mathbf{M}\mathbf{x}(t_f) \tag{7.3}$$

where $\mathbf{Q} \in \mathbb{R}^{n \times n}$ and $\mathbf{M} \in \mathbb{R}^{n \times n}$ are constant positive semi-definite matrices and $\mathbf{M} \in \mathbb{R}^{m \times m}$ is a constant positive-definite matrix. This is commonly called linear quadratic regulator (LQR) control. The term $\mathbf{x}(t)^T \mathbf{Q}\mathbf{x}(t)$ is a measure of state accuracy, $\mathbf{u}(t)^T \mathbf{R}\mathbf{u}(t)$ is a measure of control effort, and $\mathbf{x}(t_f)^T \mathbf{M}\mathbf{x}(t_f)$ is a measure of terminal control accuracy. For convenience of notation, the implicit time, t, will be omitted in future equations except where necessary.

7.3 Hamilton-Jacobi equation

In this section the optimization equation for the LQR problem is derived, commonly referred to as the Hamilton-Jacobi equation. This equation is used to determine a control law $\mathbf{u} = \phi(\mathbf{x}, t)$ that satisfies the cost function

$$V = \int_t^{t_f} l(\mathbf{x}, \mathbf{u}, \tau) d\tau + m[\mathbf{x}(t_f)] \tag{7.4}$$

which is identical to (7.3) if $l(\mathbf{x}, \mathbf{u}) = \mathbf{x}^T \mathbf{Q}\mathbf{x} + \mathbf{u}^T \mathbf{R}\mathbf{u}$ and $m[\mathbf{x}(t_f)] = \mathbf{x}^T(t_f)\mathbf{M}\mathbf{x}(t_f)$, and the system dynamics are represented by the nonlinear system dynamics

$$\dot{\mathbf{x}} = f(\mathbf{x}, \mathbf{u}, t) \tag{7.5}$$

The term $l(\mathbf{x}, \mathbf{u}, \tau)$, known as the loss function, and $m[\mathbf{x}(t_f)]$, the terminal cost, are generally non-negative functions. Since the generalized nonlinear form causes no problems when deriving the optimization equation, they are used here to abbreviate further mathematical

notation.

To derive an optimization equation for the LQR control problem, we use the optimality principle. The main assumption of the optimality principle is that the system can be characterized by its state $\mathbf{x}(t)$ at time t. The state essentially summarizes the effects of all inputs $\mathbf{u}(\tau)$ prior to time t. Using the optimality principle to derive these equations, initially proposed by Bellman and Dreyfus (1962), is referred to as the dynamic-programming approach.

The principle of optimality states:
If $\mathbf{u}^*(\tau)$ *is optimal over the interval* $[t, T]$*, starting at state* $\mathbf{x}(t)$*, then* $\mathbf{u}^*(\tau)$ *is necessarily optimal over the subinterval* $[t + \Delta t, T]$ *for any* Δt *such that* $T - t \geq \Delta t > 0$.

Denoting $V^*(\mathbf{x}, t)$ as the minimum value of the cost function V when the initial time is t and the initial state is $\mathbf{x}(t) = \mathbf{x}$, and denoting $\mathbf{u}[t, T]$ as the control signal defined over the interval $[t, T]$

$$V^*(\mathbf{x}, t) = \min_{\mathbf{u}[t,T]} \left\{ \int_t^T l(\mathbf{x}, \mathbf{u}, \tau) d\tau + m[\mathbf{x}(T)] \right\} \tag{7.6}$$

From the optimality principle, and the additive properties of integrals we have

$$V^*(\mathbf{x}, t) = \min_{\mathbf{u}[t,t+\Delta t]} \left\{ \int_t^{t+\Delta t} l(\mathbf{x}, \mathbf{u}, \tau) d\tau + V^*[\mathbf{x}(t + \Delta t), t + \Delta t] \right\} \tag{7.7}$$

Therefore, by using the optimality principle, finding the minimum value of the function across the interval $[t, T]$ is reduced to finding a minimum value over $[t, t + \Delta t]$.

By approximating the integral in (7.7) by $l(\mathbf{x}, \mathbf{u}, t)\Delta t$ and performing a Taylor Series expansion of $V^*(\mathbf{x}, t)$ about the initial point $(\mathbf{x}(t), t)$, and approximating $\mathbf{x}(t + \Delta t) - \mathbf{x}(t)$ by $f(\mathbf{x}, \mathbf{u}, t)\Delta t$, we obtain

$$V^*(\mathbf{x}, t) = \min_{\mathbf{u}[t]} \left\{ l(\mathbf{x}, \mathbf{u}, \tau)\Delta t + V^*(\mathbf{x}, t) + \frac{\partial V^*}{\partial t}\Delta t + \left[\frac{\partial V^*}{\partial \mathbf{x}} \right]' f(\mathbf{x}, \mathbf{u}, t)\Delta t + o(\Delta t) \right\} \tag{7.8}$$

where $\partial V^*/\partial t$ is the gradient of V^* with respect to $\mathbf{x}$, and $o(\Delta t)$ represents the higher order terms from the Taylor Series expansion. Taking the limit as Δt goes to zero yields

$$-\frac{\partial V^*}{\partial t} = \min_{\mathbf{u}[t]} \left\{ l(\mathbf{x}, \mathbf{u}, \tau) + V^*(\mathbf{x}, t) + \frac{\partial V^*}{\partial t} + \left[\frac{\partial V^*}{\partial \mathbf{x}}\right]' f(\mathbf{x}, \mathbf{u}, t) \right\} \tag{7.9}$$

$$V^*(\mathbf{x}, T) = m(\mathbf{x})$$

which is known as the Hamilton-Jacobi optimization equation.

To obtain the solution we perform the indicated minimization. This leads to a generalized control law taking the form

$$\mathbf{u}^* = \psi\left(\frac{\partial V^*}{\partial \mathbf{x}}, \mathbf{x}, t\right) \tag{7.10}$$

This is substituted back into (7.9) and then solve the nonlinear partial differential equation

$$-\frac{\partial V^*}{\partial t} = l(\mathbf{x}, \psi, t) + \left[\frac{\partial V^*}{\partial \mathbf{x}}\right]' f(\mathbf{x}, \psi, t) \tag{7.11}$$

for $V^*(\mathbf{x}, t)$ subject to the boundary condition

$$V^*(\mathbf{x}, t) = m(\mathbf{x}) \tag{7.12}$$

Finally, the optimal state-feedback control law is produced by computing the gradient of $V^*(\mathbf{x}, t)$ with respect to $\mathbf{x}$, yielding

$$\mathbf{u}^* = \psi\left(\frac{\partial V^*}{\partial \mathbf{x}}, \mathbf{x}, t\right) = \phi(\mathbf{x}, t) \tag{7.13}$$

7.4 Matrix Riccati equation

The first step in determining the solution to the LQR problem is the minimization of the Hamilton-Jacobi equation

$$\mathbf{x}^T\mathbf{Q}\mathbf{x} + \mathbf{u}^T\mathbf{R}\mathbf{u} + \left[\frac{\partial V^*}{\partial \mathbf{x}}\right]' (\mathbf{A}\mathbf{x} + \mathbf{B}\mathbf{u}) \tag{7.14}$$

with respect to $\mathbf{u}$. This can be done by setting the gradient of (7.14) to zero. This is both a *necessary* and *sufficient* condition when $\mathbf{R}$ is a positive-definite matrix. Setting the gradient equal to zero and solving for $\mathbf{u}$ gives

$$\mathbf{u}^* = -\frac{1}{2}\mathbf{R}^{-1}\mathbf{B}^T\frac{\partial V^*}{\partial \mathbf{x}} \tag{7.15}$$

It is known that an integral-quadratic form evaluated for a linear system is a quadratic form in the initial state of the system. Therefore, it is reasonable to assume

$$V^*(\mathbf{x}, t) = \mathbf{x}^T\mathbf{\Gamma}(t)\mathbf{x} \tag{7.16}$$

where $\mathbf{\Gamma} \in \mathbb{R}^{n\times n}$ is symmetric. It then follows that

$$\frac{\partial V^*(\mathbf{x}, t)}{\partial \mathbf{x}} = 2\mathbf{\Gamma}(t)\mathbf{x} \tag{7.17}$$

When V^* from (7.16) and (7.17) are substituted into (7.11), we arrive at

$$-\mathbf{x}^T\dot{\mathbf{\Gamma}}\mathbf{x} = \mathbf{x}^T\left[\mathbf{A}^T\mathbf{\Gamma} + \mathbf{\Gamma}\mathbf{A} + \mathbf{Q} - \mathbf{\Gamma}\mathbf{B}\mathbf{R}^{-1}\mathbf{B}^T\mathbf{\Gamma}\right]\mathbf{x} \tag{7.18}$$

with the boundary condition

$$V^*(\mathbf{x}, T) = \mathbf{x}^T\mathbf{M}\mathbf{x} \tag{7.19}$$

Since (7.18) must be true for all $\mathbf{x}$, we arrive at the matrix Riccati equation

$$-\dot{\mathbf{\Gamma}} = \mathbf{A}^T\mathbf{\Gamma} + \mathbf{\Gamma}\mathbf{A} + \mathbf{Q} - \mathbf{\Gamma}\mathbf{B}\mathbf{R}^{-1}\mathbf{B}^T\mathbf{\Gamma}\mathbf{x} \tag{7.20}$$

$$\mathbf{\Gamma}(T) = \mathbf{M}$$

and the optimal state-feedback control law is

$$\mathbf{u}^* = -\mathbf{K}(t)\mathbf{x} = -\mathbf{R}^{-1}\mathbf{B}^T\mathbf{\Gamma}(t)\mathbf{x} \tag{7.21}$$

7.5 Solving the matrix Riccati equation

The matrix Riccati equation can be solved by solving the following system of linear equations

$$\begin{bmatrix} \dot{\mathbf{X}} \\ \dot{\mathbf{Y}} \end{bmatrix} = \begin{bmatrix} \mathbf{A} & -\mathbf{B}\mathbf{R}^{-1}\mathbf{B}^T \\ -\mathbf{Q} & -\mathbf{A}^T \end{bmatrix} \begin{bmatrix} \mathbf{X} \\ \mathbf{Y} \end{bmatrix} \tag{7.22}$$

where $\mathbf{X} \in \mathbb{R}^{n\times n}$ and $\mathbf{Y} \in \mathbb{R}^{n\times n}$ and satisfy the boundary conditions

$$\begin{bmatrix} \mathbf{X}(T) \\ \mathbf{Y}(T) \end{bmatrix} = \begin{bmatrix} \mathbf{I} \\ \mathbf{M} \end{bmatrix} \tag{7.23}$$

The solution of the matrix Riccati equation from (7.20) is

$$\mathbf{\Gamma}(t) = \mathbf{Y}(t)\mathbf{X}(t)^{-1} \tag{7.24}$$

The matrix in (7.22)

$$\mathbf{H} = \begin{bmatrix} \mathbf{A} & -\mathbf{B}\mathbf{R}^{-1}\mathbf{B}^T \\ -\mathbf{Q} & -\mathbf{A}^T \end{bmatrix} \tag{7.25}$$

is called the Hamiltonian matrix. First, note that if λ is an eigenvalue of $\mathbf{H}$, then so is $-\lambda$. This comes from the fact that $\mathbf{H}^T$ is mathematically similar to $-\mathbf{H}$. Let $\mathbf{U} \in \mathbb{R}^{2n \times 2n}$ be a nonsingular transformation such that

$$\mathbf{U}^{-1}\mathbf{H}\mathbf{U} = \begin{bmatrix} \mathbf{\Lambda}_s & \mathbf{0} \\ \mathbf{0} & \mathbf{\Lambda}_u \end{bmatrix} \tag{7.26}$$

where $\mathbf{\Lambda}_s \in \mathbb{R}^{n \times n}$ is a Jordan block with all eigenvalues having negative real parts (stable) and $\mathbf{\Lambda}_u \in \mathbb{R}^{n \times n}$ is a Jordan block with all eigenvalues having positive real parts (unstable). If $\mathbf{H}$ has no eigenvalues that are purely imaginary this transformation always exists. Additionally, let $\mathbf{U}$ be partitioned into four $n \times n$ blocks

$$\mathbf{U} = \begin{bmatrix} \mathbf{U}_{11} & \mathbf{U}_{12} \\ \mathbf{U}_{21} & \mathbf{U}_{22} \end{bmatrix} \tag{7.27}$$

where

$$\begin{bmatrix} \mathbf{U}_{11} \\ \mathbf{U}_{21} \end{bmatrix} \tag{7.28}$$

has columns made up of the generalized eigenvectors of $\mathbf{H}$ corresponding to eigenvalues with negative real parts, and where

$$\begin{bmatrix} \mathbf{U}_{21} \\ \mathbf{U}_{22} \end{bmatrix} \tag{7.29}$$

has columns made up of the generalized eigenvectors of $\mathbf{H}$ corresponding to eigenvalues with positive real parts. With the transformation

$$\begin{bmatrix} \mathbf{X} \\ \mathbf{Y} \end{bmatrix} = \mathbf{U} \begin{bmatrix} \hat{\mathbf{X}} \\ \hat{\mathbf{Y}} \end{bmatrix} \tag{7.30}$$

the differential equation in (7.22) becomes

$$\frac{d}{dt}\begin{bmatrix}\hat{\mathbf{X}}\\ \hat{\mathbf{Y}}\end{bmatrix} = \begin{bmatrix}\mathbf{\Lambda}_s & \mathbf{0}\\ \mathbf{0} & \mathbf{\Lambda}_u\end{bmatrix}\begin{bmatrix}\hat{\mathbf{X}}\\ \hat{\mathbf{Y}}\end{bmatrix} \tag{7.31}$$

From the decoupled equations in (7.31), $\hat{\mathbf{X}}$ and $\hat{\mathbf{Y}}$ at a final time T can be computed as

$$\begin{aligned}\hat{\mathbf{X}}(T) &= e^{\mathbf{\Lambda}_s(T-t)}\hat{\mathbf{X}}(t) \\ \hat{\mathbf{Y}}(T) &= e^{\mathbf{\Lambda}_u(T-t)}\hat{\mathbf{Y}}(t)\end{aligned} \tag{7.32}$$

Evaluating (7.30) at the boundary T now gives

$$\begin{aligned}\mathbf{I} &= \mathbf{U}_{11}\hat{\mathbf{X}}(T) + \mathbf{U}_{12}\mathbf{Y}(T) \\ \mathbf{M} &= \mathbf{U}_{21}\hat{\mathbf{X}}(T) + \mathbf{U}_{22}\mathbf{Y}(T)\end{aligned} \tag{7.33}$$

We can solve for $\hat{\mathbf{Y}}(t)$ in terms of $\hat{\mathbf{X}}(t) - \hat{\mathbf{Y}}(t) = \mathbf{G}\hat{\mathbf{X}}(t)$ where

$$\mathbf{G} = -\left[\mathbf{U}_{22} - \mathbf{M}\mathbf{U}_{12}\right]^{-1}\left[\mathbf{U}_{21} - \mathbf{M}\mathbf{U}_{11}\right] \tag{7.34}$$

Combing (7.32-7.34) we obtain

$$\begin{aligned}\mathbf{X}(t) &= \left[\mathbf{U}_{11} + \mathbf{U}_{12}e^{-\mathbf{\Lambda}_u(T-t)}\mathbf{G}e^{-\mathbf{\Lambda}_s(T-t)}\right]e^{-\mathbf{\Lambda}_s(T-t)}\hat{\mathbf{X}}(t) \\ \mathbf{X}(t) &= \left[\mathbf{U}_{21} + \mathbf{U}_{22}e^{-\mathbf{\Lambda}_u(T-t)}\mathbf{G}e^{-\mathbf{\Lambda}_s(T-t)}\right]e^{-\mathbf{\Lambda}_s(T-t)}\hat{\mathbf{X}}(t)\end{aligned} \tag{7.35}$$

Substituting (7.35) into (7.24) we arrive at

$$\mathbf{\Gamma}(t) = \left[\mathbf{U}_{21} + \mathbf{U}_{22}e^{-\mathbf{\Lambda}_u(T-t)}\mathbf{G}e^{-\mathbf{\Lambda}_s(T-t)}\right]\left[\mathbf{U}_{11} + \mathbf{U}_{12}e^{-\mathbf{\Lambda}_u(T-t)}\mathbf{G}e^{-\mathbf{\Lambda}_s(T-t)}\right]^{-1} \tag{7.36}$$

7.6 Algebraic Riccati equation

When the data is time-invariant and the optimization interval is infinite ($T \to \infty$), the optimal control problem is referred to as the steady-state LQR problem. The solution to (7.20) is time-invariant; therefore, the equation becomes

$$\mathbf{0} = \mathbf{A}^T\bar{\mathbf{\Gamma}} + \bar{\mathbf{\Gamma}}\mathbf{A} + \mathbf{Q} - \bar{\mathbf{\Gamma}}\mathbf{B}\mathbf{R}^{-1}\mathbf{B}^T\bar{\mathbf{\Gamma}} \tag{7.37}$$

which is called the algebraic Riccati equation (ARE). Taking the limit of the more general Riccati solution in (7.36) as $T \to \infty$ gives the solution to (7.37) as

$$\bar{\mathbf{\Gamma}} = \mathbf{U}_{21}\mathbf{U}_{11}^{-1} \tag{7.38}$$

The optimal control for the steady-state problem via the ARE is then

$$\mathbf{u}^* = -\mathbf{K}\mathbf{x} = -\mathbf{R}^{-1}\mathbf{B}^T\bar{\mathbf{\Gamma}}\mathbf{x} \tag{7.39}$$

These concepts will be revisited when developing a nonlinear form of the optimal control problem and solving for the feedback gains in the next chapter.

References

Bellman R, Dreyfus S: *Applied dynamic programming* (Princeton, NJ: Princeton New Jersey Press 1962)

Dorato P, Abdallah C, Cerone V: *Linear quadratic control: An introduction* (Malbar, FL: Krieger 2000)

Chapter 8

Approximation of the neural controller using the nonlinear state-dependent Riccati equation during postural responses to large magnitude sagittal plane perturbations

Abstract

This study investigated the use of a nonlinear controller to simulate responses to large magnitude postural perturbations. A three DOF model of the human body was developed and controlled with the state-dependent Riccati equation (SDRE). Parameters of the SDRE were optimized to fit the experimentally recorded kinematics. Unlike other forms of nonlinear control, the SDRE provides meaningful parameters for interpretation in the system identification. This approach was successful at stabilizing the system with the initial parameter seed for the case of a single perturbation. When additional perturbations were included, the controller was unable to stabilize the system. Several reasons may account for this which include: 1) poor selection of initial parameters, 2) inability of the SDRE to account for cognitive control, 3) the state-dependent coefficient realization was inadequate for this task, or 4) unknown stabilizability and controllability with the addition of time-delay to SDRE. One possible solution to address stabilizability and controllability is to reformulate the controlled dynamics into the Roesser state space form.

8.1 Introduction

The linear quadratic regulator (LQR) is a well-known optimal control method that has demonstrated its usefulness in biomedical applications such as modeling neural signal transduction (Gadkar et al., 2005) and other internal physiological processes (Brenner et al., 1995; Kovacs et al., 2004), implementing robotic surgical assistance (Vanne and Hynynen, 2003), and analysis of human gait (Matjacic and Bajd, 1998). The regulator problem is defined by imposing an invariant point of equilibrium in the phase plane (e.g., $x = 0$, $\dot{x} = 0$ in a dynamic system with one degree of freedom). Attraction to this equilibrium state is regulated by a controlled input that optimally penalizes the state error via a set of full-state feedback gains. LQR methodology is well-suited for modeling upright stance since the body continuously regulates an approximately vertical position based on kinematic feedback from the vestibular, visual, and somatosensory organs (Shumway-Cook and Woollacott, 1995). The approximately vertical position is an imposed (or controlled) equilibrium since the natural dynamics of an uncontrolled inverted link-segment system are marginally stable at best. In addition, LQR provides a structured framework for relevant physiological interpretation since the performance criteria are always known and have meaning.

Only a few studies involving upright stance have utilized LQR control. He et al. (1991) first used this technique to simulate standing posture in a model of the cat hind limb controlled by 10 muscle-tendon actuators. During small platform perturbations, the LQR-controlled model was able to reproduce ground reaction forces similar to experimentally collected data. A investigation by Kuo (1995) employed the LQR to simulate postural strategy ("ankle strategy" or "hip strategy") selection during recovery from platform perturbations in humans. Adding to the LQR design, Kuo (2005) incorporated an optimal state estimator in a model of quiet stance that successfully predicted statistical properties of human sway. Recently, Qu et al. (2007) developed an LQR controlled model that included feedback time-delay. This model was used to predicted changes due to aging and fatigue in

parameters related to postural sway.

This investigation expands upon previous LQR-based approaches to postural modeling by introducing a nonlinear quadratic regulator (NQR) (Beeler, 2004) with time-delayed sensory feedback to simulate large magnitude postural perturbations. Most physiological systems exhibit a high degree of nonlinearity (Westwick and Kearney, 2003). In dynamical systems these nonlinearities, represented by higher order terms in the equations of motion (EOM), become more significant as the system kinematics exceed the linear operating region. Since large magnitude perturbations have a much broader kinematic range than the small magnitude perturbations (such as in Chapter 6), it becomes necessary to account for the nonlinearities of the EOM in the simulations.

Nonlinearities within physiological systems also exist in the mode of control (Westwick and Kearney, 2003). There are few methods to design nonlinear controllers, most of which are dependent upon particular characteristics of the system such as the nature of the nonlinearities or the size of the system (Beeler et al., 2000). When more generalized control structures are used such as artificial neural networks, fuzzy control, and other "black box" methods, the resulting parameters have little meaning and are difficult to interpret. In this study we attempt to implement a NQR that has meaningful and interpretable parameters.

The NQR used in this investigation is based upon the state-dependent Riccati equation (SDRE), which has gained attention in recent years as a useful method of design (Banks et al.; Beeler, 2004; Beeler et al., 2000; Bogdanov, 2004; Friedland, 1996; Shamma and Cloutier, 2001). The SDRE is an extension of the familiar algebraic Riccati equation to nonlinear systems. It differs in that the coefficients in the solution of the SDRE are functions of the state instead of being constant valued (Beeler et al., 2000). Likewise, it is reasonable to assume that the neural controller in the human body is state-dependent since the state information is readily available to the neural controller.

The purpose of this study was to accurately simulate experimentally recorded kinematics during the response to large postural perturbations. A method of system identification

similar to that used during small perturbations (Chapter 6) was employed to parameterize a sagittal plane model of the human body that is controlled with a nonlinear controller. We hypothesized that the SDRE would be able to accurately reproduce the recorded kinematics during large perturbations. If successful, this method of the nonlinear system identification may be used to gain insight into the neural control of upright stance without making potentially limiting assumptions of linearity in the equations of motion and neural controller.

8.2 Methods

In all but a few details the experimental procedure was similar to that in Chapters 3 & 6, and will only be summarized here. Ballistic pendulums were used to administer anteriorly-directed (AD) and posteriorly-directed (PD) postural perturbations in the mid-sagittal plane. Each pendulum was pulled back from the participant and individually released from a distance that corresponded to a specified AD or PD velocity just before impact. Perturbation magnitude was defined as the linear momentum just before impact. For each series of perturbation, an equal number of AD and PD perturbations were administered in a random order. The participant was allowed to complete the balance recovery motion before the subsequent perturbation began. Instructions to "stand in a relaxed manner" were given to the participant before and during each series of perturbations (Allum et al., 2002; Otten, 1999).

The experiment began with an initial series of 20 moderately low magnitude (10 N·s AD, 7 N·s PD) perturbations to allow any adaptation to occur. Afterward, the maximum perturbation that could be withstood without stepping was determined by applying a series of AD and PD perturbations beginning at 6 N·s AD and 5 N·s PD and increasing incrementally by 2 N·s AD and 1 N·s PD after each successful recovery without stepping. Sixteen perturbations were then administered at a perturbation magnitude of 4 N·s and 2 N·s below the maximal AD and PD perturbations that could be withstood without stepping, respectively.

During the experiment the participant was instrumented with five pairs of reflective

markers that were placed on the shoulders, greater trochanters, ankles, calcaneous, and 5th metatarsal joints (Vicon Motion Analysis System, Lake Forest, CA). Marker position data were sampled at 100 Hz and low-pass filtered at 5 Hz (3rd order zero-phase-lag Butterworth) during post-processing. A sagittal plane representation of the body was formed by averaging each marker pair and creating three body segments (foot, lower body, upper body) that were defined by angles relative to the adjacent inferior segment (Figure 8.1). An inline load cell (Cooper Instruments and Systems, Warrenton, VA) was attached to the pendulum to determine perturbation onset time and time series of force magnitude for implementation into the dynamic simulations.

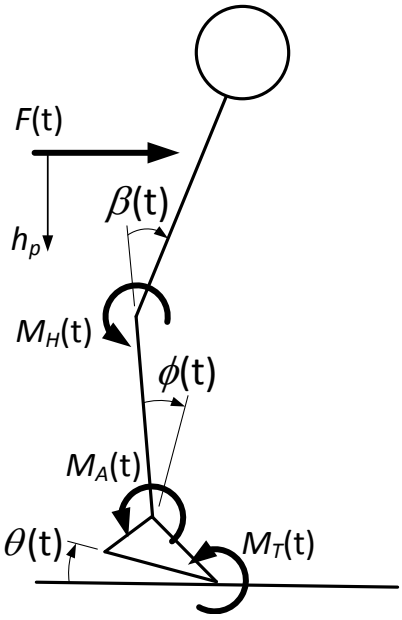

Figure 8.1: Free body diagram of the human model (i.e., the plant). $F(t)$ represents the experimentally recorded pendulum force applied to the participant. $M_T(t)$, $M_A(t)$, and $M_H(t)$ are the corrective torques produced by the neural controller. $\theta(t)$, $\phi(t)$, and $\beta(t)$ are relative segment angles of the foot, lower body, and upper body. h_P is the height of the pendulum upon contact with the participant.

8.2.1 Equations of motion

A 2D three degree of freedom link segment dynamic model was used to simulate the perturbations. The three segments included in the model were foot, lower body, and upper body (note: the foot and lower body segment accounted for the left and right feet and legs, respectively). Derivation of the equations of motion was accomplished with the Lagrangian method based on the kinetic energy, potential energy, and dissipation functions in the following equations:

$$\frac{d}{dt}\left(\frac{\partial T}{\partial \dot{q}}\right) - \frac{\partial T}{\partial q} + \frac{\partial V}{\partial q} + \frac{\partial D}{\partial \dot{q}} = Q_q^* \tag{8.1}$$

where generalized coordinates, q, were θ, ϕ, and β (Figure 8.1). Kinetic energy and potential energy scalars were defined as

$$T = \frac{1}{2}\left(m_F \mathbf{v}_F \cdot \mathbf{v}_F + I_F \boldsymbol{\omega}_F \cdot \boldsymbol{\omega}_F\right) + \frac{1}{2}\left(m_{LB} \mathbf{v}_{LB} \cdot \mathbf{v}_{LB} + I_{LB} \boldsymbol{\omega}_{LB} \cdot \boldsymbol{\omega}_{LB}\right) + \frac{1}{2}\left(m_{UB} \mathbf{v}_{UB} \cdot \mathbf{v}_{UB} + I_{UB} \boldsymbol{\omega}_{UB} \cdot \boldsymbol{\omega}_{UB}\right) \tag{8.2}$$

and

$$V = g\left(m_F \mathbf{r}_F + m_{LB} \mathbf{r}_{LB} + m_{UB} \mathbf{r}_{UB}\right) \cdot \mathbf{n}_1 + \frac{1}{2} K_A \phi^2 + \frac{1}{2} K_H \beta^2 \tag{8.3}$$

where subscripts F, LB, and UB denote the foot, lower body, and upper body segments included in the model; m is the mass and I is the moment of inertia about the center of mass of each segment; $\mathbf{r}$, $\mathbf{v}$, and $\boldsymbol{\omega}$ are the position, linear velocity, and angular velocity vectors, respectively, calculated from an inertial coordinate system; g is the gravitational acceleration; $\mathbf{n}_1$ is the vertical unit vector; and K_A and K_H represent the instrinsic stiffness constants about the ankle and hip, respectively. The value of K_A was taken from Hof (1998).

The dissipation constant was calculated as

$$D = \frac{1}{2}B_A\dot{\phi}^2 + \frac{1}{2}B_H\dot{\beta}^2 \tag{8.4}$$

where B_A and B_H are the intrinsic damping constants at the ankle and hip, respectively. B_A was calculated using the formula from Loram et al. (2001) as

$$B_A = 0.76\sqrt{4J_BK_A} \tag{8.5}$$

where J_B is the moment of inertia of the body about the ankle joint. Since intrinsic stiffness and damping values for the hip were not available, K_H and B_H were estimated to be 50% of K_A and B_A, respectively.

The generalized forces Q_j^* were calculated to be

$$\begin{aligned} Q_\theta^* &= Fh_p - M_T \\ Q_\phi^* &= F(h_p - h_A\cos\theta - d_A\sin\theta) - M_A \\ Q_\beta^* &= F(h_p - h_A\cos\theta - h_H\cos(\theta+\phi) - d_A\sin\theta) - M_H \end{aligned} \tag{8.6}$$

where F is the recorded pendulum force; h_p is the pendulum height above the ground; h_A is the vertical distance to the height joint; d_A is the horizontal distance from the 5^{th} metatarsal to the ankle joint, h_H is the distance from ankle to hip; M_T, M_A, and M_H are the controlling joint torques at the toe, ankle, and hip joints, respectively. The resulting equations of motion were decoupled with respect to acceleration and placed in the following matrix form:

$$\begin{Bmatrix} \ddot{\theta} \\ \ddot{\phi} \\ \ddot{\beta} \end{Bmatrix} = \mathbf{M}^{-1}\mathbf{f}\left(\theta, \dot{\theta}, \phi, \dot{\phi}, \beta, \dot{\beta}\right) + \mathbf{M}^{-1}\begin{Bmatrix} Q_\theta^* \\ Q_\phi^* \\ Q_\beta^* \end{Bmatrix} \tag{8.7}$$

where $\mathbf{M}^{-1} \in \mathbb{R}^{3\times3}$ is the inverse of the mass matrix, $\mathbf{M}^{-1}\mathbf{f}\left(\theta, \dot{\theta}, \phi, \dot{\phi}, \beta, \dot{\beta}\right)$ describes the transient state-dependent components of acceleration, and $\mathbf{M}^{-1}[\ Q_\theta^* \quad Q_\phi^* \quad Q_\beta^*\ ]^T$ describes the forced dynamics.

The simulation began with the heel in contact with the ground. In this situation, the dynamic equations are reduced to two segments (lower body, upper body). When a positive toe torque is required to keep the foot on the ground, the dynamics change so that the foot is unconstrained and it makes a smooth transition off the ground. When the heel comes back into contact with the ground we assumed a pure plastic impact in which the angular momentum of the system about the 5^{th} metatarsal joint and the ankle joint is conserved according to:

$$\mathbf{H}^- \begin{Bmatrix} \dot{\theta}^- \\ \dot{\phi}^- \\ \dot{\beta}^- \end{Bmatrix} = \mathbf{H}^+ \begin{Bmatrix} \dot{\phi}^+ \\ \dot{\beta}^+ \end{Bmatrix} \tag{8.8}$$

where (-) denotes the instant before heel contact and (+) denotes the instant after heel contact; $\mathbf{H}^- \in \mathbb{R}^{2\times3}$ and $\mathbf{H}^+ \in \mathbb{R}^{2\times2}$ are matrices that map the segmental velocities to angular momenta calculated about the 5^{th} metatarsal joint and the ankle joint.

The dynamics were placed into state-dependent coefficient (SDC) form for implementation into the neural controller (see below). SDC form is a nonlinear realization that has an appearance similar to the familiar linear matrix form $\dot{\mathbf{x}} = \mathbf{A}\mathbf{x} + \mathbf{B}\mathbf{u}$; however, the state matrix and input matrix are each a function of the system state:

$$\begin{Bmatrix} \dot{\theta} \\ \ddot{\theta} \\ \dot{\phi} \\ \ddot{\phi} \\ \dot{\beta} \\ \ddot{\beta} \end{Bmatrix} = \mathbf{A}\left(\theta, \dot{\theta}, \phi, \dot{\phi}, \beta, \dot{\beta}\right) \begin{Bmatrix} \theta \\ \dot{\theta} \\ \phi \\ \dot{\phi} \\ \beta \\ \dot{\beta} \end{Bmatrix} + \mathbf{B}\left(\theta, \dot{\theta}, \phi, \dot{\phi}, \beta, \dot{\beta}\right) \begin{Bmatrix} M_T \\ M_A \\ M_H \end{Bmatrix} \tag{8.9}$$

For this reason, the SDC form is sometimes referred to as a "quasi-linearization", "apparent linearization", and "extended linearization" (Beeler, 2004). The SDC matrices $\mathbf{A}\left(\theta, \dot{\theta}, \phi, \dot{\phi}, \beta, \dot{\beta}\right)$ and $\mathbf{B}\left(\theta, \dot{\theta}, \phi, \dot{\phi}, \beta, \dot{\beta}\right)$ are not unique and must be carefully chosen. In this investigation, the coefficients in the state-dependent matrices were chosen in a manner that preserved most of the nonlinearities and avoided sparse matrices (see Appendix B).

8.2.2 Development of the state-dependent Riccati equation

The neural controller (Figure 8.2), which is responsible for central processing of sensory information in order to produce the controlling joint torques, was based on the SDRE. The SDRE represents a method of 'suboptimal' control based upon the algebraic Riccati equation (ARE).

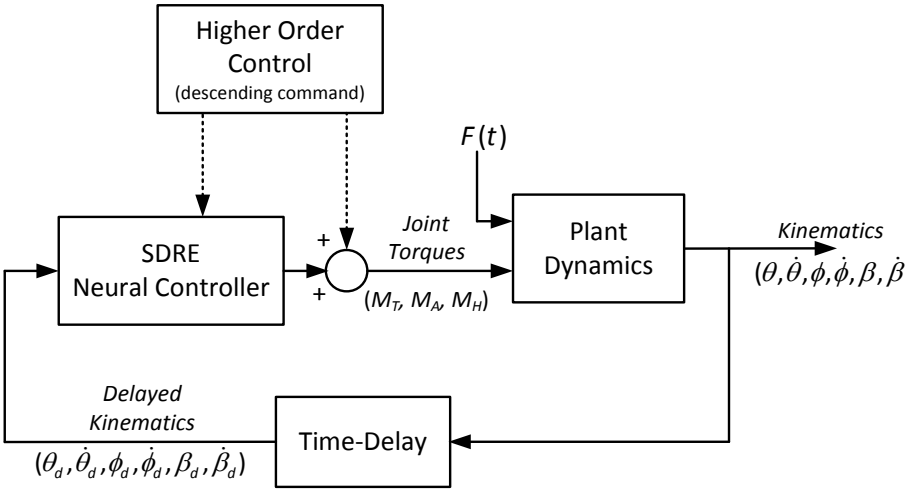

Figure 8.2: Schematic of the controlled system. The input into the system is the experimentally measured pendulum force, $F(t)$. The neural controller is based on the state-dependent Ricatti equation with a time-delayed input. The neural controller produced state-dependent corrective joint torques about the toe, ankle, and hip joint torques for maintenance of upright stance. The higher order control represents to the neural controller such as adjustments in reference angles, performance parameters within the $\mathbf{Q}$ and $\mathbf{R}$ matrices, and voluntary joint torque control. Higher order control was not included in the current model.

Recall from Chapter 7 that the solution to the ARE was used to compute the optimal full-state feedback gains for the regulator problem in a system with steady-state linear dynamics

of the form

$$\dot{\mathbf{x}} = \mathbf{A}\mathbf{x} + \mathbf{B}\mathbf{u} \tag{8.10}$$

where $\mathbf{x} \in \mathbb{R}^n$ is a vector containing the n system states, $\mathbf{u} \in \mathbb{R}^m$ is a vector of the system inputs, $\mathbf{A} \in \mathbb{R}^{n\times n}$ is the state matrix, and $\mathbf{B} \in \mathbb{R}^{n\times m}$ is the input matrix. The system is controlled with the optimal gain matrix $\mathbf{K} \in \mathbb{R}^{m\times n}$ by the control law

$$\mathbf{u}^* = -\mathbf{K}\mathbf{x} \tag{8.11}$$

where

$$\mathbf{K} = \mathbf{R}^{-1}\mathbf{B}^T\bar{\mathbf{\Gamma}} \tag{8.12}$$

and $\bar{\mathbf{\Gamma}} \in \mathbb{R}^{n\times n}$ is the solution to the ARE

$$\mathbf{A}^T\bar{\mathbf{\Gamma}} + \bar{\mathbf{\Gamma}}\mathbf{A} + \mathbf{Q} - \bar{\mathbf{\Gamma}}\mathbf{B}\mathbf{R}^{-1}\mathbf{B}^T\bar{\mathbf{\Gamma}} = \mathbf{0} \tag{8.13}$$

The matrices $\mathbf{Q} \in \mathbb{R}^{n\times n}$ and $\mathbf{R} \in \mathbb{R}^{m\times m}$ penalize the state and control according to the scalar function

$$\int_0^{t_f} \mathbf{x}^T\mathbf{Q}\mathbf{x} + \mathbf{u}^T\mathbf{R}\mathbf{u}dt \tag{8.14}$$

the values of which are typically set by the design engineer to affect the response characteristics of the system.

To arrive at the SDRE, the plant dynamics must be placed into SDC form

$$\dot{\mathbf{x}} = \mathbf{A}(\mathbf{x})\mathbf{x} + \mathbf{B}(\mathbf{x})\mathbf{u} \tag{8.15}$$

Substituting the SDC state and input matrices into the ARE gives

$$\mathbf{A}(\mathbf{x})^T\mathbf{\Gamma}(\mathbf{x}) + \mathbf{\Gamma}(\mathbf{x})\mathbf{A}(\mathbf{x}) + \mathbf{Q} - \mathbf{\Gamma}(\mathbf{x})\mathbf{B}(\mathbf{x})\mathbf{R}^{-1}\mathbf{B}(\mathbf{x})^T\mathbf{\Gamma}(\mathbf{x}) = \mathbf{0} \tag{8.16}$$

In all systems but those with special structures, an analytic solution for $\mathbf{\Gamma}(\mathbf{x})$ does not exist (Banks et al.; Beeler et al., 2000). Therefore, $\mathbf{\Gamma}(\mathbf{x})$ must be calculated for each new state $\mathbf{x}$. Accordingly, yet another name for the SDRE is the "frozen Riccati equation" (Doyle et al., 1998). The resulting state feedback gains are then state-dependent and calculated for each new state as

$$\mathbf{K}(\mathbf{x}) = \mathbf{R}^{-1}\mathbf{B}(\mathbf{x})^T\mathbf{\Gamma}(\mathbf{x}) \tag{8.17}$$

and the control law becomes

$$\mathbf{u}^* = -\mathbf{K}(\mathbf{x})\mathbf{x} = -\mathbf{R}^{-1}\mathbf{B}(\mathbf{x})^T\mathbf{\Gamma}(\mathbf{x})\mathbf{x} \tag{8.18}$$

Although $\mathbf{K}(\mathbf{x})$ is the optimal set of gains for a particular state (i.e., a particular set of dynamic equations since $\mathbf{A}(\mathbf{x})$ and $\mathbf{B}(\mathbf{x})$), this control is considered to be suboptimal for a time interval over which the state changes (Beeler et al., 2000).

8.2.3 SDRE control with time-delayed feedback and position references

The derivation of the SDRE controller was based on a complete set of state information. In this experiment, kinematic information is readily available to the neural controller in the human body from redundant sensory feedback from the vestibular and somatosensory systems. Since this information must be transmitted from locations distal to the central processing center, an associated delay exists. Therefore, inputs to the neural controller in the simulations were delayed by τ_d seconds. In addition, reference angles for the lower body and upper body segments were incorporated to accommodate a forward lean during upright

stance. The three controlling joint torques were calculated as

$$\begin{Bmatrix} M_T \\ M_A \\ M_H \end{Bmatrix} = \mathbf{K}\left(\theta_d, \dot{\theta}_d, \phi_d, \dot{\phi}_d, \beta_d, \dot{\beta}_d\right) \begin{Bmatrix} \theta_d \\ \dot{\theta}_d \\ \phi_d - \phi_{ref} \\ \dot{\phi}_d \\ \beta_d - \beta_{ref} \\ \dot{\beta}_d \end{Bmatrix} \tag{8.19}$$

where $\mathbf{K}\left(\theta_d, \dot{\theta}_d, \phi_d, \dot{\phi}_d, \beta_d, \dot{\beta}_d\right)$ is a 3×6 matrix of feedback gains. The subscript d indicates a time-delay of 188 msec, which was the average time-delay value taken from the young group in Chapter 6.

8.2.4 Parameter Optimization

Six SDRE parameters and four reference angles were optimized from the first two perturbations in the series. The SDRE parameters included the diagonal elements of the matrix $\mathbf{Q}$ taken from (8.14), and the reference angles were ϕ_{ref} and β_{ref} from the two perturbations. Diagonal elements of $\mathbf{R}$ were fixed at 1.0, indicating that equal constraints were placed upon the each of the joint torques. To optimize these parameters the difference between the simulated and experimentally recorded segment angles were minimized via the scalar cost function

$$\sum_{n=1}^{pert}\left(\sum_{m=1}^{sample}\left[(\hat{\theta}_{mn} - \theta_{mn})^2 + (\hat{\phi}_{mn} - \phi_{mn})^2 + (\hat{\beta}_{mn} - \beta_{mn})^2\right]\right) \tag{8.20}$$

where $\hat{\theta}_{mn}$, $\hat{\phi}_{mn}$, and $\hat{\beta}_{mn}$ are the simulated foot, lower body, and upper body angles at data point m during perturbation n, and θ_{mn}, ϕ_{mn}, and β_{mn} are the experimentally recorded foot, lower body, and upper body angles at data point m during perturbation n. A Nelder-Mead search (Lagarias et al., 1998; Nelles, 2005) was used to perform the optimization. This algorithm has shown good results for optimizing neural controller parameters during

quiet stance (Maurer and Peterka, 2005) and small magnitude perturbations (Chapter 6). The simulations began at the time of perturbation onset, and lasted for 2.5 seconds. The simulation length was chosen to allow sufficient time to fully recover an upright position following the perturbation. All simulations were performed in Fortran90 (Intel Fortran Compiler 9.1, San Jose, CA).

8.2.5 Simulations

Recorded angular position data and pendulum force data from two participants randomly chosen from the young group were used to test the nonlinear controlled model. Participant specific inertial parameters calculated using Pavol et al. (2002) and de Leva (1996) and measured anthropometry were used in the equations of motion.

The Nelder-Mead search is a local nonlinear search. As with all searches of this type, the algorithm is iterative, and to converge on the global (or a physiologically relevant) minimum, selection of the seed parameters must be based upon prior experience (Nelles, 2005). Here we considered the postural strategies involved in recovery from large magnitude perturbations. Runge et al. (1999) demonstrated that as the magnitude of postural perturbations increases, participants enact more of a "hip strategy." We assumed that parameters corresponding to a "hip strategy" include lower penalizing coefficients for the upper body kinematics (q_{55} and q_{66}) relative to those values used for the lower body kinematics (q_{33} and q_{44}). In addition, the foot kinematics were heavily penalized relative to the lower body and upper body segments (Table 8.1).

8.3 Results

Before expanding the simulations to represent two perturbations, fitting a single perturbation was attempted. Using the parameters from Table 8.1, the scalar cost function from (8.20) reduced from 296.28 to 2.77 in approximately 2000 iterations (Figure 8.3). Most of the

Table 8.1: Parameter seed and specifications for Nelder-Mead search. A hip strategy with little foot movement was assumed by enacting a relationship such that q_{11}, $q_{22} \gg q_{33}$, $q_{44} > q_{55}$, q_{66}. Initial Step Size refers to the step taken during the first series of simplexes based on each parameter.

Parameter	Starting Value	Initial Step Size
Performance function		
q_{11} (rad^{-1})	10^5	10^3
q_{22} ($\text{rad}^{-1}\cdot\text{sec}$)	10^5	10^3
q_{33} (rad^{-1})	10^3	10^2
q_{44} ($\text{rad}^{-1}\cdot\text{sec}$)	10^3	10^2
q_{55} (rad^{-1})	10^2	10^2
q_{66} ($\text{rad}^{-1}\cdot\text{sec}$)	10^2	10^2
Reference angles (for 2 perturbations)		
$\phi_{ref}(1,2)$ (rad)	0.05	0.1
$\beta_{ref}(1,2)$ (rad)	0.05	0.1

reduction occurred within the first 300 iterations, and then gradually settled into the final value.

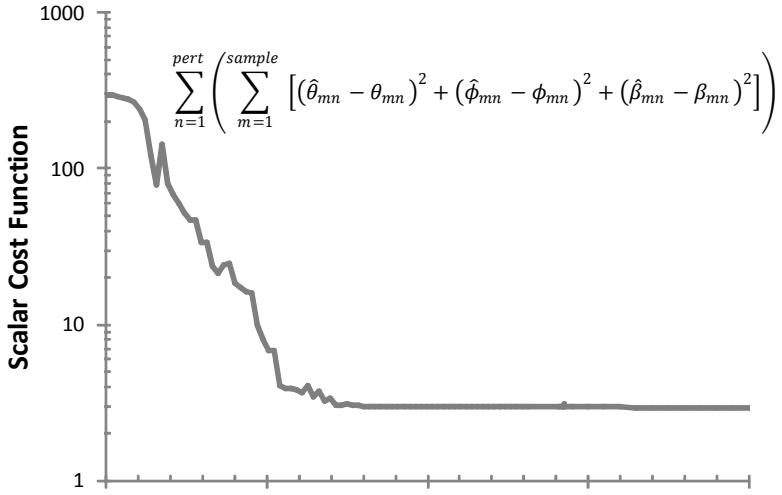

Figure 8.3: Plot of the scalar cost function versus number of iterations performed by the Nelder-Mead search. The cost function was based upon the sum of squared error in angular position across each sample and perturbation.

The optimized kinematic penalties ranged in order of magnitude from 10^1 to 10^5 (Table 8.2) and the optimized reference angles were $\phi_{ref} = -0.161$ rad ($-9.2°$) and $\beta_{ref} = -0.049$ rad ($-2.8°$). These penalties and reference angles enabled the simulation to maintain upright

stance following the perturbation. This is demonstrated by the attraction of the simulated kinematics toward equilibrium positions close to zero degrees (Figure 8.4).

Table 8.2: Values of the optimized state penalties for a single subject during a single large magnitude perturbation.

State variable	Optimized penalty
θ	72765
$\dot{\theta}$	333389
ϕ	7516
$\dot{\phi}$	13
β	1715
$\dot{\beta}$	537

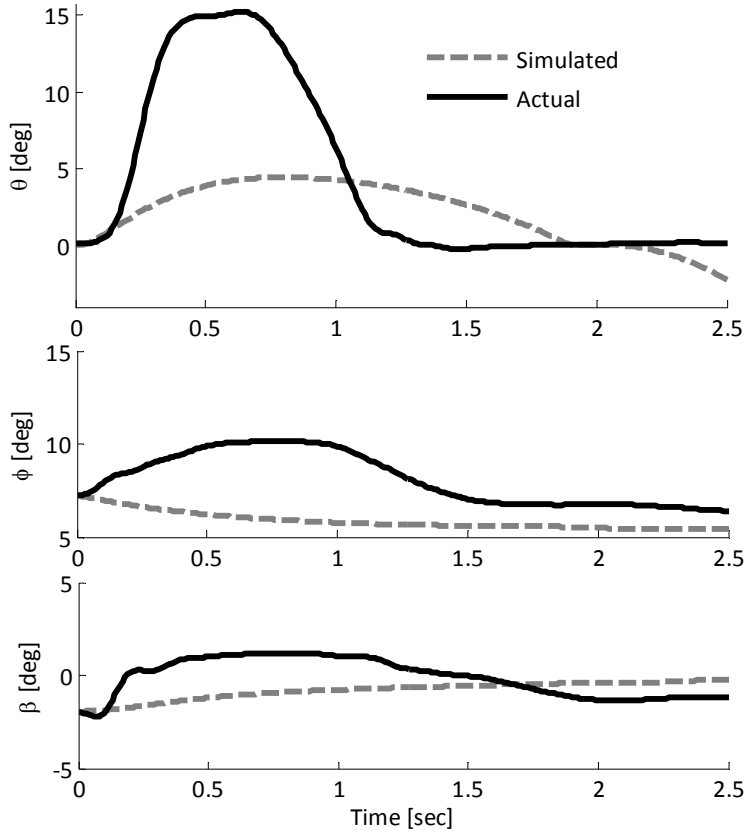

Figure 8.4: Simulated and experimental segment angles from a single subject during a large magnitude perturbation.

When the search criteria were expanded to encompass two perturbations, the solver minimized the scalar cost function found in (8.20) from 497.67 to 10.98. The model was

unable to simulate the experimental data with a high degree of accuracy, even showing unstable characteristics in some trajectories (Figure 8.5).

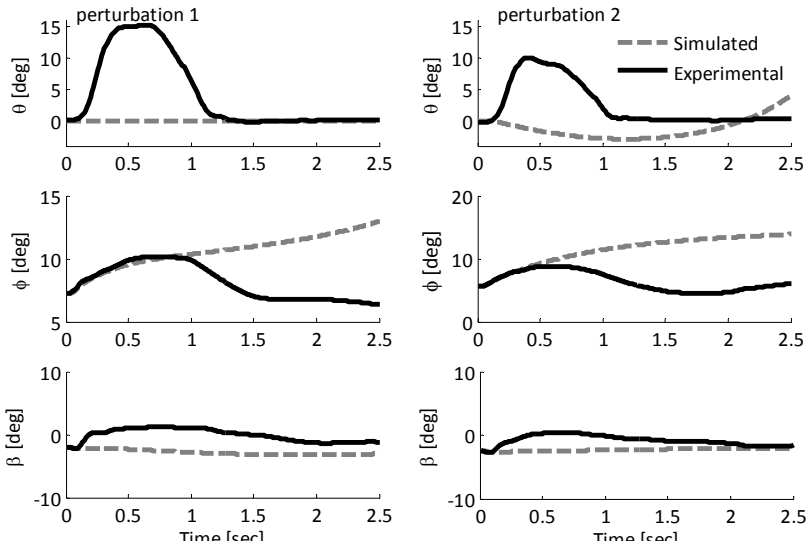

Figure 8.5: Simulated and experimental segment angles from a single subject during a series of two large magnitude perturbations. The simulated data was optimized using a scalar cost function that included data from both perturbations.

8.4 Discussion

This investigation focused on implementing an interpretable nonlinear neural controller in a model of the human body to simulate responses to large magnitude postural perturbations. The neural controller generated toe, ankle, and hip torques based upon time-delayed state-dependent feedback gains calculated using the SDRE. Parameters of the SDRE were optimized based a Nelder-Mead search, but were unsuccessful at accurately simulating the experimentally recorded kinematics. This approach was successful at stabilizing the system with the given parameter seed when considering a single perturbation, but demonstrated poor stabilizing ability when additional perturbations were included. Regardless of the results of these simulations, we must note that it is not likely that upright stance is regulated by an explicit calculation of the Riccati equation within the postural control system. Investigations of upright stance with and without postural perturbations have had success when

using this type of control (He et al., 1991; Kuo, 2005, 1995; Qu et al., 2007). The advantage of using these techniques is that much is known about the behavior of these structures through frequent application in traditional control designs.

Several things may have contributed to the inaccurate results when using SDRE control. First, it is likely that a set of parameters that more accurately simulates the experimental data exists. This is due in part to the necessity to supply the Nelder-Mead search with a good parameters seed. In this investigation we assumed that a hip strategy was used in response to the large magnitude perturbations, and estimated the parameter seed accordingly. Although the initial parameter seed produced an optimized set of parameters with kinematics consistent with a hip strategy, the large number of parameters likely provides many combinations that produce similar strategies. To search the parameter space more efficiently, a simulated annealing algorithm was also implemented. With an identical parameter seed, the simulated annealing arrived at the same set of optimized parameters as the Nelder-Mead search. This provides assurance that the local minimum was found with the search, but does not guarantee that this local minimum is also the global minimum.

A second factor to consider is that of cognitive control. There is ample time within the 2.5 second window following the perturbation for cognitive, or descending, control to be activated and affect the response to the perturbations. The SDRE controls the system in a purely automatic fashion and has no explicit means of incorporating descending control. Even though there exists a wide parameter range with which to supply the system (in this case orders of magnitude from 10 to 105), the parameters remain constant throughout the perturbation and cannot account for descending motor commands initiated after the perturbation occurs.

Third, in order to arrange the equations of motion into SDC form, it was necessary to reduce the nonlinearities in the equations by linearizing some elements. Linearization essentially introduces error into the system, especially as the state kinematics deviate from the linear operating region. The SDRE controller, which was based upon SDC equations

of motion, may have lost some nonlinear components that contributed to the irregularities represented in the experimental data.

Any dynamical system with more than one state variable has multiple SDC realizations. This may have had significant effects on the controllability and stabilizability of the system. Controllability is defined as the ability to drive the system to a desired state within a given time limit, and is a *sufficient* condition for controlled stability in linear dynamical systems. This can be assessed by calculating the rank of the controllability matrix

$$\mathbf{M} = \begin{bmatrix} \mathbf{B} & \mathbf{AB} & \mathbf{A}^2\mathbf{B} & \cdots & \mathbf{A}^{n-1}\mathbf{B} \end{bmatrix} \tag{8.21}$$

where $\mathbf{M} \in \mathbb{R}^{n \times m}$ (Kwakernaak and Sivan, 1972). A system is considered to be controllable when M has full rank (i.e., rank($\mathbf{M}$) = n). When using the SDRE, the controllability matrix is state-dependent:

$$\mathbf{M}(\mathbf{x}) = \begin{bmatrix} \mathbf{B}(\mathbf{x}) & \mathbf{A}(\mathbf{x})\mathbf{B}(\mathbf{x}) & \mathbf{A}(\mathbf{x})^2\mathbf{B}(\mathbf{x}) & \cdots & \mathbf{A}(\mathbf{x})^{n-1}\mathbf{B}(\mathbf{x}) \end{bmatrix} \tag{8.22}$$

However, this is not *sufficient* to guarantee true controllability outside a small neighborhood near the equilibrium point (Hammett et al., 1998). This state-dependency also has implications on the stabilizability of the SDRE system, a *necessary* condition for stability. A system is considered to be stabilizable if the uncontrolled poles of the system are stable (i.e., poles contain a negative real part). Recently, a method of estimating stability regions in the SDRE using vector matrix norms has been proposed by Erdem and Alleyne (2002). However, this method required knowledge of the maximum and feedback minimum gains across the interested region and was not applicable in this investigation.

Finally, another potentially confounding factor is the addition of time-delay to the SDRE control. Current SDRE theory does not account for the addition of feedback time-delay, and further reduces the prospects for creating a stable system. Including time-delay is frequently

required to create valid models of biomechanical phenomena. However, using tools that consider the effects of time-delay in dynamical systems are not prevalent in biomechanical research and have largely been relegated to theoretical mathematicians. Perhaps future research in postural control will be more successful at solving problems like those encountered here by drawing on previous research on time-delayed systems.

One approach that holds great promise is to transform the dynamics into the Roesser state space form (Roesser, 1975) and then solve the quadratic regulator problem (see Appendix C). This approach incorporates the time-delayed dynamics into a hybrid discrete/continuous system that often referred to as a 2D system (Anderson et al., 1986). An optimal control law called the 2D matrix Riccati equation has be formulated for these equations (Klein and Ramirez, 2001; Yashiki and Matsumoto, 1998), and may be beneficial to control and identification of time-delayed systems similar to this investigation. Two main advantages emerge from this approach. First, uncertainties of controllability would be alleviated since the 2D matrix Riccati equation satisfies the conditions set forth in the matrix Lyapunov stability equations (Agathoklis and Foda, 1989; Anderson et al., 1986; Bliman, 2002). Second, parameterization of the optimal control problem could allow parameterization and interpretation of descending commands since the optimal control law considers penalties on both the current and time-delayed states.

8.5 Conclusions

In summary, responses to large magnitude postural perturbations were simulated using a three DOF model of the human body that was controlled by the SDRE. The model was able to stabilize a single perturbation. However, the results did not represent the experimental data with a high degree of accuracy, and the final parameters were not interpreted. Several sources of error may have contributed to these results that include: 1) an inability to initialize the optimizing algorithm with satisfactory parameters, 2) the presence of descending

cognitive control that was not accounted for in the neural controller, 4) inability to ensure controllability or stabilizability with SDC form and addition of time-delay in feedback. Finally, a brief description of a possible solution to this problem (and other time-delay systems) was presented using Roesser state space equations.

References

Agathoklis P, Foda S (1989) Stability and the matrix lyapunov equation for delay differential systems. *Int J Contr* 49(2): 417–432

Allum JH, Carpenter MG, Honegger F, Adkin AL, Bloem BR (2002) Age-dependent variations in the directional sensitivity of balance corrections and compensatory arm movements in man. *J Physiol* 542(Pt 2): 643–63

Anderson B, Agathoklis P, Jury E, Mansour M (1986) Stability of the matrix lyapunov equation for discrete 2-dimensional systems. *IEEE Proc-G* CAS-33(3): 261–267

Banks HT, Lewis BM, Tran HT: (????) Nonlinear feedback controllers and compensators:a state-dependent riccati equation approach. Technical report

Beeler S: (2004) State-dependent riccati equation regulation of systems with state and control nonlinearities. Technical report, NASA Langley Research Center / National Institute of Aerospace

Beeler S, Tran HT, Banks HT (2000) Feedback control methodologies for nonlinear systems. *J Optim Theory and App* 107(1): 1–33

Bliman P (2002) Lyapunov equation for hte stability of 2-d systems. *Multidim Syst Sign P* 13: 201–222

Bogdanov A: (2004) Optimal control of a double inverted pendulum on a cart. Technical report, Oregan Health Sciences University

Brenner DJ, Hlatky LR, Hahnfeldt PJ, Hall EJ, Sachs RK (1995) A convenient extension of the linear-quadratic model to include redistribution and reoxygenation. *Int J Radiat Oncol Biol Phys* 32(2): 379–90

de Leva P (1996) Adjustments to zatsiorsky-seluyanov's segment inertia parameters. *J Biomech* 29(9): 1223–30

Doyle J, Huang Y, Primbs J, Freeman R, Murray R: Nonlinear control: Comparison and case studies. In *American Control Conference* (Albuquerque, NM 1998)

Erdem E, Alleyne A: (2002) Estimation of stability regions of sdre controlled systems using vector norms

Friedland B: *Advanced Control System Design* (Englewood Cliffs, NJ: Prentice Hall 1996)

Gadkar KG, Varner J, Doyle F J r (2005) Model identification of signal transduction networks from data using a state regulator problem. *Syst Biol (Stevenage)* 2(1): 17–30

Hammett K, Hall C, Ridgely D (1998) Controllability issues in nonlinear state-dependent riccati equation control. *J Guid Cont Dyn* 21(5): 767–773

He J, Levine W, Loeb G (1991) Feedback gains for correcting small perturbations to standing posture. *IEEE Trans Auto Contr* 36(3): 322–332

Hof AL (1998) In vivo measurement of the series elasticity release curve of human triceps surae muscle. *J Biomech* 31(9): 793–800

Klein E, Ramirez W (2001) State controllability and optimal regulator control of time-delayed systems. *Int J Control* 74(3): 281–289

Kovacs L, Palancz B, Almassy Z, Benyo Z (2004) Optimal glucose-insulin control in h2 space. *Conf Proc IEEE Eng Med Biol Soc* 1: 762–5

Kuo AD (1995) An optimal control model for analyzing human postural balance. *IEEE Trans Biomed Eng* 42(1): 87–101

Kuo AD (2005) An optimal state estimation model of sensory integration in human postural balance. *J Neural Eng* 2(3): S235–49

Kwakernaak H, Sivan R: *Linear Optimal Control Systems* (New York: Wiley-Interscience 1972)

Lagarias J, Reeds J, Wright M, Wright P (1998) Convergence properties of the nelder-mead simplex method in low dimensions. *SIAM J Optim* 9: 112–147

Loram I, Kelly S, Lakie M (2001) Human balancing of an inverted pendulum: is sway size controlled by ankle impedance? *J Physiol* 532(Pt 3): 879–891

Matjacic Z, Bajd T (1998) Arm-free paraplegic standing–part i: Control model synthesis and simulation. *IEEE Trans Rehabil Eng* 6(2): 125–38

Maurer C, Peterka RJ (2005) A new interpretation of spontaneous sway measures based on a simple model of human postural control. *J Neurophysiol* 93(1): 189–200

Nelles O: *Nonlinear System Identification* (Berlin: Springer 2005)

Otten E (1999) Balancing on a narrow ridge: biomechanics and control. *Philos Trans R Soc Lond B Biol Sci* 354(1385): 869–75

Pavol MJ, Owings TM, Grabiner MD (2002) Body segment inertial parameter estimation for the general population of older adults. *J Biomech* 35(5): 707–12

Qu X, Nussbaum MA, Madigan ML (2007) A balance control model of quiet upright stance based on an optimal control strategy. *J Biomech*

Roesser P (1975) A discrete time state-space model for linear image processing. *IEEE Trans Auto Contr* AC-20(1): 1–10

Runge CF, Shupert CL, Horak FB, Zajac FE (1999) Ankle and hip postural strategies defined by joint torques. *Gait Posture* 10(2): 161–70

Shamma J, Cloutier J: (2001) Existance of sdre stabilizing feeedback

Shumway-Cook A, Woollacott M: *Motor Control: Theory and Practical Applications* (Baltimore: Williams and Wilkins 1995)

Vanne A, Hynynen K (2003) Mri feedback temperature control for focused ultrasound surgery. *Phys Med Biol* 48(1): 31–43

Westwick D, Kearney R: *Identification of nonlinear physiological systems* (Piscataway, NJ: IEEE Press 2003)

Yashiki S, Matsumoto N (1998) Stabilization and optimal regulator problem for time-delay systems based on the 2d riccati matrix equation. *Electron Comm Jpn 3* 81(1): 1–8

Chapter 9

Study contributions and directions for future work

Contributions

A series of studies was presented that focused on the recovery of upright stance from sagittal plane postural perturbations. The first study investigated the effects of localized muscle fatigue (LMF) and age on balance recovery from a postural perturbation without stepping. Changes in center of mass (COM)-based measures indicated a decreased ability to recover from the perturbations without stepping following LMF. In addition, changes in center of pressure (COP)-based measures indicated an altered postural strategy with LMF that are compatible with previous findings. This investigation expanded on the experimental basis of LMF effects on perturbed stance by interpreting the COM- and COP-based measures alongside each other within the context of balance recovery.

The second study investigated neural control of upright stance during small magnitude postural perturbations with aging and LMF. The neural controller was identified using a single degree of freedom feedback-controlled model of the human body. Identified parameters included proportional gain, differential gain, and time-delay. Robustness was evaluated by considering the delay margins of the identified system. The identified parameters revealed that the older population exhibited higher time-delay and a higher differential gain. The higher differential gain contributed to greater robustness as indicated by the delay margins. No changes in neural controller gains, time-delay, or delay margin with LMF were found in either age group. In addition to evaluating the effects of aging and LMF on neural control, this investigation expanded on current models of upright stance by accounting for the forward

lean present during upright stance and also with the addition of a novel time-delay stability analysis.

The third study explored the application of the state-dependent Riccati equation (SDRE), a method of nonlinear feedback control, to the neural control of upright stance during large magnitude perturbations. A three degree of freedom model with a movable foot was developed and controlled with a time-delayed SDRE. The structure of SDRE control allows meaningful interpretation of the parameters – a property not often available in nonlinear systems. Although the optimization converged upon a stable set of parameters, the approach was unsuccessful at accurately simulating the experimental data. Some reasons for this may include: insufficient choices for initial parameters, cognitive control that was unaccounted for in the model, linearizations in the state-dependent coefficient dynamics, and the inability to ensure controllability with the SDRE due to the combination of state-dependent dynamics and the time-delay.

Future directions

Future directions for this research include developing interventions to mitigate the effects of LMF on balance recovery. These interventions could be tested in the laboratory; however, it would also be beneficial to increase the external validity of the laboratory experiments. This could be accomplished by using tasks performed by workers in high FFH risk environments and/or creating a virtual environment that provides visual stimuli like those encountered when working at elevation.

It is also necessary to continue using postural models to gain insight into the neural controller. Current models contain many assumptions about the sensory dynamics, central processing, and descending motor control commands. As we begin to understand more about the neural control of upright stance and fill in these gaps, more complex models may be developed that have the capability to account for LMF or aging in an explicit manner.

Appendix A

Laboratory setup

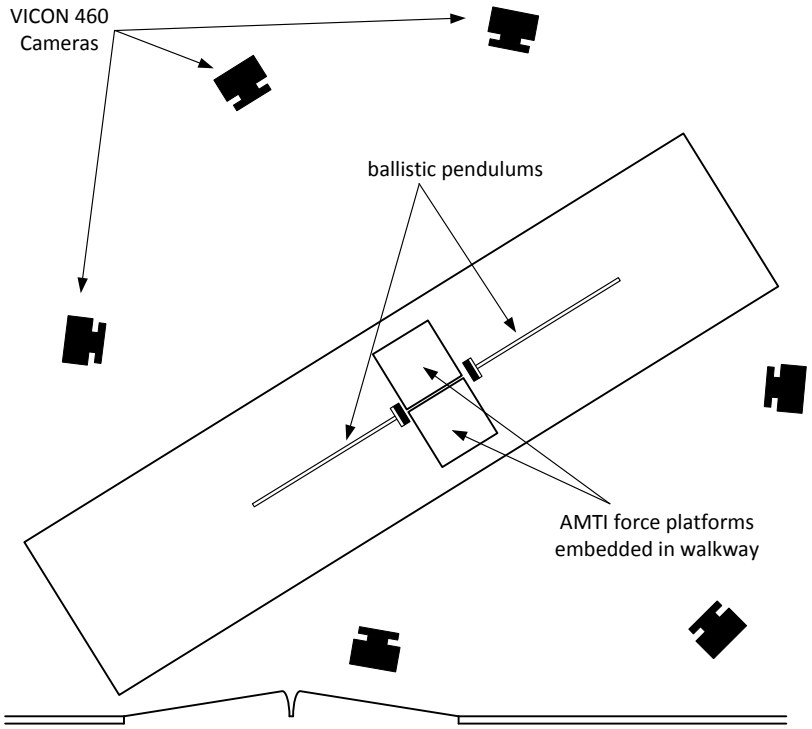

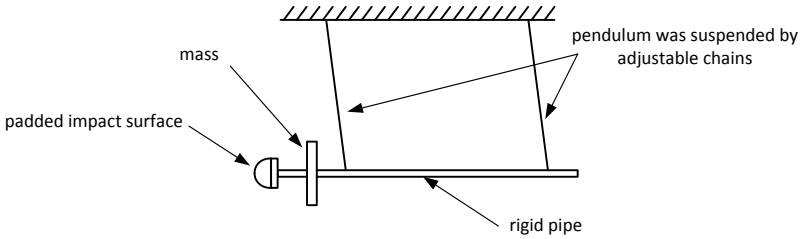

Pendulum Details

Appendix B

State-dependent coefficient dynamics

The state-dependent coefficient form used in Chapter 8 is couched in the following format:

$$\dot{\mathbf{x}} = \mathbf{A}(\mathbf{x})\mathbf{x} + \mathbf{B}(\mathbf{x})\mathbf{u} \tag{B.1}$$

where

$$\mathbf{x} = \begin{Bmatrix} \theta \\ \dot{\theta} \\ \phi \\ \dot{\phi} \\ \beta \\ \dot{\beta} \end{Bmatrix} \quad \text{and} \quad \mathbf{u} = \begin{Bmatrix} M_T \\ M_A \\ M_H \end{Bmatrix}$$

$\mathbf{A}(\mathbf{x})$ and $\mathbf{B}(\mathbf{x})$ are called the state-dependent coefficient state matrix and input matrix, respectively. Coefficients of these matrices were chosen in a systematic manner such that 1) most nonlinear terms were preserved and 2) creating a sparse matrix was avoided if possible. The 1^{st}, 3^{rd}, and 5^{th} rows in each of the matrices were populated with zeros and ones so that

they defined three identity equations on $\dot{\theta}$, $\dot{\phi}$, and $\dot{\beta}$ as follows:

$$\begin{Bmatrix} \dot{\theta} \\ \ddot{\theta} \\ \dot{\phi} \\ \ddot{\phi} \\ \dot{\beta} \\ \ddot{\beta} \end{Bmatrix} = \begin{bmatrix} 0 & 1 & 0 & 0 & 0 & 0 \\ \cdot & \cdot & \cdot & \cdot & \cdot & \cdot \\ 0 & 0 & 0 & 1 & 0 & 0 \\ \cdot & \cdot & \cdot & \cdot & \cdot & \cdot \\ 0 & 0 & 0 & 0 & 0 & 1 \\ \cdot & \cdot & \cdot & \cdot & \cdot & \cdot \end{bmatrix} \begin{Bmatrix} \theta \\ \dot{\theta} \\ \phi \\ \dot{\phi} \\ \beta \\ \dot{\beta} \end{Bmatrix} + \begin{bmatrix} 0 & 0 & 0 \\ \cdot & \cdot & \cdot \\ 0 & 0 & 0 \\ \cdot & \cdot & \cdot \\ 0 & 0 & 0 \\ \cdot & \cdot & \cdot \end{bmatrix} \begin{Bmatrix} M_T \\ M_A \\ M_H \end{Bmatrix} \tag{B.2}$$

where the dots represent the state dependent coefficients outlined in the following paragraphs.

First, the equations of motion were decoupled into three acceleration equations. All products and powers in the equations were expanded, and the individual components of each term were ordered as follows:

scalar coefficient x cosine operators x sine operators x state variable

When a state variable was present as a simple multiplier on the term, the term was divided by the state variable and the result was added to the state matrix in the row corresponding to the proper acceleration equation and the column to be multiplied by the state variable. When a state variable was not present as simple multiplier, a partial linearization was necessary to create a state variable multiplier. This was performed on only a single instance of the sine operator (Table B.1) to minimize the effects of the linearization. After the partial linearization (and creation of a state variable multiplier) the procedure continued as described above. The three rows in the input matrix containing state-dependent terms are populated with the corresponding rows of the inverse state-dependent mass matrix.

Table B.1: Terms from the acceleration equations to be linearized (if necessary) and used in the state matrix in the column corresponding to the variable linearized around. The state variables are arranged in the same column order as the state matrix.

θ	$\dot{\theta}$	ϕ	$\dot{\phi}$	β	$\dot{\beta}$
$\sin\theta$	$\dot{\theta}\dot{\phi}$	$\sin\phi$	$\dot{\beta}\dot{\phi}$	$\sin\beta$	$\dot{\beta}\dot{\theta}$
$\sin^2\beta\sin\theta$		$\sin^2\beta$		$\sin(\phi+\beta)$	
$\sin(\theta+\phi)$		$\sin(2\beta)\sin\theta$		$\sin(\theta+\phi)$	
$\sin(\theta+\phi+\beta)$		$\sin(\theta+\beta)$		$\sin(\theta+\phi+\beta)$	
$\sin\theta\sin\beta$		$\sin\phi$		$\sin\beta\sin\phi$	
		$\sin(\theta+\phi+\beta)$		$\sin\theta\sin\phi$	
		$\sin\beta\sin\theta$		$\sin\beta\sin\theta\sin\phi$	
		$\sin\beta\sin\phi$		$\sin^2\phi$	

Appendix C

Optimal control using Roesser state space equations

It has been estimated that central feedback time-delays of over 150 msec during the neural control of balance (Cordo et al., 1994). When modeling time-delayed systems such as this it is essential that the model to account for the time-delay present within the system in order to predict the true dynamics of the system. Only in recent years has time-delay gained more presence become within postural modeling. With it comes its own set of difficulties.

The time-delayed component is often included as an afterthought within the dynamic formulation via the numerical solver used. To our knowledge, only one investigation has integrally incorporated time-delay into the dynamics of balance control (Qu et al., 2007), and Chapter 6 provided the first use of time-delay when considering stability of the neurally-controlled system.

Typically the solution to the optimal regulator problem with time-delay has involved solving simultaneous partial differential based on the infinite dimensional Riccati equation, which is computationally very expensive to calculate (Ramirez, 1994). Yashiki and Matsumoto (1998) proposed a solution to the optimally regulator problem with time-delay in SISO systems by using a hybrid discrete/continuous Riccati equation. Klein and Ramirez (2001) expanded this work to encompass multi-input multi-output (MIMO) situations in addition to multiple time-delays.

In the following sections the Roesser state space form of dynamical equations are introduced. Next, an optimal solution is developed by formulating the hybrid discrete/continuous Ricatti equation. Finally, a method for solving the problem is presented.

Roesser state space form

First, the dynamics must be transformed into the contiuous/discrete state space form first proposed by Roesser (1975). To do this, pseudo-states are introduced that are equivalent to the delayed portions of the original states. For example, take the SISO system

$$\dot{x}(t) = a_0 x(x) + a_1 x(t - \tau_d) + b_0 u(t) + b_1 u(t - \tau_d) \tag{C.1}$$

where x is the state variable, u is the input, t is time, and τ_d is a constant time-delay. The Roesser state space form of this equation is expressed as the following 2D system

$$\begin{Bmatrix} x_1(t + \tau_d) \\ \dot{x}_2(t) \end{Bmatrix} = \begin{bmatrix} 0 & a_1 \\ 1 & a_0 \end{bmatrix} \begin{Bmatrix} x_1(t + \tau_d) \\ x_2(t) \end{Bmatrix} + \begin{Bmatrix} b_1 \\ b_0 \end{Bmatrix} u(t) \tag{C.2}$$

where $x_1(t)$ is the pseudo-state and is defined as the delayed portion of (C.1) such that

$$x_1(t) = a_1 x(t - \tau_d) + b_1 u(t - \tau_d) \tag{C.3}$$

and

$$x_2(t) = x(t) \tag{C.4}$$

This can be expanded to multivariable systems with a single time-delay such as

$$\dot{\mathbf{x}}(t) = \mathbf{A}_0 \mathbf{x}(t) + \mathbf{A}_1 \mathbf{x}(t - \tau_d) + \mathbf{B}_0 \mathbf{u}(t) + \mathbf{B}_1 \mathbf{u}(t - \tau_d) \tag{C.5}$$

where $\mathbf{x} \in \mathbb{R}^n$ is the state vector, $\mathbf{u} \in \mathbb{R}^m$ is the input vector, $\mathbf{A}_0 \in \mathbb{R}^{n \times n}$ and $\mathbf{A}_1 \in \mathbb{R}^{n \times n}$ are the non-delayed and delayed state matrices, respectively, and $\mathbf{B}_0 \in \mathbb{R}^{n \times m}$ and $\mathbf{B}_1 0 \in \mathbb{R}^{n \times m}$ are the non-delayed and delayed input matrices, respectively. In the Roesser form, this

becomes

$$\left\{ \begin{array}{c} \mathbf{x}_1(t+\tau_d) \\ \dot{\mathbf{x}}_2(t) \end{array} \right\} = \left[\begin{array}{cc} \mathbf{0} & \mathbf{A}_1 \\ \mathbf{I} & \mathbf{A}_0 \end{array} \right] \left\{ \begin{array}{c} \mathbf{x}_1(t+\tau_d) \\ \mathbf{x}_2(t) \end{array} \right\} + \left\{ \begin{array}{c} \mathbf{B}_1 \\ \mathbf{B}_0 \end{array} \right\} \mathbf{u}(t) \tag{C.6}$$

where $x_1(t)$ is the pseudo-state and is defined as the delayed portion of (C.1) such that

$$\mathbf{x}_1(t) = \mathbf{A}_1\mathbf{x}(t-\tau_d) + \mathbf{B}_1\mathbf{u}(t-\tau_d) \tag{C.7}$$

and

$$\mathbf{x}_2(t) = \mathbf{x}(t) \tag{C.8}$$

The state equations can be partitioned into discrete and continuous portions

$$\left\{ \begin{array}{c} \tilde{\mathbf{x}}_d(t+\tau_d) \\ \dot{\tilde{\mathbf{x}}}_c(t) \end{array} \right\} = \left[\begin{array}{cc} \tilde{\mathbf{A}}_{11} & \tilde{\mathbf{A}}_{12} \\ \tilde{\mathbf{A}}_{21} & \tilde{\mathbf{A}}_{22} \end{array} \right] \left\{ \begin{array}{c} \tilde{\mathbf{x}}_d(t) \\ \tilde{\mathbf{x}}_c(t) \end{array} \right\} + \left\{ \begin{array}{c} \tilde{\mathbf{B}}_1 \\ \tilde{\mathbf{B}}_0 \end{array} \right\} \tilde{\mathbf{u}}(t) \tag{C.9}$$

We define $\tilde{\mathbf{A}} \in \mathbb{R}^{(n+d)\times(n+d)}$ and $\tilde{\mathbf{B}} \in \mathbb{R}^{(n+d)\times m}$ as

$$\tilde{\mathbf{A}} = \left[\begin{array}{cc} \tilde{\mathbf{A}}_{11} & \tilde{\mathbf{A}}_{12} \\ \tilde{\mathbf{A}}_{21} & \tilde{\mathbf{A}}_{22} \end{array} \right] \quad \text{and} \quad \tilde{\mathbf{B}} = \left\{ \begin{array}{c} \tilde{\mathbf{B}}_1 \\ \tilde{\mathbf{B}}_0 \end{array} \right\} \tag{C.10}$$

If $\tilde{\mathbf{A}}$ and $\tilde{\mathbf{B}}$ are state-invariant, then controllability can be tested using the controllability matrix

$$\tilde{\mathbf{C}} = \left[\begin{array}{cccc} \tilde{\mathbf{B}} & \tilde{\mathbf{A}}\tilde{\mathbf{B}} & \cdots & \tilde{\mathbf{A}}^{n+d-1}\tilde{\mathbf{B}} \end{array} \right] \tag{C.11}$$

Optimal control of the Roesser equations

The optimal regulator problem in this scheme takes the same form as in Chapter 7. The quadratic cost function is defined as

$$\int_0^{t_f} \tilde{\mathbf{x}}(t)^T \tilde{\mathbf{Q}} \tilde{\mathbf{x}}(t) + \tilde{\mathbf{u}}(t)^T \tilde{\mathbf{R}} \tilde{\mathbf{u}}(t) dt \tag{C.12}$$

where $\tilde{\mathbf{x}}(t) = [\ \tilde{\mathbf{x}}_c \quad \tilde{\mathbf{x}}_d(t)\ ]^T$ The resulting hybrid discrete/continuous Riccati equation is

$$\begin{aligned} \tilde{\mathbf{A}}^T \tilde{\mathbf{\Gamma}}^c + \tilde{\mathbf{\Gamma}}^c \tilde{\mathbf{A}} + \tilde{\mathbf{A}}^T \tilde{\mathbf{\Gamma}}^d \tilde{\mathbf{A}} - \tilde{\mathbf{\Gamma}}^d - [\tilde{\mathbf{B}}^T (\tilde{\mathbf{\Gamma}}^c + \tilde{\mathbf{\Gamma}}^d \tilde{\mathbf{A}})]^T \\ \times (\tilde{\mathbf{B}}^T \tilde{\mathbf{\Gamma}}^d \tilde{\mathbf{B}} + \tilde{\mathbf{R}})^{-1} [\tilde{\mathbf{B}}^T (\tilde{\mathbf{\Gamma}}^c + \tilde{\mathbf{\Gamma}}^d \tilde{\mathbf{A}})] = -\tilde{\mathbf{Q}} \end{aligned} \tag{C.13}$$

where

$$\tilde{\mathbf{\Gamma}}^d = \begin{bmatrix} \tilde{\mathbf{\Gamma}}_1 & \mathbf{0} \\ \mathbf{0} & \mathbf{0} \end{bmatrix} \quad \text{and} \quad \tilde{\mathbf{\Gamma}}^c = \begin{bmatrix} \mathbf{0} & \mathbf{0} \\ \mathbf{0} & \tilde{\mathbf{\Gamma}}_2 \end{bmatrix} \tag{C.14}$$

the solution to this equation is used in providing the optimal control to the time-delay delayed system in the familiar form

$$\tilde{\mathbf{u}}(t) = -\tilde{\mathbf{K}} \tilde{\mathbf{x}} \tag{C.15}$$

where

$$\tilde{\mathbf{K}} = (\tilde{\mathbf{R}} + \tilde{\mathbf{B}}^T \tilde{\mathbf{\Gamma}}^d \tilde{\mathbf{B}})^{-1} [\tilde{\mathbf{B}}^T (\tilde{\mathbf{\Gamma}}^c + \tilde{\mathbf{\Gamma}}^d \tilde{\mathbf{A}})] \tag{C.16}$$

Solving the hybrid discrete/continuous Riccati equation

When (C.13), the hybrid Riccati Equation, is closely examined we discover two familiar structures. The (1,1) portion of the equation is the discrete algebraic Riccati equation.

Likewise, the (2,2) portion is the continuous algebraic Riccati equation, which was presented in great detail in Chapter 7. The solutions to these equations are well-known (Dorato, 1971; Dorato et al., 2000).

Once the matrix diagonal portions of (C.13) are solved, the solutions must satisfy the (1,2) and (2,1) portions. If the solutions do not satisfy the matrix off-diagonal portions, Klein and Ramirez (2001) have presented a unique method of reweighting the state matrix $\tilde{\mathbf{Q}}$ that satisfies the entire system.

System stability is assured if either

$$\begin{bmatrix} \tilde{\mathbf{Q}} & \mathbf{0} \\ \mathbf{0} & \tilde{\mathbf{R}} \end{bmatrix} > 0 \tag{C.17}$$

or

$$\tilde{\mathbf{Q}} + \tilde{\mathbf{\Gamma}}^T \tilde{\mathbf{R}} \tilde{\mathbf{\Gamma}} > \mathbf{0} \tag{C.18}$$

where (C.18) is the Lyapunov matrix equation (Agathoklis and Foda, 1989; Anderson et al., 1986; Bliman, 2002).

Appendix D

Institutional Review Board approval

Virginia Tech
VIRGINIA POLYTECHNIC INSTITUTE
AND STATE UNIVERSITY

Institutional Review Board

Dr. David M. Moore
IRB (Human Subjects) Chair
Assistant Vice President for Research Compliance
1880 Pratt Drive, Suite 2006(0497), Blacksburg, VA 24061
Office: 540/231-4991; FAX: 540/231-0959
email: moored@vt.edu

DATE: November 15, 2005

MEMORANDUM

TO: Michael L. Madigan Engineering Science & Mechanics 0219
Maury A. Nussbaum ISE 0118

FROM: David Moore

SUBJECT: **IRB Expedited Continuation**: "Risk Factors and Controls for Falls from Heights((Effects of Localized Muscle Fatigue on Balance-2)" IRB # 05-694 ref. 04-638

This memo is regarding the above referenced protocol which was previously granted expedited approval by the IRB on January 15, 2005. The proposed research is eligible for expedited review according to the specifications authorized by 45 CFR 46.110 and 21 CFR 56.110. Pursuant to your request of last week, as Chair of the Virginia Tech Institutional Review Board, I have granted approval for extension of the study for a period of 12 months, effective as of January 15, 2006.

Approval of your research by the IRB provides the appropriate review as required by federal and state laws regarding human subject research. It is your responsibility to report to the IRB any adverse reactions that can be attributed to this study.

To continue the project past the 12-month approval period, a continuing review application must be submitted (30) days prior to the anniversary of the original approval date and a summary of the project to date must be provided. Our office will send you a reminder of this (60) days prior to the anniversary date.

Virginia Tech has an approved Federal Wide Assurance (FWA00000572, exp. 7/20/07) on file with OHRP, and its IRB Registration Number is IRB00000667.

cc: File

Appendix E

Informed consent

VIRGINIA POLYTECHNIC INSTITUTE AND STATE UNIVERSITY

Informed Consent for Participants
In Research Projects Involving Human Subjects

Title of the Research Study
Project 1 – Effects of Localized Muscle Fatigue on Balance
Experiment 2 – Balance After a Dynamic Postural Perturbation

Investigators
Maury A. Nussbaum, Ph.D. 231-6053 – Department of Industrial and Systems Engineering
Michael L. Madigan, Ph.D. 231-1215 – Department of Engineering Science and Mechanics

I. Purpose of this Study
The purpose of this research study is to measure the effects muscle fatigue on balance. Falls from heights are a major problem in both industry and general society when measured in terms of human suffering and economic losses. Muscle fatigue has been recently shown to influence balance, and fatigue at the ankle, knee, lower torso, and shoulder are particular concerns because they are common during physical labor. The findings from this research study will contribute to the development of practical interventions aimed at minimizing the effect of fatigue on balance and decreasing the risk of falls.

II. Procedures
A total of 40 adult subjects will be used for the study.

The study will take place in either the Industrial Ergonomic Lab (Department of Industrial and Systems Engineering) or the Musculoskeletal Biomechanics Lab (Department of Engineering Science and Mechanics). Upon arriving, you will be briefed of the study protocol, asked if you have any further questions, and asked to sign this informed consent form.

During the experiment, you will be asked to perform two main tasks numerous times. The first task will involve you standing still on a force platform. While standing, you will be gently "nudged" numerous times in the upper back or upper chest. You are to try to recover your balance from this nudge without stepping. Data collected during this nudge will provide the investigators a measure of your balance. The second task will involve you performing exercises on a Biodex System (similar to a health club-type exercise apparatus). The investigators will provide detailed instructions on what to do throughout both tasks of the experiment.

You will be asked to complete three experimental sessions, once for a training session, once to fatigue your ankle, and once to fatigue your lower torso. Each of these will be on different days separated by at least 48 hours to prevent potential carry-over effects. Each experimental session is expected to take approximately 2 hours to complete.

III. Risks
The risks to involved in this study are minimal. The overall physical exertion required during this experiment is not significantly larger than that required during common manual labor.

IV. Benefits
You will receive no direct benefit from participating in this study. The scientific community will benefit through the additional information that is expected to result from the completion of this study. This information will contribute to fall-related biomechanical knowledge that will be used to develop intervention techniques to prevent falls from heights.

No promise or guarantee of benefits has been made to encourage you to participate.

V. Extent of Anonymity and Confidentiality
The results of this research study may be presented at meetings or in publications. Your identity will not be disclosed in those presentations. All subjects will be identified based only on their unique identifying number. Only the investigators and students involved in the research will have access to these identifying numbers. The video recordings from this study will be analyzed and stored in the labs under the supervision of the investigators. Some photographs or video recordings may be shown to other scientists at the University or at scientific conferences.

VI. Compensation
You will be paid $10/hour for your participation in this study.

VII. Freedom to Withdraw
Your participation in this research study is voluntary. Refusal to participate will involve no penalty or loss of benefits to which you are otherwise entitled. You are free to withdraw from the study at any time without penalty.

VIII. Approval of Research
This research project has been approved, as required, by the Institutional Review Board for Research Involving Human Subjects at Virginia Polytechnic Institute and State University.

IRB Approval Date: January 15, 2005.

Approval Expiration Date: January 14, 2007.

IX. Subject Responsibilities
I voluntarily agree to participate in this study.

X. Subject's Permission
I have read and understand the Informed Consent and conditions of this project. I have had all my questions answered. I hereby acknowledge the above and give my voluntary consent:

_____ _____
Subject signature Date

_____ _____
Witness Date

Should I have any pertinent questions about this research or its conduct, and research subjects' rights, and whom to contact in the event of a research related injury to the subject, I may contact:

Principal Investigator:	Maury Nussbaum, PhD	231-6053	nussbaum@vt.edu
Co-Investigator:	Michael Madigan, PhD	231-1215	mlmadigan@vt.edu
Chair, IRB:	David M. Moore, DVM	231-4991	moored@vt.edu

Appendix F

Data collection sheets

This section includes data collection sheets from the Practice Session (parts 1 & 2) and the Low Back session. The Ankle session data collection sheets are identical to the Low Back session except for the following elements:

- The data recording area during fatiguing exercises differs slightly in teh Ankle section due to different means of recording the maximum voluntary contraction
- The Low Back session contains two additional series of perturbations in the eyes open and eyes closed conditions

Name: _____ Practice Session
Number: _____
Date: _____
Session: _____

R-01 STUDY
Practice Session (Part 1) Setup Checklist

1. Turn on: (allow 30 minutes to warm up)
   - ☐ Vicon datastation
   - Force Platform Amplifiers
     - ☐ AMTI 1
     - ☐ AMTI 2
   - ☐ Load cell amplifiers
2. ☐ Open workstation software and create Vicon directory with subject name and session name (*Practice*)
3. ☐ Move camera if necessary (plug in cord to splitter box)
4. ☐ Change load cell cable if necessary
5. ☐ Calibrate Vicon Cameras
   - Make sure calibration is adequate:
     - System > Calibrate cameras
     - wand visibility > 70 %
     - static reproducibility < 1.0%
6. Check Vicon data collection settings
   - ☐ System > Video Setup
     - video sampling rate: 100 Hz
   - ☐ System > Analog Setup
     - analog sampling rate: 1000 Hz
     - collection channels: 1-21 (apply to current session)
7. ☐ Place reflective markers on pendulum
8. ☐ Ensure that force platforms are not in contact with walking platform
9. ☐ Secure and mark poster sheet on force platform, prepare soft surface
10. Autobalance equipment:
    - ☐ Load Cell Amplifiers
11. ☐ Complete randomization details on data collection sheet

R-01 STUDY
Practice Session (part 1) Collection Sheets

Subject name: _____ Date: _____

1. ☐ Record beginning time: _____
2. ☐ Give summary of protocol and demonstrate
3. ☐ Give subject proper clothing in which to change (shorts, tank top) and ask if they need to use the restroom
4. ☐ Ask subject to remove shoes
5. ☐ Position participant on force platform and trace outline of feet on poster sheet

6. ☐ Apply reflective markers: [*(sm)* denotes small marker]

☐ right head	☐ right greater troch	☐ right maleolus *(sm)*
☐ left head	☐ left greater troch	☐ left maleolus *(sm)*
☐ right jaw	☐ right thigh	☐ right heel *(sm)*
☐ left jaw	☐ left thigh	☐ left heel *(sm)*
☐ right shoulder	☐ right lateral epicondile	☐ right 5th meta *(sm)*
☐ left shoulder	☐ left lateral epicondile	☐ left 5th meta *(sm)*
☐ right iliac crest	☐ right shin	☐ C7
☐ left iliac crest	☐ left shin	

7. ☐ Collect baseline force platform signals
   (trial type: *baseline analog*)

   Data is saved as: *sub#_P_1*

   comments: _____

8. ☐ Collect static marker calibration
   (trial type: *subject calibration*)

   Data is saved as: *sub#_P_2*

   comments: _____

9. ☐ Label subject markers in Vicon (*trial > create autolabel calibration , save trial*)

☐ 10. Static Sway Collections (3 replications of each condition)

EOH – eyes open/hard surface ECH – eyes closed/hard surface
EOS – eyes open soft surface ECS – eyes closed/soft surface
ROM – Romberg stance UNI – unilateral stance

There are 18 total collections in which the order appearance is completely randomized according to the sequence #.

Record time using a stopwatch for Romberg and unilateral stances. Romberg and unilateral stances are to be self-selected concerning foot placement, but must remain consistent after selection. Be sure to monitor participant closely during Romberg and unilateral stances.

Instruct participant to, "Remain as still as possible".

Data is saved as: *sub#_P_sway_#*

collection:	condition:	time:	
1	_____	_____	comments: _____
2	_____	_____	comments: _____
3	_____	_____	comments: _____
4	_____	_____	comments: _____
5	_____	_____	comments: _____
6	_____	_____	comments: _____
7	_____	_____	comments: _____
8	_____	_____	comments: _____
9	_____	_____	comments: _____
10	_____	_____	comments: _____
11	_____	_____	comments: _____
12	_____	_____	comments: _____
13	_____	_____	comments: _____
14	_____	_____	comments: _____
15	_____	_____	comments: _____
16	_____	_____	comments: _____
17	_____	_____	comments: _____
18	_____	_____	comments: _____

☐ 11. Static and Dynamic Stability

Data is saved as: *sub#_P_stab_#*

Static Stability: (3 sec collection)

1 _____ comments: _____
2 _____ comments: _____
3 _____ comments: _____
4 _____ comments: _____
5 _____ comments: _____
6 _____ comments: _____
7 _____ comments: _____
8 _____ comments: _____
9 _____ comments: _____
10 _____ comments: _____
11 _____ comments: _____
12 _____ comments: _____

Dynamic Stability (AP): (20 sec collection)

13 _____ comments: _____
14 _____ comments: _____
15 _____ comments: _____
16 _____ comments: _____
17 _____ comments: _____
18 _____ comments: _____

☐ 12. Adjust height of pendulums and record
behind height: _____ cm front height: _____ cm
Adjust position of pendulums to accommodate a 10 cm gap between both front and back of participant and record
behind position: _____ cm front position: _____ cm

☐ 13. Perturbation Adaptation (perturb.vi – blue)
Apply 20 moderate level perturbations to habituate the participant. All will be applied at levels 3 (10 N·s) and 3 (7 N·s) for forwards and backwards, respectively (randomized direction).

VICON data is saved as: *sub#_P_adapt*

Tell participant to, "Stand in a relaxed manner. Try not to step, and try to keep your feet flat on the ground at all times."

perturbation:	direction:	
1	F	comments: _____
2	F	comments: _____
3	B	comments: _____
4	B	comments: _____
5	F	comments: _____
6	B	comments: _____
7	F	comments: _____
8	F	comments: _____
9	B	comments: _____
10	B	comments: _____
11	B	comments: _____
12	F	comments: _____
13	B	comments: _____
14	F	comments: _____
15	B	comments: _____
16	B	comments: _____
17	F	comments: _____
18	F	comments: _____
19	F	comments: _____
20	B	comments: _____

☐ 14. Initial Perturbations to Step

VICON data is saved as: *sub#_P_step*
Remind participant to, "Remain completely relaxed, and try not to step."
Collection #: 2a
EMG Column #: ___

collection:	direction:	F mag:	B mag:	comments:	2b:
1	F	1		_____	B
2	F	2			F
3	B		1		F
4	F	3			B
5	B		2	_____	F
6	B		3		F
7	F	4			B
8	B		4		B
9	F	5			F
10	B		5		F
11	F	6		_____	F
12	F	7			B
13	B		6		B
14	F	8			F
15	B		7		B
16	F	9		_____	B
17	F	10			F
18	B		8	_____	B
19	B		9	_____	F
20	B		10		B
21	F	11		_____	
22	F	12			
23	B		11	_____	
24	B		12		
25	F				
26	B		____		

F: _____ B: _____

15. Unfatigued Dynamic Collections (perturb_back.vi – blue)
Forward Level: _____ Backward Level: _____

Collection #: 3b
EMG Column #: ___

perturbation:	direction:	
1	B	comments: _____
2	F	comments: _____
3	F	comments: _____
4	B	comments: _____
5	F	comments: _____
6	F	comments: _____
7	B	comments: _____
8	B	comments: _____
9	F	comments: _____
10	F	comments: _____
11	F	comments: _____
12	B	comments: _____
13	B	comments: _____
14	F	comments: _____
15	B	comments: _____
16	B	comments: _____
17	F	comments: _____
18	B	comments: _____
19	F	comments: _____
20	B	comments: _____

☐ 16. Remove reflective markers from participant

☐ 17. Correctly set up and record Biodex positions for Torso, Thigh, and Leg:

Torso:
(1-3) C: _____ Dynamometer Position
(5-7) D: _____ Dynamometer Height
(1-2) _____ Attachment Setting
(75-80) _____ Pelvic Height

Thigh:
_____45_____ Dynamometer Rotation
J: _____45_____ Seat Rotation
K: _____85_____ Backrest Rotation (relative to seat)
(0-1) C: _____ Dynamometer Position
(1-2) D: _____ Dynamometer Height
(18-19) E: _____ Chair Platform adjustment
(5) F: _____ Seat Height
(3-4) G: _____ Lateral Position of backrest to seat
(12-13) _____ Attachment Setting

Plantar/Dorsi Flexion:
J: _____90_____ Seat Rotation
K: _____70_____ Backrest Rotation (relative to seat)
(15-17) C: _____ Dynamometer Position
(12-13) D: _____ Dynamometer Height
(24-27) E: _____ Chair Platform adjustment
(2-4) F: _____ Seat Height
(0-3) G: _____ Lateral Position of backrest to seat
(5-7) _____ Legrest Height
(6-7) _____ Attachment Setting
(0-3) _____ Attachment Foot Position

Inversion/Eversion:
J: _____90_____ Seat Rotation
K: _____70_____ Backrest Rotation (relative to seat)
_____65_____ Dynamometer Tilt
(-) C: _____ Dynamometer Position
(-) D: _____ Dynamometer Height
(-) E: _____ Chair Platform adjustment
(-) F: _____ Seat Height
(-) G: _____ Lateral Position of backrest to seat
(-) _____ Legrest Height
(-) _____ Attachment Setting
(-) _____ Attachment Foot Position

□ 18. Record end time: _____
□ 19. Turn off equipment:
- Vicon system
- force platform amplifiers (AMTI 1 & AMTI 2)
- load cell amplifiers
□ 20. Reapply adhesive to reflective markers
□ 21. Clean up the laboratory

General Comments:

_____
_____
_____
_____
_____
_____
_____

R-01 STUDY

Practice Session (Part 2) Setup Checklist

1. Turn on: (allow 30 minutes to warm up)
   - □ Biodex
   - □ EMG amplifier
   - Motor Equipment
     - □ CPU
     - □ Amplifier

□ 2. Open LabView VI's (equip_baseline_new.vi; EMG_max_P.vi; force_control.vi; reaction_time.vi; reflex.vi; proprioception.vi)
□ 3. Calculate Biodex baseline and scale factor for position and torque and enter the values into the open LabView VI's: (equip_baseline.vi – maroon)
   - Position Baseline _____ V
   - Position Scale Factor _____ Deg/V
   - Torque Baseline _____ V
   - Torque Scale Factor _____ N·m/V

□ 4. Enter subject #s, baseline and scale factor values in LabView VI's
□ 5. Get out supplies:
   - EMG electrodes
   - Co-flex
   - alcohol
   - razor
   - bathroom scale
   - athletic tape

□ 6. Initialize motor and set zero-position
□ 7. Complete randomization details on data collection sheet

R-01 STUDY

Practice Session (Part 2) Collection Sheets

Subject name: _____ Date: _____

☐ 1. Record beginning time: _____
☐ 2. Give summary of protocol and demonstrate
☐ 3. Obtain informed consent
☐ 4. Give subject proper clothing in which to change (shorts, tank top) and ask if they need to use the restroom
☐ 5. Ask subject to remove shoes
☐ 6. Collect anthropometric measurements:

age: _____ weight: _____ lbs height: _____ cm

Stance measurements taken during comfortable standing:

left length: _____cm left width: _____cm
right length: _____cm right width: _____cm
dist between malleoli: _____cm

Anthropometric Measurements (from Pavol et al., 2002):

head width:	_____	head diameter = (width+depth)/2:	
head depth:	_____	_____	h_{body}
head circumference:	_____	c_{head}	
neck circumference:	_____	c_{neck}	
C7 height:	_____	h_{C7}	
acromion height:	_____	h_{acr}	
shoulder height:	_____	h_{shl}	
shoulder-to-shoulder width:	_____	w_{shl}	
shoulder level trunk depth:	_____	D_{shl}	
chest height:	_____	h_{bst}	
chestlevel trunk width:	_____	w_{bst}	
chestlevel trunk depth:	_____	D_{bst}	
axis depth* at breast:	_____	δ_{bst}	
mid chest–L_3L_4 trunk width:	_____	w_{mid}	
mid chest–L_3L_4 trunk depth:	_____	D_{mid}	
axis depth* at mid chest–L_3L_4:	_____	δ_{mid}	
L_3L_4 height:	_____	h_{L34}	
L_3L_4 width:	_____	w_{L34}	
L_3L_4 depth:	_____	D_{L34}	
axis depth* at L_3L_4:	_____	δ_{L34}	
waist circumference:	_____	c_{waist}	
hip height:	_____	h_{hip}	
hip-to-shoulder angle**:	_____	θ_{hs}	
hip-level torso circumference:	_____	c_{hip}	
thigh length (hip to tibial plat)	_____	l_{thigh}	
mid-thigh circumference:	_____	c_{thigh}	
leg length (tibial plat to lat mal)	_____	l_{leg}	
leg maximum circumference:	_____	c_{leg}	
foot length	_____	l_{foot}	
lateral malleolus height:	_____	h_{ankle}	ASIS width: _____ w_{ASIS}
ankle width (lat to med mal):	_____	w_{ankle}	knee width: _____ w_{knee}

* measured depth, at the indicated height, between hip-to-shoulder axis and the surface of the back
** angle, from vertical in the sagittal plane, of the hip-to-shoulder axis when the trunk is erect; angle is positive when the shoulder is anterior to the hip

☐ 7. Body Fat %:

triceps:	_____	_____	_____	_____mm
subscapula:	_____	_____	_____	_____mm
abdomen:	_____	_____	_____	_____mm
suprailiac:	_____	_____	_____	_____mm
front thigh:	_____	_____	_____	_____mm
chest/rear thigh:	_____	_____	_____	_____mm

body fat percentage: _____ % sum: _____mm

☐ 8. Measure maximum grip strength using dominant hand and self-selected posture (3 trials separated by 1 minute rest)

grip 1: _____ N
grip 2: _____ N [circle best strength]
grip 3: _____ N

☐ 9. Apply EMG electrodes:
from *Introduction to Surface Electromyography* by Cram and Kasman

☐ L ref- tibial tuberosity
☐ L1- gastroc nemius (medially, upper half, vertical)
☐ L2- soleus (lateral, lower third of calf, near vertical plane)
☐ L3- tibialis anterior (one third down from knee, vertical plane)
☐ L4- peronius brevis (above lateral melleolus, vertical)

☐ 10. Correctly set up Biodex positions for leg and record EMG maximum for normalization:

☐ peronius brevis max absolute torque: _____
(ch L4) gain: _____

☐ gastroc/soleus max absolute torque: _____
(ch L1) gastroc gain: _____
(ch L2) soleus gain: _____

☐ anterior tibialis max absolute torque: _____
(ch L3) gain: _____

☐ 11. Ankle Force Control (force_control.vi – grey)

Force control test consists of the participant maintaining 10% isometric plantar flexion MVE for 1.25 minutes by matching lines on a visual display.

MVE: _____ (from above)

Press Collect and time with stopwatch for at least 3 minutes.
Data is saved as: *#_P_FC.txt*

R-01 STUDY
Practice Session (Part 2) Collection Sheets

Subject name: _____ Date: _____

☐ 1. Record beginning time: _____
☐ 2. Give summary of protocol and demonstrate
☐ 3. Obtain informed consent
☐ 4. Give subject proper clothing in which to change (shorts, tank top) and ask if they need to use the restroom
☐ 5. Ask subject to remove shoes
☐ 6. Collect anthropometric measurements:

age: _____ weight: _____ lbs height: _____ cm

Stance measurements taken during comfortable standing:

left length: _____cm left width: _____cm
right length: _____cm right width: _____cm
dist between malleoli: _____cm

Anthropometric Measurements (from Pavol et al., 2002):

head width:	_____	head diameter = (width+depth)/2:	
head depth:	_____	_____	h_{body}
head circumference:	_____	c_{head}	
neck circumference:	_____	c_{neck}	
C7 height:	_____	h_{C7}	
acromion height:	_____	h_{acr}	
shoulder height:	_____	h_{shl}	
shoulder-to-shoulder width:	_____	w_{shl}	
shoulder level trunk depth:	_____	D_{shl}	
chest height:	_____	h_{bst}	
chestlevel trunk width:	_____	w_{bst}	
chestlevel trunk depth:	_____	D_{bst}	
axis depth* at breast:	_____	δ_{bst}	
mid chest–L_3L_4 trunk width:	_____	w_{mid}	
mid chest–L_3L_4 trunk depth:	_____	D_{mid}	
axis depth* at mid chest–L_3L_4:	_____	δ_{mid}	
L_3L_4 height:	_____	h_{L34}	
L_3L_4 width:	_____	w_{L34}	
L_3L_4 depth:	_____	D_{L34}	
axis depth* at L_3L_4:	_____	δ_{L34}	
waist circumference:	_____	c_{waist}	
hip height:	_____	h_{hip}	
hip-to-shoulder angle**:	_____	θ_{hs}	
hip-level torso circumference:	_____	c_{hip}	
thigh length (hip to tibial plat)	_____	l_{thigh}	
mid-thigh circumference:	_____	c_{thigh}	
leg length (tibial plat to lat mal)	_____	l_{leg}	
leg maximum circumference:	_____	c_{leg}	
foot length	_____	l_{foot}	
lateral malleolus height:	_____	h_{ankle}	ASIS width: _____ w_{ASIS}
ankle width (lat to med mal):	_____	w_{ankle}	knee width: _____ w_{knee}

* measured depth, at the indicated height, between hip-to-shoulder axis and the surface of the back
** angle, from vertical in the sagittal plane, of the hip-to-shoulder axis when the trunk is erect; angle is positive when the shoulder is anterior to the hip

☐ 7. Body Fat %:

triceps:	_____	_____	_____	_____mm
subscapula:	_____	_____	_____	_____mm
abdomen:	_____	_____	_____	_____mm
suprailiac:	_____	_____	_____	_____mm
front thigh:	_____	_____	_____	_____mm
chest/rear thigh:	_____	_____	_____	_____mm

body fat percentage: _____ % sum: _____mm

☐ 8. Measure maximum grip strength using dominant hand and self-selected posture (3 trials separated by 1 minute rest)
grip 1: _____ N
grip 2: _____ N [circle best strength]
grip 3: _____ N

☐ 9. Apply EMG electrodes:
from *Introduction to Surface Electromyography* by Cram and Kasman
☐ L ref- tibial tuberosity
☐ L1- gastroc nemius (medially, upper half, vertical)
☐ L2- soleus (lateral, lower third of calf, near vertical plane)
☐ L3- tibialis anterior (one third down from knee, vertical plane)
☐ L4- peronius brevis (above lateral melleolus, vertical)

☐ 10. Correctly set up Biodex positions for leg and record EMG maximum for normalization:

☐ peronius brevis max absolute torque: _____
(ch L4) gain: _____

☐ gastroc/soleus max absolute torque: _____
(ch L1) gastroc gain: _____
(ch L2) soleus gain: _____

☐ anterior tibialis max absolute torque: _____
(ch L3) gain: _____

☐ 11. Ankle Force Control (force_control.vi – grey)
Force control test consists of the participant maintaining 10% isometric plantar flexion MVE for 1.25 minutes by matching lines on a visual display.

MVE: _____ (from above)

Press Collect and time with stopwatch for at least 3 minutes.
Data is saved as: *#_P_FC.txt*

□ 12. Reaction Time (reaction_time.vi – green)

While seated in the Biodex Chair with ankle attachment, the participant is required to immediately plantar flex when the signal appears on the monitor. Leg EMG and BIODEX torque data is recorded.

Repeat 3 times
Data is saved as: *#_P_RT.txt*

Be certain to adjust thigh support so that reaction only comes from leg muscles and not thigh muscles.

□ 13. Vibration Threshold
Place vibration actuator on achilles tendon and determine amplitude just below palpable level and record.
volume level: _____ (remember to take foot off of platform)

□ 14. Rotate BIODEX chair 90° and add spacers on JPS/JMS device to align ankle with axis
No. of spacers _____

□ 15. Ankle Reflex (reflex.vi – khaki)

Instruct the participant to close their eyes and remain completely relaxed throughout the test.

Repeat 3 times
Data is saved as: *#_P_REF.txt* note: readjust ankle between each test

Record first column numbers: (circle vibration tests 1-3[odd] or 4-6[even])
Test 1: _____ Test 4: _____
Test 2: _____ Test 5: _____
Test 3: _____ Test 6: _____

□ 16. Ankle Joint Position Sense (proprioception.vi – red)

While seated in the Biodex Chair (knee at 90°) and with eyes closed, the participant's foot is passively plantar flexed or dorsiflexed 15°. After returning to the starting position, the participant is asked to reposition the foot to that angle and accuracy is assessed.

Data is saved as: *#_P_PROP.txt*

<u>0° to 15° extension</u>

Non-vibration:
Passive Placement
Passive -First Column #: ___ comments: _____
__ Trial 1 – First Column #: ___ comments: _____
Trial 2 – First Column #: ___ comments: _____
Trial 3 – First Column #: ___ comments: _____
Vibration Trials:
Passive Placement
Passive -First Column #: ___ comments: _____
__ Trial 1 – First Column #: ___ comments: _____
Trial 2 – First Column #: ___ comments: _____
Trial 3 – First Column #: ___ comments: _____

<u>15° extension to 0°</u>
Non-vibration:
Passive Placement
Passive -First Column #: ___ comments: _____
__ Trial 1 – First Column #: ___ comments: _____
Trial 2 – First Column #: ___ comments: _____
Trial 3 – First Column #: ___ comments: _____
Vibration Trials:
Passive Placement
Passive -First Column #: ___ comments: _____
__ Trial 1 – First Column #: ___ comments: _____
Trial 2 – First Column #: ___ comments: _____
Trial 3 – First Column #: ___ comments: _____

□ 12. Reaction Time (reaction_time.vi – green)

While seated in the Biodex Chair with ankle attachment, the participant is required to immediately plantar flex when the signal appears on the monitor. Leg EMG and BIODEX torque data is recorded.

Repeat 3 times
Data is saved as: *#_P_RT.txt*

Be certain to adjust thigh support so that reaction only comes from leg muscles and not thigh muscles.

□ 13. Vibration Threshold
Place vibration actuator on achilles tendon and determine amplitude just below palpable level and record.
volume level: _____ (remember to take foot off of platform)

□ 14. Rotate BIODEX chair 90° and add spacers on JPS/JMS device to align ankle with axis
No. of spacers _____

□ 15. Ankle Reflex (reflex.vi – khaki)

Instruct the participant to close their eyes and remain completely relaxed throughout the test.

Repeat 3 times
Data is saved as: *#_P_REF.txt* note: readjust ankle between each test

Record first column numbers: (circle vibration tests 1-3[odd] or 4-6[even])
Test 1: _____ Test 4: _____
Test 2: _____ Test 5: _____
Test 3: _____ Test 6: _____

□ 16. Ankle Joint Position Sense (proprioception.vi – red)

While seated in the Biodex Chair (knee at 90°) and with eyes closed, the participant's foot is passively plantar flexed or dorsiflexed 15°. After returning to the starting position, the participant is asked to reposition the foot to that angle and accuracy is assessed.

Data is saved as: *#_P_PROP.txt*

<u>0° to 15° extension</u>

Non-vibration:
Passive Placement
Passive -First Column #: ___ comments: _____
__ Trial 1 – First Column #: ___ comments: _____
Trial 2 – First Column #: ___ comments: _____
Trial 3 – First Column #: ___ comments: _____
Vibration Trials:
Passive Placement
Passive -First Column #: ___ comments: _____
__ Trial 1 – First Column #: ___ comments: _____
Trial 2 – First Column #: ___ comments: _____
Trial 3 – First Column #: ___ comments: _____

<u>15° extension to 0°</u>
Non-vibration:
Passive Placement
Passive -First Column #: ___ comments: _____
__ Trial 1 – First Column #: ___ comments: _____
Trial 2 – First Column #: ___ comments: _____
Trial 3 – First Column #: ___ comments: _____
Vibration Trials:
Passive Placement
Passive -First Column #: ___ comments: _____
__ Trial 1 – First Column #: ___ comments: _____
Trial 2 – First Column #: ___ comments: _____
Trial 3 – First Column #: ___ comments: _____

Name: _____ Low Back Fatigue
Number: _____
Date: _____
Session: _____

R-01 STUDY
Low Back Fatigue Setup Checklist

1. Turn on: (allow 30 minutes to warm up)
   - ☐ Vicon datastation
   - ☐ EMG amplifier
   - ☐ Biodex
   - ☐ Load cell amplifiers
   - Force Platform Amplifiers:
     - ☐ AMTI 1
     - ☐ AMTI 2
2. ☐ Open workstation software and create Vicon directory with subject name and session name (*Back*)
3. ☐ Open LabView VI's (equip_baseline_new.vi; perturb_back.vi; body_part.vi; MVE_back.vi; EMG_back_submax_ses#.vi)
4. ☐ Calculate Biodex baseline and scale factor for position and torque and enter the values into the open LabView VI's: (equip_baseline.vi – maroon)
   - Position Baseline _____ V
   - Position Scale Factor _____ deg/V
   - Torque Baseline _____ V
   - Torque Scale Factor _____ N·m/V
5. ☐ Enter subject #s, baseline and scale factor values in LabView VI's
6. ☐ Enter maximum torque values into LabView VI's (if 3rd session)
7. ☐ Get out supplies:
   - EMG electrodes - razor - alcohol swabs
   - Co-flex - reflective markers
8. ☐ Move camera if necessary (plug in cord to splitter box)
9. ☐ Change load cell cable if necessary
10. ☐ Calibrate Vicon Cameras
    - Make sure calibration is adequate:
      - System > Calibrate cameras
      - wand visibility > 70 %
      - static reproducibility < 1.0%
11. Check Vicon data collection settings
    - ☐ System > Video Setup
      - video sampling rate: 100 Hz
    - ☐ System > Analog Setup
      - analog sampling rate: 1000 Hz
      - collection channels 1-21 (apply to current session)
12. ☐ Set up pendulums for desired height and perturbation according to Practice Session
    - behind: height – _____ front: height - _____
    - pos – _____ pos – _____
13. ☐ Place reflective markers on pendulum
14. ☐ Ensure that force platforms are not in contact with walking platform
15. ☐ Secure poster sheet on force platform
16. ☐ Autobalance Load Cell Amplifiers
17. ☐ Complete Biodex settings in collection packet
18. ☐ Correctly configure Biodex with torso attachment
19. ☐ Open subjects Excel Fatigue workbook

F: _____ B: _____ Last mod.4/27/06

R-01 STUDY
Low Back Fatigue Collection Sheets

Subject name: _____ Date: _____

1. ☐ Record beginning time: _____
2. ☐ Give subject proper clothing in which to change (shorts, tank top) and ask if they need to use the restroom
3. ☐ Ask subject to remove shoes
4. ☐ Apply EMG electrodes:
   from *Introduction to Surface Electromyography* by Cram and Kasman
   - ☐ L ref- tibial tuberosity
   - ☐ L1- soleus (lateral, lower third of calf, near vertical plane)
   - ☐ L2- tibialis anterior (one third down from knee, vertical plane)
   - ☐ R ref- head of fibula
   - ☐ R1- rectus abdominus (3 cm lateral to naval)
   - ☐ R2- erector spinae (4 cm lateral to L3 – even with iliac crest)
   - ☐ R3- vastus lateralis (lateral surface, 6 cm above kneecap, 20° from vert)
   - ☐ R4- biceps femoris (halfway between hip and knee)
5. ☐ Perform MVCs and set EMG gains: (EMG_back_submax_ses#.vi – orange)
   Data is saved as: *#_P_EMG.txt*

Torso:
☐ Correctly position participant in BIODEX with low back attachment

Settings –
C: _____ Dynamometer Position
D: _____ Dynamometer Height
_____ Attachment Setting
_____ Pelvic Height

☐ rectus abdominus (30° flexion) max absolute torque: _____
(ch R1) gain: _____

☐ erector spinae (30° flexion) max absolute torque: _____
(ch R2) gain: _____

Thigh:
☐ Correctly position participant in BIODEX with knee attachment

Settings –
____45_____ Dynamometer Rotation
J: ____45_____ Seat Rotation
K: ____85_____ Backrest Rotation (relative to seat)
C: _____ Dynamometer Position
D: _____ Dynamometer Height
E: _____ Chair Platform adjustment
F: _____ Seat Height
G: _____ Lateral Position of backrest to seat
_____ Attachment Setting

☐ vastus lateralis (45° flexion) max absolute torque: _____
(ch R3) gain: _____

☐ biceps femoris (45° flexion) max absolute torque: _____
(ch R4) gain: _____

Leg:

☐ Correctly position participant in BIODEX with ankle attachment (plantar-dorsi flexion) and record settings onto *Biodex Setup Sheet* (page 11).

J: ____90_____ Seat Rotation
K: ____70_____ Backrest Rotation (relative to seat)
C: _____ Dynamometer Position
D: _____ Dynamometer Height
E: _____ Chair Platform adjustment
F: _____ Seat Height
G: _____ Lateral Position of backrest to seat
_____ Legrest Height
_____ Attachment Setting
_____ Attachment Foot Setting

☐ gastroc/soleus max absolute torque: _____
(ch L1) gain: _____

☐ anterior tibialis max absolute torque: _____
(ch L2) gain: _____

☐ 6. Apply reflective markers: [*(sm)* denotes small marker]

☐ right head	☐ right greater troch	☐ right maleolus *(sm)*
☐ left head	☐ left greater troch	☐ left maleolus *(sm)*
☐ right jaw	☐ right thigh	☐ right heel *(sm)*
☐ left jaw	☐ left thigh	☐ left heel *(sm)*
☐ right shoulder	☐ right lateral epicondile	☐ right 5th meta *(sm)*
☐ left shoulder	☐ left lateral epicondile	☐ left 5th meta *(sm)*
☐ right iliac crest	☐ right shin	☐ C7
☐ left iliac crest	☐ left shin	

☐ 7. Collect baseline force platform signals (trial type: R01 *baseline analog*)
saved as: sub*#_B_base*

comments: _____

☐ 8. Collect static marker calibration (trial type: RO1 *subject calibration*)
saved as: *sub#_B_cal*

comments: _____

☐ 9. Label subject markers in Vicon (*trial > create autolabel calibration , save trial*)

☐ 10. Perturbation Adaptation (perturb_back.vi – blue)
Apply 12 moderate level perturbations to habituate the participant. All will be applied at levels 3 (10 N·s) and 3 (7 N·s) for forwards and backwards, respectively (randomized direction).
VICON data saved as: *sub#_B_#*
LabView data appended to: *#_B_pert_emg.txt*

Collection #: 1
EMG Column #: ___

Tell participant to, "Stand in a relaxed manner and try not to step."

perturbation:	direction:	
1	F	comments: _____
2	B	comments: _____
3	F	comments: _____
4	B	comments: _____
5	F	comments: _____
6	F	comments: _____
7	B	comments: _____
8	F	comments: _____
9	B	comments: _____
10	B	comments: _____
11	F	comments: _____
12	F	comments: _____
13	F	comments: _____
14	B	comments: _____
15	B	comments: _____
16	F	comments: _____
17	B	comments: _____
18	B	comments: _____
19	F	comments: _____
20	B	comments: _____

11. Unfatigued Low Level Perturbations

Forward Level: 1 Backward Level: 1

Collection #: 2
EMG Column #: ___

perturbation:	direction:	
1	B	comments: _____
2	F	comments: _____
3	F	comments: _____
4	B	comments: _____
5	F	comments: _____
6	B	comments: _____
7	F	comments: _____
8	F	comments: _____
9	B	comments: _____
10	B	comments: _____
11	B	comments: _____
12	F	comments: _____

_____
_____
_____
_____
_____
_____
_____
_____
_____

12. Unfatigued Perturbations to Step

Collection #: 3a
EMG Column #: ___

collection:	direction:	F mag:	B mag:	comments:	3b:
1	B		1	_____	F
2	B		2		B
3	F	1		_____	B
4	F	2			F
5	B		3		F
6	F	3			B
7	B		4	_____	B
8	B		5		B
9	F	4			F
10	B		6	_____	B
11	B		7		F
12	F	5			F
13	B		8	_____	F
14	B		9	_____	B
15	B		10		F
16	F	6		_____	B
17	F	7		_____	F
18	F	8			B
19	B		11		F
20	F	9			B
21	B		12		
22	F	10		_____	
23	F	11		_____	
24	F	12			
25	B				
26	F				

F: _____ B: _____

☐ 13. Unfatigued Dynamic Collections (perturb_back.vi – blue)
Forward Level: _____ Backward Level: _____

Collection #: 3b
EMG Column #: ___

perturbation:	direction:	
1	F	comments: _____
2	B	comments: _____
3	B	comments: _____
4	F	comments: _____
5	F	comments: _____
6	B	comments: _____
7	B	comments: _____
8	B	comments: _____
9	F	comments: _____
10	B	comments: _____
11	F	comments: _____
12	F	comments: _____
13	F	comments: _____
14	B	comments: _____
15	F	comments: _____
16	B	comments: _____
17	F	comments: _____
18	B	comments: _____
19	F	comments: _____
20	B	comments: _____

☐ 14. 10-minute rest

☐ 15. Post-Rest Dynamic Collections (perturb_back.vi – blue)
Collection #: 4
EMG Column #: ___

perturbation:	direction:	
1	F	comments: _____
2	B	comments: _____
3	B	comments: _____
4	B	comments: _____
5	F	comments: _____
6	B	comments: _____
7	B	comments: _____
8	B	comments: _____
9	F	comments: _____
10	B	comments: _____
11	F	comments: _____
12	B	comments: _____
13	F	comments: _____
14	F	comments: _____
15	B	comments: _____
16	F	comments: _____
17	F	comments: _____
18	F	comments: _____
19	B	comments: _____
20	F	comments: _____

Fatiguing Protocol (MVE_back.vi – purple)

☐ 16. 10 warm-up reps

☐ 17. Calculate Body Parts Torque (body_part.vi – grey)

☐ 18. Enter "Body Parts Torque" and "Maximum Erector Spinae Torque" into MVE_back.vi

☐ 19. Perform MVEs

	MVE (N-m)	50% MVE for Biodex
1.	_____	_____
2.	_____	_____
3.	_____	_____
4.	_____	_____
5.	_____	_____
6.	_____	_____

☐ 20. Calculate Workload for Isotonic Biodex Torque
(45 % MVE _____ – BP Torque _____ * sin45) x 0.74 = _____ ft·lbs

☐ 21. Fatigue Protocol
Metronome: 46 bpm Target MVE: _____ (from Excel sheet)

Time	% MVE	Reps
0: 00		10
1:		
3:		
5:		
7:		
9:		
11:		
13:		
15:		

☐ 22. Begin stopwatch

☐ 23. Collect fatigued EMG sub-maximum contraction

☐ 24. Fatigued Dynamic Collections (perturb_back.vi – blue)

Fatigued Perturbations to Step

Collection #: 5a elapsed time: _____ (since end of fatigue)

collection:	direction:	F mag:	B mag:	comments:	5b:
1	F	1		_____	B
2	F	2		_____	B
3	F	3			B
4	B		1		F
5	F	4		_____	F
6	F	5			F
7	B		2	_____	B
8	B		3	_____	F
9	B		4		B
10	F	6			F
11	B		5	_____	F
12	B		6		B
13	F	7		_____	B
14	F	8		_____	F
15	F	9			B
16	B		7	_____	F
17	B		8	_____	
18	B		9		
19	F	10			
20	B		10		
21	F	11		_____	
22	F	12		_____	
23	F				
24	B		11	_____	
25	B		12	_____	
26	B		_____	_____	

Collection #: 5b elapsed time: _____ (since end of fatigue)

perturbation:	direction:	
1	B	comments: _____
2	B	comments: _____
3	B	comments: _____
4	F	comments: _____
5	F	comments: _____
6	F	comments: _____
7	B	comments: _____
8	F	comments: _____
9	B	comments: _____
10	F	comments: _____
11	F	comments: _____
12	B	comments: _____
13	B	comments: _____
14	F	comments: _____
15	B	comments: _____
16	F	comments: _____

_____
_____
_____
_____
_____
_____
_____
_____

□ 25. Fatigued Low Level Perturbations

elapsed time: _____ (since end of fatigue)

Forward Level: 1 Backward Level: 1

Collection #: 6
EMG Column #: ___

perturbation:	direction:	
1	F	comments: _____
2	F	comments: _____
3	B	comments: _____
4	F	comments: _____
5	B	comments: _____
6	F	comments: _____
7	B	comments: _____
8	B	comments: _____
9	F	comments: _____
10	B	comments: _____

_____
_____
_____
_____
_____
_____
_____
_____

□ 26. Collection #: 7 elapsed time: 4 min (since end of fatigue)
EMG Column #: ___

perturbation:	direction:	
1	F	comments: _____
2	B	comments: _____
3	B	comments: _____
4	B	comments: _____
5	F	comments: _____
6	F	comments: _____
7	B	comments: _____
8	F	comments: _____
9	F	comments: _____
10	B	comments: _____
11	B	comments: _____
12	F	comments: _____
13	B	comments: _____
14	F	comments: _____
15	B	comments: _____
16	F	comments: _____

□ 27. Collection #: 8 elapsed time: 7 min (since end of fatigue)
EMG Column #: ___

perturbation:	direction:	
1	F	comments: _____
2	B	comments: _____
3	F	comments: _____
4	B	comments: _____
5	F	comments: _____
6	B	comments: _____
7	B	comments: _____
8	B	comments: _____
9	F	comments: _____
10	F	comments: _____
11	B	comments: _____
12	F	comments: _____
13	B	comments: _____
14	F	comments: _____
15	B	comments: _____
16	F	comments: _____

28. Collection #: 9 elapsed time: 10 min (since end of fatigue)
EMG Column #: ___

perturbation:	direction:	
1	B	comments: _____
2	F	comments: _____
3	F	comments: _____
4	B	comments: _____
5	F	comments: _____
6	B	comments: _____
7	F	comments: _____
8	F	comments: _____
9	B	comments: _____
10	B	comments: _____
11	B	comments: _____
12	F	comments: _____
13	B	comments: _____
14	F	comments: _____
15	B	comments: _____
16	F	comments: _____

29. Collection #: 10 elapsed time: 13 min (since end of fatigue)
EMG Column #: ___

perturbation:	direction:	
1	F	comments: _____
2	B	comments: _____
3	B	comments: _____
4	F	comments: _____
5	B	comments: _____
6	B	comments: _____
7	F	comments: _____
8	F	comments: _____
9	F	comments: _____
10	B	comments: _____
11	B	comments: _____
12	F	comments: _____
13	B	comments: _____
14	B	comments: _____
15	F	comments: _____
16	F	comments: _____

□ 30. Recovery Perturbations to Step

Collection #: 11 elapsed time: 15 min (since end of fatigue)
EMG Column #: ___

collection:	direction:	F mag:	B mag:	comments:
1	B		1	
2	F	1		_____
3	F	2		_____
4	F	3		
5	B		2	_____
6	B		3	
7	F	4		
8	B		4	_____
9	B		5	
10	F	5		_____
11	F	6		
12	B		6	_____
13	B		7	_____
14	B		8	
15	F	7		_____
16	F	8		_____
17	F	9		
18	B		9	
19	F	10		
20	B		10	
21	F	11		_____
22	F	12		
23	B		11	_____
24	B		12	_____
25	B			
26	F			

□ 31. Collection #: 12 elapsed time: 17 min (since end of fatigue)
EMG Column #: ___

perturbation:	direction:	
1	B	comments: _____
2	F	comments: _____
3	F	comments: _____
4	B	comments: _____
5	F	comments: _____
6	B	comments: _____
7	B	comments: _____
8	F	comments: _____
9	B	comments: _____
10	F	comments: _____
11	B	comments: _____
12	B	comments: _____
13	F	comments: _____
14	F	comments: _____
15	B	comments: _____
16	F	comments: _____

_____
_____
_____
_____
_____
_____
_____
_____

☐ 32. Collection #: 13 elapsed time: 21 min (since end of fatigue)
EMG Column #: ___

perturbation:	direction:	
1	F	comments: _____
2	B	comments: _____
3	B	comments: _____
4	B	comments: _____
5	F	comments: _____
6	F	comments: _____
7	B	comments: _____
8	F	comments: _____
9	F	comments: _____
10	B	comments: _____
11	B	comments: _____
12	B	comments: _____
13	F	comments: _____
14	B	comments: _____
15	F	comments: _____
16	F	comments: _____

☐ 33. Collection #: 14 elapsed time: 25 min (since end of fatigue)
EMG Column #: ___

perturbation:	direction:	
1	B	comments: _____
2	F	comments: _____
3	B	comments: _____
4	B	comments: _____
5	F	comments: _____
6	F	comments: _____
7	B	comments: _____
8	F	comments: _____
9	F	comments: _____
10	F	comments: _____
11	B	comments: _____
12	B	comments: _____
13	F	comments: _____
14	F	comments: _____
15	B	comments: _____
16	B	comments: _____

☐ 34. Collection #: 15 elapsed time: 30 min (since end of fatigue)
EMG Column #: ___

perturbation:	direction:	
1	B	comments: _____
2	F	comments: _____
3	B	comments: _____
4	F	comments: _____
5	B	comments: _____
6	B	comments: _____
7	F	comments: _____
8	B	comments: _____
9	F	comments: _____
10	B	comments: _____
11	F	comments: _____
12	B	comments: _____
13	F	comments: _____
14	F	comments: _____
15	F	comments: _____
16	B	comments: _____

☐ 35. Record end time: _____
☐ 36. Remove EMG electrodes and reflective markers from the participant
☐ 37. Turn off equipment:
- Vicon system
- force platform amplifiers (AMTI 1 & AMTI 2)
- load cell amplifiers
- EMG amplifier

☐ 38. Reapply adhesive to reflective markers
☐ 39. Reconstruct and process Vicon data
☐ 40. Clean up the laboratory

General Comments:

Vita

Bradley Davidson was born in Knoxville, Tennessee on September 15, 1979. He attended Cocke County High School in Newport, Tennessee and was honored as class Valedictorian in 1997. He completed a Bachelor of Science in Civil Engineering, graduating *summa cum laude* from Tennessee Technological University in the Spring of 2002. In the Spring of 2005, he obtained a Master of Science in Engineering Mechanics at Virginia Polytechnic and State University, and in the Fall of 2007, a Doctor of Philosophy in Biomedical Engineering from the Virginia Tech–Wake Forest School of Biomedical Engineering and Sciences. Bradley's research was conducted in the Kevin P. Granata Musculoskeletal Biomechanics Laboratory on the topic of localized muscle fatigue effects on the postural control system. During his graduate studies he published manuscripts in several peer-reviewed academic journals and conference proceedings, and received several awards including Outstanding Researcher at the VT–WFU Student Research Symposium, Best Student Paper at The Virginia Academy of Sciences annual meeting, and was a finalist in the ASB Clinical Biomechanics Research Paper Award. Bradley is currently a Postdoctoral Fellow at the University of Colorado Health Sciences Center and serves as an adjunct instructor in Bioengineering at the University of Colorado (Denver) and the Colorado School of Mines. In his free time he enjoys spending time with his wife, Becky, and can often be found outside rock climbing, cycling, or backpacking.

Bradley Davidson can be contacted at the following address:
4791 S Grant Street
Englewood, Colorado 80113